**ISTANBUL TECHNICAL UNIVERSITY ★ GRADUATE SCHOOL OF SCIENCE ENGINEERING AND TECHNOLOGY**

# SYNTHESIS OF CONDUCTING POLYMERS AND INVESTIGATION OF THEIR ELECTRICAL PROPERTIES

**Ph.D. THESIS**

**Esma ÖZEROL**

**Department of Polymer Science and Technology**

**Polymer Science and Technology Programme**

**JULY 2015**

**ISTANBUL TECHNICAL UNIVERSITY ★ GRADUATE SCHOOL OF SCIENCE ENGINEERING AND TECHNOLOGY**

# SYNTHESIS OF CONDUCTING POLYMERS AND INVESTIGATION OF THEIR ELECTRICAL PROPERTIES

**Ph.D. THESIS**

**Esma ÖZEROL**
**515092006**

**Department of Polymer Science and Technology**

**Polymer Science and Technology Programme**

**Thesis Advisor: Prof. Dr. Bahire Filiz ŞENKAL**
**Thesis co-Advisor: Doç. Dr. Mustafa OKUTAN**

**JULY 2015**

**İSTANBUL TEKNİK ÜNİVERSİTESİ ★ FEN BİLİMLERİ ENSTİTÜSÜ**

# İLETKEN POLİMERLERİN SENTEZİ VE ELEKTRİKSEL ÖZELLİKLERİNİN İNCELENMESİ

**DOKTORA TEZİ**

**Esma ÖZEROL**
**(515092006)**

**Polimer Bilim ve Teknolojisi Anabilim Dalı**

**Polimer Bilim ve Teknolojisi Programı**

**Tez Danışmanı: Prof. Dr. Bahire Filiz ŞENKAL**
**Eş Danışmanı: Doç. Dr. Mustafa OKUTAN**

**TEMMUZ 2015**

**Esma ÖZEROL**, **a Ph.D.** student of ITU **Graduate School of Science, Engineering and Technology** student ID **515092006**, successfully defended the **thesis** entitled "Synthesis Of Conducting Polymers and Investigation of Their Electrical Properties", which she prepared after fulfilling the requirements specified in the associated legislations, before the jury whose signatures are below.

| | | |
|---|---|---|
| **Thesis Advisor :** | **Prof. Dr. Bahire Filiz ŞENKAL**<br>İstanbul Technical University | ..... |
| **Co-advisor :** | **Doç.Dr. Mustafa OKUTAN**<br>İstanbul Technical University | ..... |
| **Jury Members :** | **Prof. Dr. Sait Eren SAN**<br>Gebze Technical University | ..... |
| | **Prof. Dr. Esma SEZER**<br>İstanbul Technical University | ..... |
| | **Prof. Dr. Ayfer SARAÇ**<br>Yildiz Technical University | ..... |

**Date of Submission :** June 19, 2015
**Date of Defense :** July 10, 2015

***To my lovely SPOUSE and my lovely PARENTS,***

## FOREWORD

I would like to express my sincere thanks to my supervisor Prof. Dr. Bahire Filiz ŞENKAL, for encouragement, gracious support throughout the whole study and for providing me a peaceful environment to work at Istanbul Technical University. I am grateful for her, patience and consideration.

I express my appreciation to my co-supervisor Assoc. Prof. Dr. Mustafa OKUTAN who provides the laboratories at which I contacted my physical experiments at Yıldız Technical University and at Gebze Technical University. I also want to thank to him for his creative ideas and sharing his wisdom.

Prof. Dr. Yeşim GÜRSEL, whom I like to give my special thanks for giving me an opportunity to share her knowledge.

I am grateful to my doctoral committee members Prof. Dr. Sait Eren SAN, Prof. Dr. Esma SEZER, Prof. Dr. Ayfer SARAÇ for their constructive suggestions and fruitful discussions at various stages of my research work. In addition, I am indebted to Prof. Dr. Sait Eren SAN, from Gebze Technical University for allowing the use of scientific equipments at Department of Physics.

I would like to thank my colleague and close friends who are always willing to help me: Res. Assist. Gülçin Torunoğlu TURAN, Res. Assist. Dr. Erdem YAVUZ for invaluable support and help. I also want to thank to Res. Assist. Dr. Ayşegül Çelik BOZDOĞAN for her help and support.

I would like to thank to my parents Prof. Dr. Mehmet AHLATCIOĞLU and Yıldız AHLATCIOĞLU for their moral supports and sharing all the difficulties with me throughout this study. They have been exceptionally supportive and loving during all stages of my life. Without the support of my parents, I could not have finished this thesis. Without them, I would not be where I am today. I would especially like to thank my lovely father is very special person in both my social and academic life. He is always guide for my life. His special advices have been very valuable in my way of life. I am so glad i have my parents…

I want to thank my other lovely family members Beyza-Serkan-Burak ÖZKÖK and Aykut-Esra-Mehmet AHLATCIOĞLU for being with me. I am so glad I have you…

Finally, words are not enough to express my emotions; I would special thanks to my husband Bilal ÖZEROL for all the support, understanding and love during the final stages of my work. I am so blessed to have you in my life…

July 2015

Lecturer Esma ÖZEROL
(Physicist)

**TABLE OF CONTENTS**

**Page**

## ABBREVIATIONS

**PANI** : Poly(aniline)
**PPy** : Poly(pyrole)
**NVC** : Poly(N-vinyl carbazole)
**PEDOT** : Poly(ethylenedioxythiophene)
**TP** : Poly(thiophene)
**$BN_3$** : Boron nitride
**CNT** : Carbon nanotube
**NC** : Nano clay
**GH** : Graphite
**LC** : Liquid Crystal
**DMAEM** : Poly(2-(dimethylamino)ethylmetactylate) (DMAEM)
**NMP** : N-Methyl-2-pyrrolidone
**THF** : Tetrahydrofuran
**DMF** : Dimethylformamide
**AIBN** : Azobisisobutyronitrile
**ITO** : Indiumtinoxide
**CBH** : Correlated Barrier Hoping
**QMT** : Quantum Mechanical Tunneling
**Cs** : Chalcone substitued aniline
**LC8** : 8-(4-cyanobiphenyl-4'-oxy) octan-1-ol
**XRD** : X-Ray Diffraction
**GPC** : Gel Permeation Chromatography
**FESEM** : Field Emission Scanning Electron Microscopy
**$^1$H-NMR** : $^1$H Nuclear magnetic resonance
**POM** : Polarizing optical microscope
**EPR** : Electron Paramagnetic Resonance

**LIST OF TABLES**

**Page**

**LIST OF FIGURES**

**Page**

**SYNTHESIS OF CONDUCTING POLYMERS AND INVESTIGATION OF THEIR ELECTRICAL PROPERTIES**

## SUMMARY

This thesis is consisting of two parts. First part concerning with synthesis of new conducting polymers. For this purpose, chemical polymerization of aniline in the presence of propiolic acid as dopant and synthesis and polymerization of chalcone substituted aniline, and the other one is preparation of the poly (N-vinyl carbazole)-co-poly (2-(dimethylamino) ethyl methacrylate) based hydrogen bonded side-chain liquid crystal copolymer.

Among the conducting polymers, polyaniline is one of the important electronic materials because of its easy synthesis, environmental stability, reversible proton dopability, redox recyclability, cost-effectiveness, and reasonable electrical conductivity. Polyaniline is one of the most promising conducting materials for applications in optoelectronics and microelectronics devices.

In the present work, polyaniline (PANI) was synthesized in the presence of propiolic acid. The effects of the dopant on the course of oxidation and properties of final products have been studied by Fourier Transform Infrared Spectroscopy (FTIR) spectroscopy, and conductivity measurements. The dielectric properties of PANI and doped PANI were investigated using the impedance spectroscopy (IS) dependency of the frequency and the temperatures.

New chalcone substituted aniline derivative, was synthesized by starting from 3-aminoacetophenone and 4-pyrridinecarboxyaldehyde in the presence of NaOH. The obtained chalcone containing aniline was polymerized oxidatively in water in the presence of dopant such as methanesulfonic acid, formic acid, HBr and acetic acid using ammonium persulfate as oxidant at room temperature for 24h. Chalcone containing polyaniline (Cs-PANI) was characterized by using FTIR and physical methods.

Side-chain liquid crystalline polymers (SLCPs), which represent a combination of liquid crystalline behavior and polymeric properties, have been the subject of intensive research during the last decade since these polymers are regarded as materials with promising optical and electro-optical properties for potential applications in optical switching and image storage. The liquid crystallinity and physical properties of LCPs depend on the molecular structures chosen for polymer design. In this study, new side chain liquid crystalline copolymers were prepared from N-vinyl carbazole (NVC) and 2-(dimethylamino) ethyl methacrylate) (DMAEM) as a hydrogen bond acceptor copolymer and 8-(4-cyanobiphenyl-4'-oxy) octan-1-ol (LC8) by molecular self-assembly processes via hydrogen bond formation between nitrogen of (DMAEM) and hydroxyl group of the LC8.The formation of H bond was confirmed by using FTIR spectroscopy. The liquid crystalline behavior of

the copolymers and homopolymer of the (DMAEM) was investigated using a differential scanning calorimeter (DSC) and polarized optical microscopy. The dielectric relaxation properties of H-bonded Side Chain LC Copolymers (HB-LCP) doped 8-(4-cyanobiphenyl-4'-oxy) octan-1-ol (LC8) and pure LC8 liquid crystals have been investigated by the dielectric spectroscopy (DS) method.

The second part of the thesis, conducting polymer composites was prepared physical and chemical characterizations were performed. PANI was interacted with nanoclay, magnetite and graphite to obtain its composites.

The thermal stability, mechanical strength, gas barrier, fire retardant properties, processability, etc. can be enhanced by the synthesis of the composites. The formation of polyaniline composites with inorganic materials provides new synergistic properties that cannot be attained from individual materials. The combination of clays and functional polymers interacting at atomic level constitutes the basis for the preparation of an important class of inorganic–organic nanostructured materials. In this study, aniline was polymerized oxidatively in the presence of boric acid as dopant and nanoclay with different weight percentage. The electrical properties of polyaniline nanoclay composite were studied using impedance spectroscopy.

The magnetic nanoparticles were synthesized by mixing a water solution of $FeCl_2.4H_2O$ (1.0 M) and $FeCl_3.6H_2O$ (1.5 M). Composites of poly (aniline) and magnetite were prepared by using oxidative polymerization of aniline in the presence of different weight percentage of magnetite (2%, 5% and 10%). Field Emittion Scanning electron microscopy (FESEM) and FTIR analyses were performed to understand the structure of PANI-magnetite composites. The magnetic and electric properties of PANI, magnetite, magnetite doped PANI were investigated by electron paramagnetic resonance and impedance spectroscopy techniques, respectively. Also, dielectric properties were investigated by impedance spectroscopy for undoped PANI, magnetite and different weight percentage of magnetite doped Polyaniline–magnetite composites.

In this work, synthesis and characterization of composite materials based on graphite (GH) and boric acid doped PANI were studied. PANI + GH composites were prepared via a simple in situ polymerization of aniline in graphite dispersion. The resulting composites of the PANI + GH were characterized by using spectroscopic, morphologic and physical methods.

Polythiophene-boron nitride composites were prepared and characterized accordingly. Polythiophene/different weight percentage of Boron nitride (BN) (1% and 2%) (BN) composites were prepared via in situ oxidative polymerization of thiophene by using $FeCl_3$ as oxidant at room temperature for 48 h. FESEM and FTIR spectroscopy were used to characterize the morphology and structure of the samples. Also, electrical characterizations of the composites have been investigated by impedance spectroscopy.

# İLETKEN POLİMERLERİN SENTEZİ VE ELEKTRİKSEL ÖZELLİKLERİNİN İNCELENMESİ

## ÖZET

Tez iki kısımdan oluşmaktadır. Birinci kısım yeni iletken polimerlerin sentezidir. Bu amaç doğrultusunda dopant ajanı olarak propiolik asit varlığında anilin sentezi ile kalgon substitute anilinin polimerizasyonundan oluşmaktadır.Diğer kısım ise poli (N-vinil karbazol)- co-poli (2-(dimetilamino) etil metilakrilat) bazlı hidrojen bağlı yan zincir sıvı kristal kopolimer sentezinden oluşmaktadır.

İletken polimer kavramı, kendi örgüsü içerisindeki elektronlarla yeterli düzeyde elektriksel iletkenliği sağlayan polimerler için kullanılır. Polimerlerin elektronik iletkenlik gösterebilmesi için, polimer örgüsünde, elektronların zincir boyunca taşınmasını sağlayan uygun yerlerin bulunması gerekmektedir. Bu koşulu ana zincirinde konjuge çift bağlar bulunan polimerler sağlamaktadır. Konjügasyon yüksek düzeyde iletkenlik için tek başına yeterli olmaktadır. Konjuge çift bağlı polimerlerin iletkenliğinin artırılabilmesi için hareketli yük taşıyıcılarının (dopant) eklenmesi gerekmektedir. Bu durum konjuge π yapısına sahip olan polimerlerin elektron alan veya elektron veren gruplarla yükseltgenmesi veya indirgenmesi işlemleri ile sağlanmaktadır.

Diğer iletken polimerler arasında polianilin (PANI), kolay sentezi çevresel stabil olması, tersinir proton doplanabilmesi, etkili elektriksel iletkenli gibi özelliklerden dolayı önemli elektronik malzemelerden biridir. Polianilin optoelektronik, mikroelektronik aletlerde kullanılan dikkat çeken iletken polimerlerden biri olmaktadır.

Bu çalışmada polianilin propiolik asit varlığında sentezlenmiştir. Dopant ajanının oksidasyona etkisi ve elde edilen polimerin FTIR (Fourier Dönüşümlü Kızılötesi Spektroskopisi) ve iletkenlik ölçümleri yapılmıştır. Doplu ve dopsuz polianilinin dielektrik özellikleri frekansa ve sıcaklığa bağlı olarak empedans özellikleri incelenmştir.

Yeni kalgon sübstitiye anilin türevi, NaOH varlığında 3-aminoasetofenon and 4-piridinkarboksialdehit ile başlanarak sentezlenmiştir. Elde edilen kalgon içeren anilin, suda metansülfonik asit, formik asit, HBr ve asetik asit gibi dopantlar varlığında amonyumpersülfat başlatıcısı ile oda sıcaklığında 24 saat sure ile polimerizasyonu gerçekleşmiştir. Elde edilen kalgon sübstitiye anilin FTIR ve dielektriksel metodlar ile karakterize edilmiştir.

Son yıllarda teknolojide yaygın olarak kullanılan sıvı kristal materyallere olan ilgi artmakta, farklı yapıdaki yeni sıvı kristallerin tasarımı ve fiziksel özelliklerinin belirlenmesini kapsayan araştırmalara hızla yenileri eklenmektedir. Sıvı kristaller, termal, elektriksel ve manyetik alanlar gibi dış etkilere duyarlı olmalarından dolayı çok sayıda farklı uygulamalarda kullanılabilmektedir. Yan zincirli sıvı kristal polimerler, sıvı kristal davranış ile polimerik özelliklerin bir arada bulunduğu özelliğe sahip malzemeler olmaktadır. Yan zincir sıvı kristal polimerler genellikle rijid

mezojenlerin polimer ana zincirine, bir ara yapı üzerinden kovalent bağ ile bağlanmasıyla elde edilir. Son on yılda bu malzemeler elektro-optik özellikler ile alakalı uygulamalarda yoğun çalışmalar yapılmaktadır. Poli(vinil karbazol) bilinen en eski ve çoğunlukla polimerik fotoiletken polimerlerden bir tanesi olmaktadır. Polimerik ışık emisyonu diyot (LED), organik fotorefraktif malzemelerde, fotovoltaik cihazlarda kullanıldığında dikkat çekici özelliğe sahip olmaktadır.

Bu çalışmada, N-vinil karbazol (NVC) and 2-(dimetilamino) etil metakrilat) (DMAEM) kullanılarak H bağı akseptörü olan yeni yan zincir sıvı kristal kopolimerler hazırlanmıştır. Hazırlanan kopolimerler 8-(4-siyanobifenil-4'-oksi) oktan-1-ol (LC8) ile kendiliğinden (DMAEM)'de ki azot ile LC8'de ki OH grubu ile hidrojen bağı oluşumu ile elde edilmiştir. Bileşiklerdeki H-bağ oluşumu FT-IR spektroskopisi ile saptanmıştır. Mesojenik birimlerin yapı tayinleri $^1$H-NMR ve FT-IR spektroskopi ile gerçekleştirilmiştir. Sentezlenen bileşiklerin termal ve mesomorfik özellikleri sırasıyla diferansiyel taramalı kalorimetri (DSC), ve polarize optik mikroskop (POM) ile incelenmiştir. Malzemelerin dielektrik relaksasyon özellikleri dielektrik spektroskopisi (DS) ile tayin edilmiştir.

Tezin ikinci kısmında iletken polimer kompozitlerin fiziksel ve kimyasal karakterizasyonu incelenmiştir. Polianilinin nanokil, magnetit, ve grafit ile kompozitleri ve politiyofenin bor nitrit ile kompozitleri elde edilmiştir.

Kompozit terimi, iki veya daha fazla farklı maddenin karıstırılması veya belli bir düzende birlestirilmesi ile hazırlanan sistemler için kullanılmaktadır. Kompozit yapımında iki polimer matriksi birbiri içine difüzlenerek bir karısım olusturulmaktadır. Bu yöntemde genellikle bir polimer süspanse edilmekte veya çözülmekte ve bu sistemin üzerinde baska bir monomer polimerlestirilerek kompozit elde edilmektedir. Yalıtkan polimer matriksi kullanılarak iletken kompozit hazırlanmasındaki temel amaç, hem yalıtkan polimer matriksinin mekanik özelliklerini tasıyan hem de iletken polimerlere yakın iletkenlik gösteren kompozitler olusturmaktır. Polimer kompozitlerinin kullanımındaki artısın sebebi, yeni polimer sentezlemeye ihtiyaç duyulmadan polimer özelliklerinin modifikasyonu için metot sağlanması olmaktadır. Bu özelliklerden kimyasal rezistans, termal kararlılık ve mekanik dayanım, var olan iki ya da daha fazla polimerin olusturdugu kompozit ile artırılabilmektedir.

Termal kararlılık, mekaniksel güç, alev geciktirici özellikler, işlenebilirlik gibi özellikler kompozit sentezleri ile artırılabilmektedir. Polianilinin inorganik malzemelerle kompozitleri yeni sinerjik özellikler sağlar. Kil ile foksiyonel polimerlerin atomik seviyede etkileşiminde önemli inorganik-organik nanoyapıda malzeme sınıfı oluşturmaktadır. Bu çalışmada anilin, dopant ajanı olarak borik asit varlığında ve ağırlıkça farklı yüzdelerde nano kil varlığında oksidatif polimerizasyon ile elde edilmiştir. Polianilin nanokil kompozitlerinin elektriksel özellikleri, empedans spektroskopisi incelenmiştir.

Magnetik nanoparçacıklar sulu $FeCl_2.4H_2O$ (1.0 M) ve $FeCl_3.6H_2O$ (1.5 M) çözeltisinde hazırlanmıştır. Polianilin magnetit kompozitleri farklı ağırlıkça yüzde oranlarında ki (%2, %5, %10) magnetit varlığında oksidatif polimerizasyonla elde edilmiştir. Polianilin-magnetit kompozitlerin yapılar alan emisyonlu taramalı elektron mikroskobu (FESEM) ve FTIR spektroskopisinde incelenmiştir. Elektron paramagnetik resonans ile magnetitin ve magnetit doplu polianilinin magnetik özellikleri araştırılmıştır. Aynı zamanda magnetit ve farklı ağırlıkça yüzde oralarında

magnetit polianilin kompozitlerin impedans spektroskobisi ile dielektrik özellikleri araştırılmıştır.

Bu kompozit çalışmalarından birisi de, borik asit doplu polianilinin grafit bazlı kompozitlerinin sentezi ve karakterizasyonu olmaktadır. Polianilin grafit kompozitleri basit bir şekilde grafit çözeltisi içinde in situ polimerizasyonu ile elde edilmiştir. Elde edilen polianilin grafit kompozitleri spektroskopik, morfolojik, ve fiziksel metodlar ile elde edilmiştir.

Yapılarının çeşitliliği ve çevresel kararlılıklarının iyi olmasından dolayı, politiyofen ve onun türevleri iletken polimerler alanında fazlaca kullanılmıştır ve pek çok bilim adamının ilgisini çekmiştir. Politiyofen bor nitrit kompozitleri'nde ise farklı ağırlıkça yüzde oranlardında ki bor nitrit ile $FeCl_3$'ü oksidant olarak kullanarak tiyofenin oksidatif polimerizasyonuyla 48 saat sonunda oda sıcaklığında elde edilmştir. FESEM ve FTIR spektroskopisi ile morfolojileri ve yapıları karakterize edildi. Ayrıca empedans spektroskopisi ile elektriksel karakterizasyonları yapılmıştır.

## 1. INTRODUCTION

Conducting polymers in organic electronics have a number of advantages against small molecules, particularly because of mechanical properties their stability and ease of processing [1,2].

Polyaniline (PANI) has received an enormous amount of research attention, because it has very interesting and useful physical properties for the practical fabrication of an electrical all- organic device, as well as remarkable tensile properties. Therefore, it is important to modifying the conductivity and processability of PANI through the selection of a suitable dopant and suitable level of doping and also by controlling its structure during synthesis [3,4]. Photosensitive polymers with photocrosslinkable groups have gained a considerable interest in recent years owing to a wide variety of applications in the field of macro- and microlithography, printing, liquid crystalline display, nonlinear optical materials, holographic head-up-display, integrated circuit technology, photocurable coatings, photoconductors, energy exchange materials, etc [5].

Polymer containing pendant α, β-unsaturated carbonyl groups (also named chalcone groups, e.g., cinnamoyl groups) either in the backbone or as pendant group undergo crosslinking upon irradiation with UV light or an electron beam, and are being used as photoresists in the field of printing technology [6], microlithography [7], non-linear optical materials [8], holographic head-up display [9], liquid crystals [10,11], energy exchange materials [12], etc.

These polymers with the following properties: good solubility, the ability to form films, high photosensitivity, resistance towards solvents after crosslinking, thermal stability and resistance towards plasma and etching agents, are very important for practical use as commercial negative photoresist materials.

In this study, propiolic acid doped PANI and chalcone subtitued PANI were prepared and characterized by using physical and chemical methods.

Polythiophene materials can be used as electrical conductors, nonlinear optical devices, polymer LEDs, electrochromic or smart windows, photoresists, antistatic

coatings, sensors, batteries, electromagnetic shielding materials, artificial noses and muscles, solar cells, electrodes, microwave absorbing materials, new types of memory devices, nanoswitches, optical modulators and valves, imaging materials, polymer electronic interconnects, nanoelectronic and optical devices and transistors.

Side chain liquid-crystalline polymers (SCLCPs) are usually prepared by covalently linking rigid mesogens to a polymer backbone through flexible spacers. Self-assembly through specific interactions, such as hydrogen-bonding [14–16] ionic, ionic dipolar, and charge transfer interactions, [13] was used as a strategy for constructing (SCLCPs).

A new copolymers were prepared from radical copolymerization of N-vinyl carbazole (NVC) and 2-(Dimethylamino)ethyl methacrylate) (DMAEM). And these copolymers were interacted with 8-(4-cyanobiphenyl-4'-oxy) octan-1-ol (LC8) as a hydrogen bond acceptor. The liquid crystalline side chain copolymers were obtained by molecular self-assembly processes via hydrogen bond formation between nitrogen of (DMAEM) and (LC8) hydroxyl group.

The formation of polyaniline (PANI) composites with inorganic materials provides new synergistic properties that cannot be attained from individual materials [17,18]. The combination of clays and functional polymers interacting at atomic level constitutes the basis for the preparation of an important class of inorganic–organic nanostructured materials. In the present study, transition metal ions were exchanged with the interlamellar cations of montmorillonite clays and polymerization of aniline was done within the layers.

In this study, aniline was polymerized oxidatively in the presence of nanoclay, graphite and magnetite with different weight percentage. The electrical properties of a poly(aniline) composites were studied using impedance spectroscopy as a function of the frequency of the applied AC–DC signal at various temperatures and four point probe technique.

Composites of BN and Poly(thiophene) are interesting for their application as electrochromic and photovoltaic materials.

In this study, different weight percentage of BN (0%, 1%, 2%) and chemical polymerization was performed by using $FeCl_3$ as oxidant at room temperature for 48 h.

# 2. THEORETICAL PART

## 2.1 Conducting Polymer

Even in the fifth decade of the last century, because polymers were well known as electrically insulating materials, they are used the insulating area such as insulating cover for electrical somethings in modern civilization [19]. In these polymers has not be ability of electrical conductivity because of no any free electrons, which are responsible for electrical conductivity. It can be called insulating polymers which are insulating in nature due to the saturated [19].

The main difference is their structure between in insulating polymers and intrinsically conductive polymers. Insulating polymer contains unsaturated conjugated structure. However, insulators have not conjugated structure. Structures of few conjugated polymers approach the ideal of fully extended, defect free backbones and are generally partly crystalline or non crystalline. Because of this, their conjugation and backbone does not be in order and disorder, respectively. [20]

It can be said polymers with conjugated backbones can be made metallic because of high density of conjugated regions, which are ability of high degree of connectivity. However, semiconducting polymers with saturated backbones containing only localized conjugated regions.

### 2.1.1 Doping mechanism

In terms of electrical conductivity, the materials can be classified as three categories, which are insulators, semiconductor and conductors. This difference can be explained “Band Theory”.

Delocalized positive charges (holes) are occurred on the polymer chain when the electrons move away from valance band and this situation can be called as oxidation of polymer. Anion from solution move to delocalized charges on polymer chain for the purpose of neutralization of these charges. In conjugated polymers, these are first $\pi$ electrons from the HOMO (Highest Occupied Molecular Orbital) level. Therefore, they act as electron acceptors, which are referred to as p-type dopants. As a result,

holes are occured. Negative charges are occurred during reduction of conducting polymers. Cation moves from solution to polymer for the purpose of neutralization of these charges. Therefore they act as electron donors, which are referred as n-type dopants. These electrons occupy states at near the LUMO (Lowest Occupied Molecular Orbital) level [21]. Representative anionic and cationic dopings are describted in Eq (2.1) and (2.2) for Poly(pyrole) (P(Py)) and Poly(p-phenylene) (P(PP)), respectively.

Anionic Doping:

$$P(Py) + n\ ClO_4^- \rightarrow P(Py)_n + (ClO4)_n(n-) \quad \textbf{(2.1)}$$

Cationic Doping:

$$P(PP) + n\ Li \rightarrow (Li)_n(n+)\ P(PP)(n-) \quad \textbf{(2.2)}$$

### 2.1.2 Conduction mechanism of conducting polymers

The electronic property of a material is related to electronic structure. “Band Theory” is the most effective expository for the electronic structure of materials. In terms of electrical conductivity, the materials can be classified as three categories, which are insulators, semiconductor and conductors at room temperature. Electronic bands occur when their molecular electronic status overlap each other at all materials. Valance band occurs when valance electrons overlap each other and when electronic states of the above of the valance band overlap each other, conducting band occurs. The band gap (EG) is the gap in energy between the valence band and conduction band.

The insulators have large energy band gap. Therefore, it is difficult to excited electron into the conduction band. If the energy ban gap is small, (e.g. 1.0 eV), then electrons can be excited from the valence band into the conduction band by different excitation ways. After that electrons are mobile in a sense. It can be called as semiconductor materials. For a conducting material, there is no energy band gap between conduction bands and valence bands. The conduction band is partially occupied resulting in a “high” electrical conductivity. The conductivity classes are shown as schematic according to their band gaps in Figure 2.1.

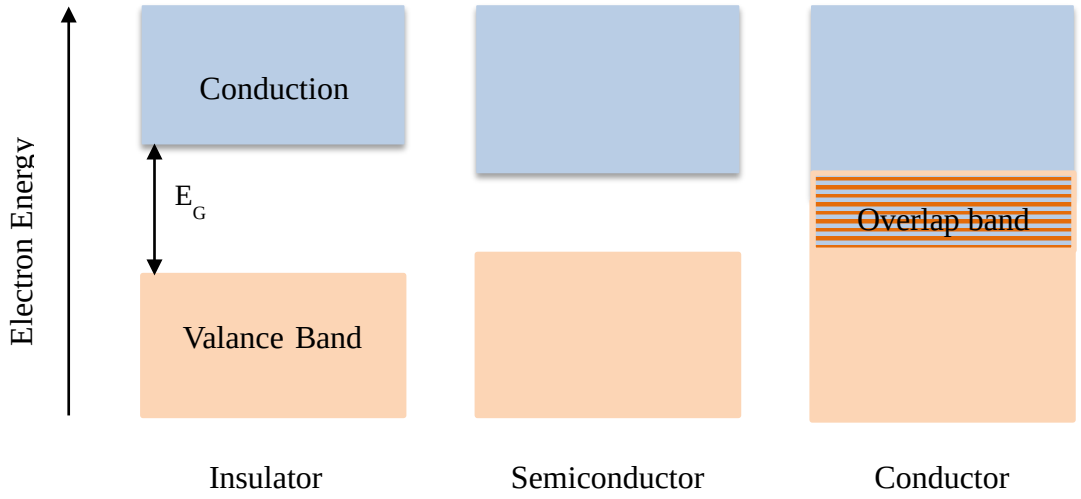


**Figure 2.1 :** Schematic comparison of the electronic band structures of conductor, semiconductor and insulator.

## 2.2 The Types of Conducting Polymers

### 2.2.1 Poly(aniline) (PANI)

Polyaniline (PANI) is one of the most attractive conducting polymers and has been studied intensively over the past decades because of its simple synthesis, controllable electrical conductivity, good environmental stability and striking electronic and optical properties [22].

The existence of nitrogen atoms as imine (in $sp^2$) or amine (in $sp^3$ hybridized state) forms, and their relative ratio in the overall polymer backbone chain determines the resulting structure and the different features of PANI [23].

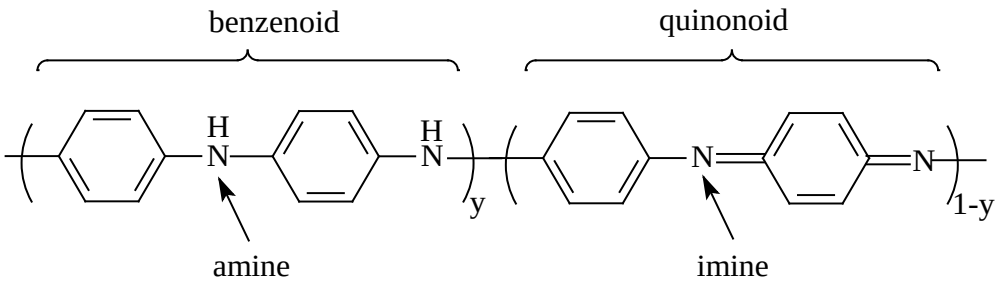


**Figure 2.2 :** General chemical structure of PANI [23].

PANI exists in three different oxidation states, which are pernigraniline, leucoemeraldine, and emeraldine which are both pH and potential dependent

The general chemical structure of polyaniline is shown in Fig 2.2. It contains y (reduced) and (1-y) oxidizing units. The value of y can vary from 0, (all quinonoid units) to give completely oxidized form (pernigraniline), to 1 (all benzenoid units) which gives a completely reduced leucoemeraldine. When y=0.5, i.e. the number of reduced units equals the number of oxidized units, it is known as emeraldine base [23]. It is shown that there is more room to modify the molecular structure according to other conducting polymer [24].

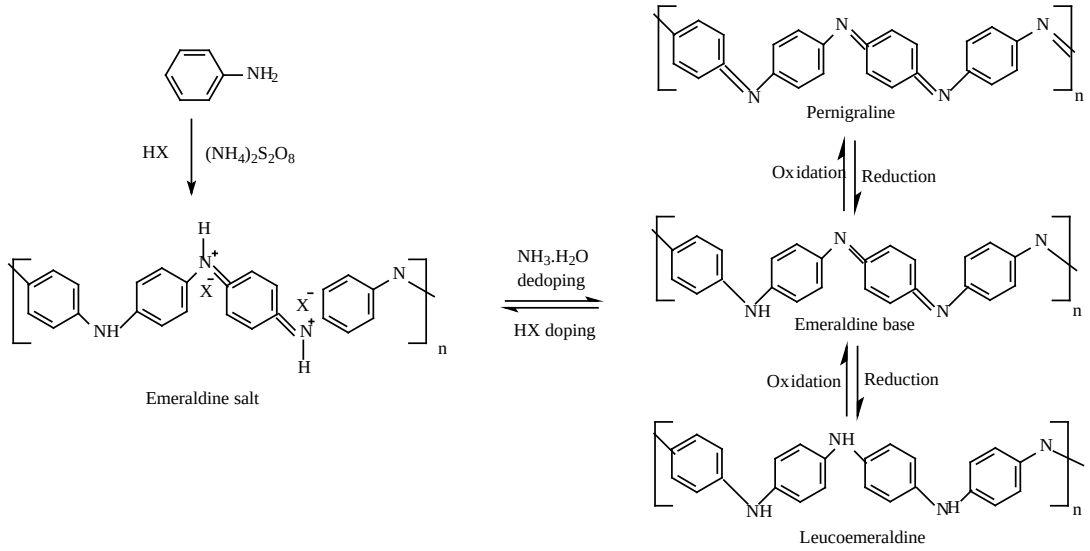


**Figure 2.3 :** The idealized oxidation states of polyaniline [25].

These oxidation states are most reduced and most oxidized states which are called as leucoemeraldine (y=1) and pernigraline (y=0), respectively. The emeraldine (y=0.5) is an intermediate oxidation state. When the emeraldine base state is doped via a strong protonic acid, it is obtained the conducting emeraldine salt state (Figure 2.3) [26].

### 2.2.1.1 Synthesis of polyaniline

The most widely employed synthetic routes are the chemical oxidative polymerization in the presence aqueous acid and the electrochemical polymerization to obtain polyaniline from the aniline monomer. Chemical oxidative polymerization (radical cationic reaction) of aniline is usually conducted in acidic medium with a suitable oxidizing agent such as ammonium persulfate (APS) and proceeds to form polyaniline. As produced polyaniline can be rendered electrically conducting by an additional acid treatment (doping) after its polymerization reaction [27].

Oxidation of aniline is initiated with the aim of a resonantly stabilized anilinium radical. Polymerization proceeds in the dimer formation by “head to tail” reaction between the radical cation and its resonant form in acidic media through preferential coupling with other anilinium radical cations. Propagation subsequently proceeds through the radical cation monomer or with the radical cation dimer to form, respectively, a trimer or a tetramer. If the above steps persist, the polyaniline (PANI) is occured (Figure 2.4) [28].

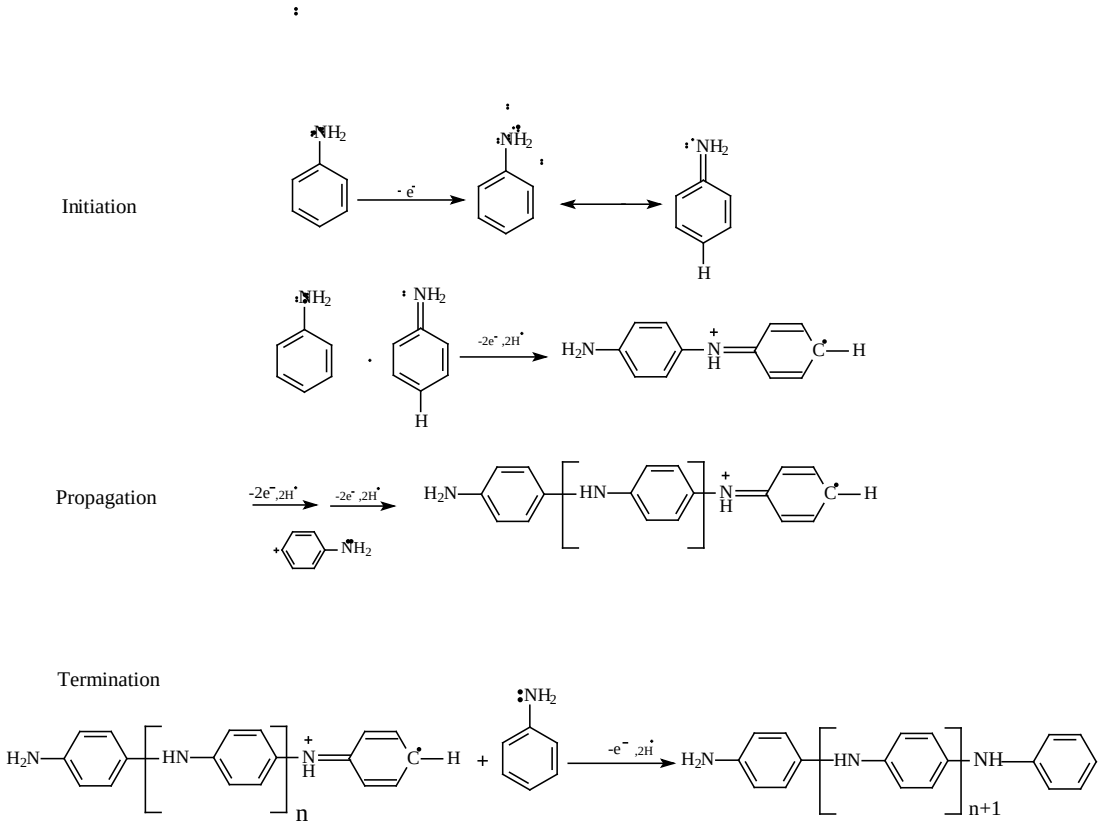


**Figure 2.4 :** The polymerization steps of aniline [29].

### 2.2.2 Poly(thiophene)

Although the obtention of polymeric materials from thiophene derivatives has been known for long, the origin of the intensive research efforts aiming the optimization of the preparation of poly(thiophenes) is in keeping with the emergence of the widespread general interest for conducting polymers in the early 1980s [30]. Poly(thiophenes) display a variety of electronic and optical properties that make them interesting to study. The polymers have also demonstrated a greater environmental stability in the conducting state than the parent conjugated polymer, polyacetylene [31]. These properties and others have resulted in much research into

their potential applications in electronic, optoelectronic, electrochromic and battery devices [30].

Poly(thiophene) is a conducting polymer composed of five-membered heteroaromatic rings [32]. The general structure of poly(five-membered heterocycles) corresponds to the coupling of monomeric units in 2,5 positions with preservation of the aromatic nucleus as shown in Figure 2.5.

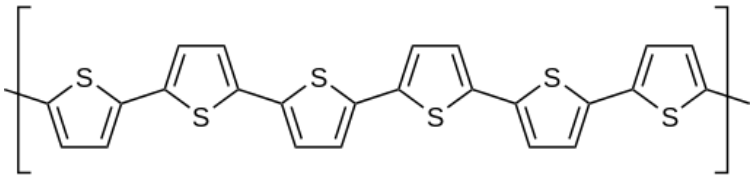

**Figure 2.5 :** Structure of Poly (thiophene) [33].

### 2.2.3 Poly(N-vinyl carbazole)

Poly(vinyl carbazole) is the oldest known and most widely characterized polymeric photoconductor. Poly(N-vinylcarbazole) (PNVK) is more attractive photoconductive polymer because of wide potential applications as polymeric light emitting diodes, organic photorefractive materials, and photovoltaic devices [34].

Since the first successful use of PVNK in electrophotographic applications [35,36], polymers with carbazole moieties have been often studied. N-vinylcarbazole (NVK) monomer undergoes feasible cationic polymerization with a variety of cationic initiators to give PNVK and the living cationic polymerization of NVK initiated by hydrogen iodide has been achieved [37]. Free radical initiators, including azo compounds and peroxides, easily polymerize NVK. Accordingly, radical polymerization is currently used in the manufacture of such polymers [35]. To expand the range of applications and to investigate the effect of the polymer compositions and functionalities on the morphology, the block copolymerization has been also attempted. One can consider the synthesis of PNVK-based block copolymers with monomers typically used in radical polymerization and stabilized by resonance such as styrenes, methacrylates, methacrylamides but their preparations using a single polymerization technique remains a challenge.

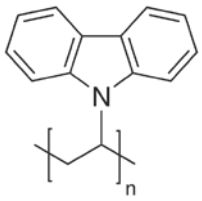

**Figure 2.6 :** Chemical structure of NVC [38].

### 2.2.4 The other common conducting polymers

#### 2.2.4.1 Poly(ethylenedioxythiophene) (PEDOT)

This polymer is poly(thiophene) derivative and called as PEDOT. It is used for various applications and most commercially successful conducting polymer. It was initially developed to give a soluble conducting polymer that lacked the presence of undesired α,β and β,α couplings within the polymer backbone [39] .

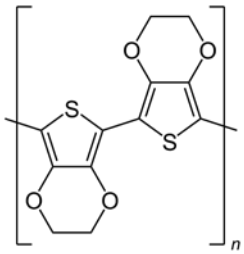

**Figure 2.7 :** Chemical structure of PEDOT [40].

#### 2.2.4.2 Poly(pyrrole)

Polypyrrole (PPy) is generally electrochemically and chemically synthesized conducting polymer.

Poly(pyrrole) is attractive conducting polymers because of many important properties. These are easily deposited from aqueous and non-aqueous media, very adherent to many types of substrates, and are well-conducting and stable. [41]

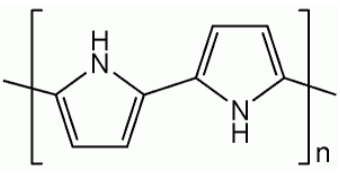

**Figure 2.8 :** Chemical structure of poly(pyrole) [42].

### 2.2.4.3 Poly(acetylene)

Hideki Shirakawa, Alan Heeger, and Alan MacDiarmid discovered the high electrical conductivity of poly(acetylene). This discovery was known by the Nobel Prize in 2000 After this discovery, polyacetylene has arrest to scientists attention. n the usage of in microelectronics. Polyacetylene, which has a planar structure, consists of a long chain of carbon atoms. Their sequence continue alternating single and double bonds and the geometry of double bonds can have either cis or trans forms.

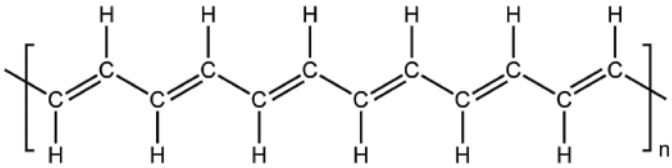

**Figure 2.9 :** Chemical structure of poly(acetylene) [43].

## 2.3 Composites

Conducting polymer are attractive materials due to remarkable properties such as their simple synthesis, good environmental stability and electrical conductivity. On the other hand, conducting polymers have some handicaps in aspect of their processing because of insoluable, low mechanical properties etc.

The formation of copolymers and composites is one of the most useful ways in order to overcome these limitations. Thus physical and mechanical properties of a polymer can be controlled and enhanced. The researchers synthesize copolymer or composites, to improve the mechanical and physical properties of conducting polymers.

Composites are materials consist of two or more component materials with significantly different physical or chemical properties, The main objective of making composites is to combine the good properties of the their components. The two materials work together to give the composite unique properties. The finished composite material may be preferred for many causes such as more stronger, lighter or less expensive properties than to their components.

Composites are combinations of two materials in which one of the materials, called the reinforcing phase and matrix material. The reinforcing phase can be in the form

of fibers, particles or sheets. The reinforcing phase is embedded in the matrix material which can be polymer, ceramic or metal [44].

Polymer composites are attained by combination with filler and polymer matrix. Polymer composites have outstanding properties such as high strength, dimensional and thermal stability, hardness and abrasion resistance.

### 2.3.1 Clay

Clay is a common name for a whole family of layered aluminosilicates. It is used in wide variety of applications like ceramic, decorating and industrial products depending upon its form and properties. The most commonly used clays in nanocomposite are organically modified montmorillonite which have widely been used to synthesize polymer-clay nanocomposites due to their good swelling behavior, and low cost [45]. Their crystal lattice consists of two-dimensional, 1 nm thick layers formed by fusing two silica tetrahedral sheets with an edge-shared octahedral sheet of alumina or magnesium [46].

### 2.3.2 Magnetite

Magnetite ($Fe_3O_4$) is the strongest magnetic material in aspect of natural mineral; beside this, it has not only magnetic properties but also electrical properties [47-49]. Moreover, magnetite has several curious applications such as magnetic storage media, printing inks, ferro-fluids and magnetic guided drug delivery [50].

Containing both ferrous (reduced) and ferric (oxidized) iron species, magnetite is oftentimes described as ironII,III oxide.

This naturally occurring magnetic compound clearly contains many interesting properties and potential for various applications [51].

### 2.3.3 Graphite

Carbon is the sixth element on the periodic table and can be found in abundance in the sun, stars, comets and atmospheres of most planets. Carbon is in three allotropic forms like as amorphous carbon, graphite and diamond.

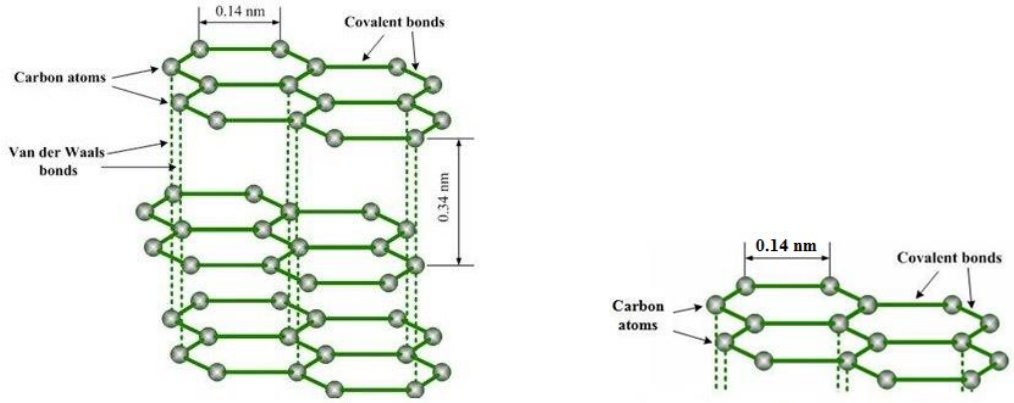


**Figure 2.10 :** The crystal structures of graphite [52].

Graphite structure arises a sequence of layers parallel to the basal plane of hexagonally connected carbon atoms. The ideal graphite structure is shown in Figure 2.10.

Graphite can be found in abundance and not high cost. It is widely used such as electronically conducting filler with the purpose of making conducting polymer composites [53].

### 2.3.4 Graphene

Graphene is an allotrope of carbon. It is one single layer of graphite. In other words, it has a layer of $sp^2$ bonded carbon atoms arranged in hexagonal lattice. Graphene offers extraordinary properties. These properties are lighter than steel by weight, heat and electrical conductivity and better mechanical properties than graphite. Because graphite is brittle but graphene is the strongest material.

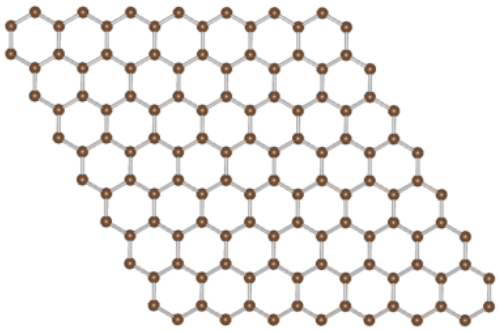

**Figure 2.11 :** The crystal structure of graphene [54].

### 2.3.5 Carbon nanotube (CNT)

Carbon nanotubes (CNTs) are also allotropes of carbon but it is a cylindrical nanostructure and well ordered. Their hexagonal arrangements of carbon atoms which have been rolled into tubes. It can said that the cylindrical graphite layer or layers [55].

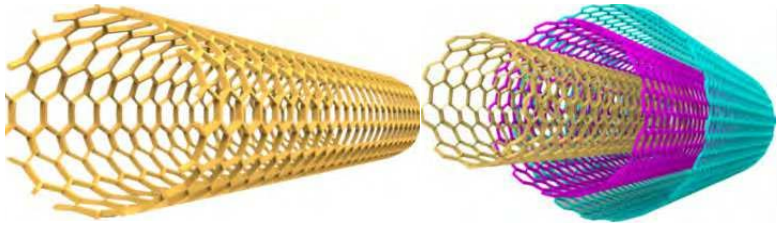

**Figure 2.12 :** The structure of carbon nanotube.

These cylindrical graphite layer have magnifique properties such as high thermal conductivity, good mechanical and electrical properties. Because of these extraordinary properties, it is used nanotechnology, electronics and materials science and technology fields.

### 2.3.6 Boron nitrite (BN)

Boron nitride is a chemical compound which their chemical formula BN. Their chemical structure consisting of equal numbers of nitrogen and boron atoms.

Boron nitride (BN) is an advanced engineering ceramic material, and it has used widespread attention with the development of high technology [56, 57].

It has a wide range of fascinating features such as thermal and chemical stability and high thermal conductivity, a low dielectric constant, good mechanical properties and corrosion and oxidation resistance, and thanks to these properties, it has high potential applications such as high-temperature ceramic applications, electronic material etc. [58, 59].

Boron nitrite exists in forms analogous both to diamond and to graphite, so that there has been much work [60, 61] on these structures.

## 2.4 Liquid Crystal

The liquid crystalline (LC) phase exhibiting the properties of both a crystalline solid and a liquid. The molecules in crystal are high orientational and positional order but

the molecules in a liquid are low positional order, this is the difference between crystal and liquids (Figure 2.13).

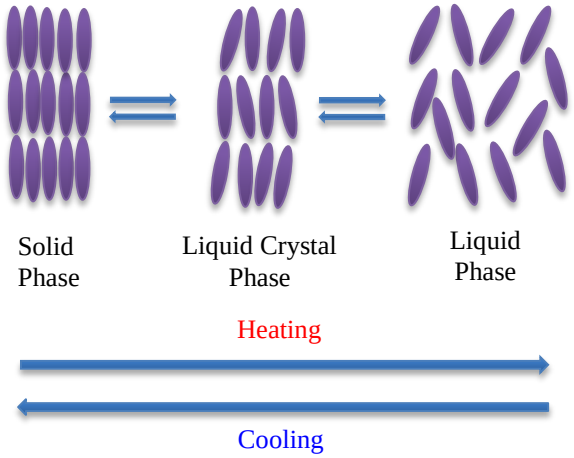


**Figure 2.13 :** Arrangements of molecules in crystal, in a liquid and in a liquid crystal.

When a molecular material which consists of anisotropic molecules is heated from the solid phase, at the melting point, there is the possibility that the positional order either fully or partially disappears while some degree of orientational order is protected. Therefore, this phase called as "liquid crystal" (LC).The other name used which means intermediate phase is mesophase or mesomorphic phase. A compound that exhibits a mesophase (mesomorphic phase) is called a mesogenic compound [62].

Transitions to the mesophases may be created in two different ways, which are thermal processes and the influence of solvation [62].

Thermotropic liquid crystal is the formation of liquid crystals phases obtained by temperature changes.

Lyotropics liquid crystal is the formed when a molecule is dissolved in a suitable solvent with spesific concentration at a particular temperature.

In a nematic phase (the term means "thread-like") the molecules are aligned in the same direction but are free to drift around randomly, very much as in an ordinary liquid. Owing to their polarity, the alignment of the rod-like molecules can be controlled by applying an electric field; this is the physical basis for liquid crystal displays and certain other electrooptic devices [63].

In smectic ("soap-like") phases, the molecules are arranged in layers, with the long molecular axes approximately perpendicular to the laminar planes. The only long-range order extends along this axis, with the result that individual layers can slip over each other (hence the "soap-like" nature) in a manner similar to that observed in graphite. Within a layer there is a certain amount of short-range order. There are a large number of sub-categories of smectic phases, which will not go into here [63].

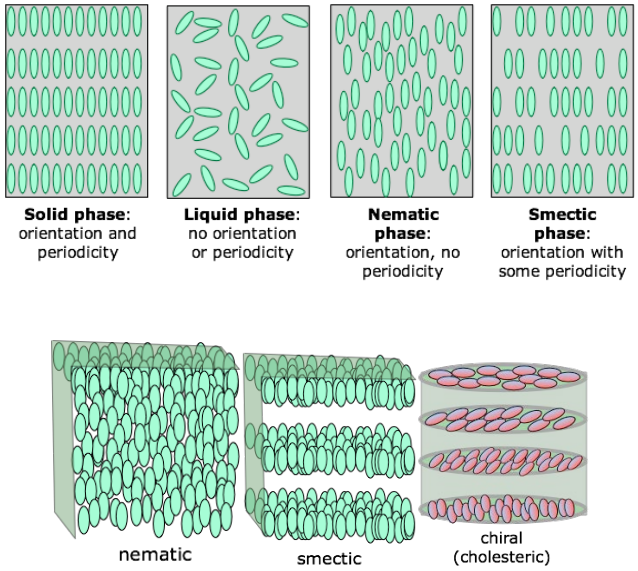


**Figure 2.14 :** Liquid crystal phases [63].

Chiral phases, special cases of nematic and smectic phases are sometimes formed by molecules that display chirality that is, they can exist in either left- or right-handed forms that cannot be superposed on each other. In the resulting chiral phase, successive molecules positioned along the long axis are rotated around this axis, giving rise to a periodicity that repeats itself at distances corresponding to a complete rotation. These twisted phases are able to rotate the plane of polarized light that passes along the axis. If the molecules are polar, this twisting can be turned off by imposing an external electric field at either end of the long axis. Besides the very important application of this property (known as ferroelectricity) to liquid crystal displays, these materials can be used to make electrooptic shutters which can be switched open and closed in microseconds [63].

## 2.5 Chalcone

Chalcone is a compound consists of two aromatic rings linked by an unsaturated α,β-ketone. They contain many various substituents on these aromatic rings. Chalcone

could be easily found in most of the plants naturally and is an intermediate precursor of flavonoids and isoflavonoids [64].

They are essential chemical compounds and studied widely owing to their varied application area. In the fields of biology and biochemistry, they have been suggested to have a vital role in treatment of some inflammatory diseases, such as malaria. They may also have some important antitumor activity. It has been documented as well, that the chalcone possesses a notable nonlinear optical (NLO) property, which is a crucial element for optical communications devices [65].

Pendant chalcone groups on polymers have similar properties such ad pendant cinnamate groups, which have been used as photosensitive polymers for their excellent resolving power, high flexibility, and respectable resistance to solvents after exposure and good thermal stability [66]. Polymers with chalcone or either in the backbone or side chain undergo crosslinking through [2π + 2π] cycloaddition of the carbon–carbon double bond upon irradiation with UV light and such polymers are regarded as negative-type photoresists. If polymer is less soluble in a solvent after exposure to UV, it is named negative photoresist [67]. The technological applications of photosensitive polymers are applied in the fields of microlithography, photoconductors, nonlinear optical materials, energy exchange materials, liquid crystalline display etc. [68].

These polymers are very significant in terms of commercial photoresist applications because of some remarkable properties such as high photosensitivity, the ability to form films, good solubility before irradiation, resistance to solvents and etching agents after crosslinking and good thermal stability [67].

### 2.6 Dielectrical Properties of Semiconducting Polymers

Dielectrical materials exist in nature as solid, liquid and gas. Each of them has specific molecular structure. Dielectric materials do not conduct electric current when an electric field is applied. However, they are affected by electrical field and on the effect of electrical field the electrons and atoms replace. The electrical field causes a slight shift in the balance of charge within the material to form an electrical dipole. These dipoles create electrical charge buildup and capacitive effect on surface of dielectric material.

Impedance Spectroscopy (IS) is shown that the materials are situated in which electromagnetic radiation depending on structure and use purposes. On the other

hand, Dielectric Spectroscopy (DS) informs that interactions of electrons, atoms, dipoles and self interfacial depending on frequency in terms of property of polarizable. Dielectric mechanism can be explain some parameters such as polarization, dielectric constant, dielectric strength, dielectric relaxation and dielectric relaxation time.

### 2.6.1 Dielectric constant

The complex impedance Z(ω) is commonly used to separate the surface and bulk material properties. The complex impedance and its complex conjugate of Z(ω) for express the sample,

$$Z(\omega)= Z'(\omega)+ i\, Z''(\omega) = R(\omega)+i\, X(\omega) \quad \textbf{(2.3a)}$$

$$Z^*(\omega)= Z'(\omega)- i\, Z''(\omega) = R(\omega)+i\, X(\omega) \quad \textbf{(2.3b)}$$

respectively. In this Eq. (2.3), ω is the angular frequency, Z(ω) and $Z^*(\omega)$ are the complex impedance and its complex conjugate, respectively. $Z'(\omega)$ and $Z''(\omega)$ are the real part, and the imaginary part of the complex impedance, respectively. R(ω) is the resistance and X (ω) is the reactance the response to an alternating current (AC). The magnitude of the complex conjugate impedance [69],

$$Z(\omega)\text{x } Z^*(\omega) = (Z'(\omega))^2 + (Z''(\omega))^2 \quad \textbf{(2.4)}$$

and the phase angle,

$$\theta=\tan^{-1}(Z''(\omega)/ Z'(\omega)) \quad \textbf{(2.5)}$$

include the complex impedance.

Alternative current (AC) measurements is one of the most effective techniques for electrical characterization of material which is known as impedance spectroscopy. Impedance consist of two parts which are real and imaginary. In the complex plane, the complex impedance for all materials can be explain as:

$$Z^*(\omega) = Z'(\omega) - Z''(\omega) = R_s - \frac{j}{\omega C_s}, \quad \textbf{(2.6)}$$

where $\omega$ angular frequency ($\omega = 2\pi f$), f is frequency, $Z'(\omega)$ the real part of impedance, $Z''(\omega)$ the imaginary part of impedance, $R_S$ serial real resistivty and $C_s$ serial capacitance.

Real part of dielectric permittivity can be calculated from capacitance value of dielectric material between two electrodes. Basically, this calculation is related with capacitance value of air layer ($C_0$) and capacitance value of dielectric material [69] ($C_p$) (Figure 2.15).

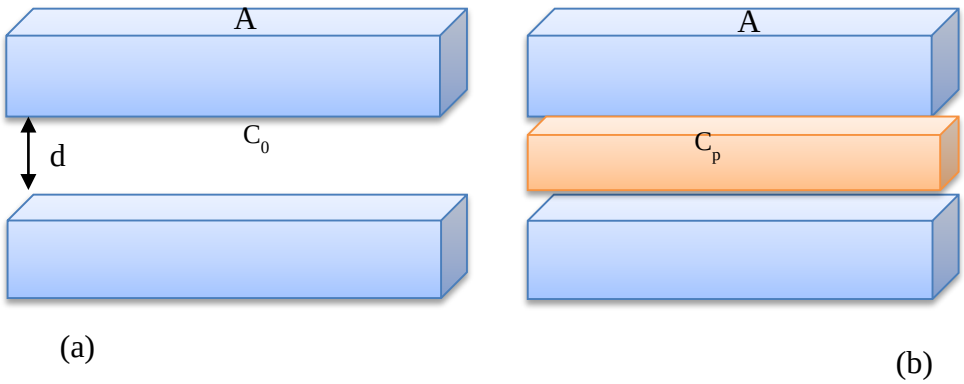


**Figure 2.15 :** Empty (a) and full (b) capacitors of two electrolyte system [1].

capacitance value of air layer ($C_0$) is

$$C_0 = \varepsilon_0 \frac{A}{d}, \quad \textbf{(2.7)}$$

where $\varepsilon_0$ is permittivity of free space

$$\varepsilon_0 = 8.8542 \times 10^{-12} F/m$$

$$\varepsilon_0 = \frac{1}{c^2 \mu_0} \quad \textbf{(2.8)}$$

where c speed of light, $\mu_0$ is permeability of free space, d is distance between electrodes, and A is surface area of electrode. Real dielectric constant $\varepsilon'(\omega)$ is variable depending on angular frequency and $\varepsilon'(\omega)$ is [69]

$$\varepsilon'(\omega) = \frac{C_p}{C_0} \quad \textbf{(2.9)}$$

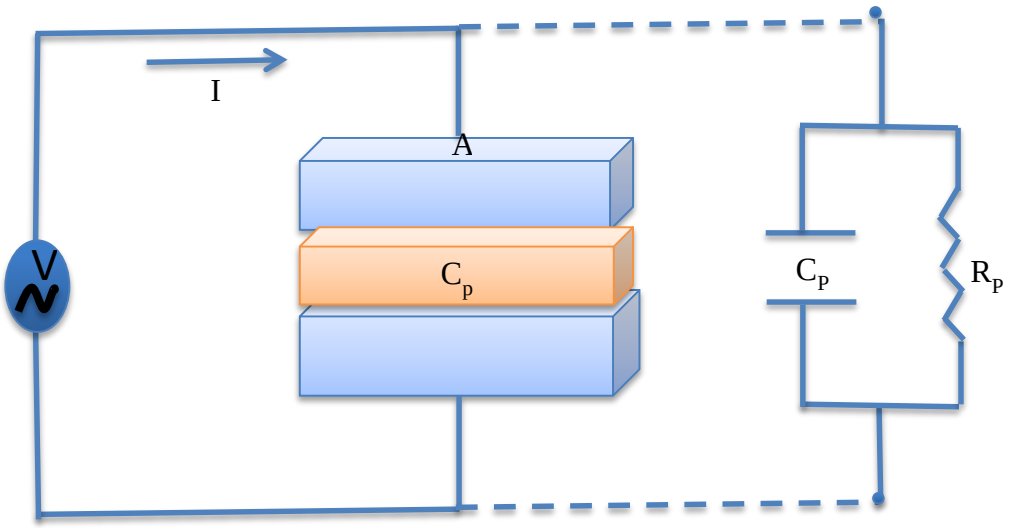


**Figure 2.16 :** Two electrodes system with dielectric material with $R_P$ and $C_P$ parallel equivalent circuit with AC supply [69].

The complex dielectric constant $\varepsilon$ is expressed in terms of the real $\varepsilon'$ and imaginary $\varepsilon''$ components, which represents the stored and dissipated energy components of the material, respectively. The dielectric constant is expressed as [70],

$$\varepsilon(\omega) = \varepsilon'(\omega) + i\varepsilon''(\omega) \quad \textbf{(2.10)}$$

The real part of the dielectric constant $\varepsilon'$ of a material is the normalized permittivity with respect to the permittivity of vacuum. It is also a measure of the amount of polarization in a material according to [71] and can be indirectly calculated from the following equation using the capacitance data and if it is applied alternative current to this geometric structure as Figure 2.16, the real dielectric constant is

$$\varepsilon' = C_p d/(\varepsilon_0 A) \quad \textbf{(2.11)}$$

where *Cp* is the parallel capacitance, *d* is the inter electrode distance, $\varepsilon_0$ is the permittivity of the free space and *A* is the sample area.

Imaginer dielectric constant is

$$\varepsilon'' = \frac{1}{R_p \omega C_0} \quad \textbf{(2.12)}$$

The tan δ is given by

$$tan\delta = \frac{\varepsilon''}{\varepsilon'} \quad \textbf{(2.13)}$$

where $\delta = 90 - \varphi$ and $\varphi$ is the phase angle. Dissipation factor (tan δ) is also a typical dielectric parameter.

Complex adding function of real and imaginary part of dielectric material is

$$\varepsilon^*(\omega) = \varepsilon'(\omega) - j\varepsilon''(\omega) = \frac{-j}{2\pi f Z^*(\omega) C_0} \quad \textbf{(2.14)}$$

and this equation is called as dielectric function.

### 2.6.2 Polarization

The creation of an electrical dipole is called polarization. The dielectric properties have a wide spectrum of interaction according to studied the range of the frequency. There are several contributions to polarization: electronic polarization; dipolar (orientation) polarization; atomic polarization; electronic polarization. Thanks to this spectrum, it is understood that how a polarization mechanism depending on structure feature of dielectrical material (Figure 2.17).

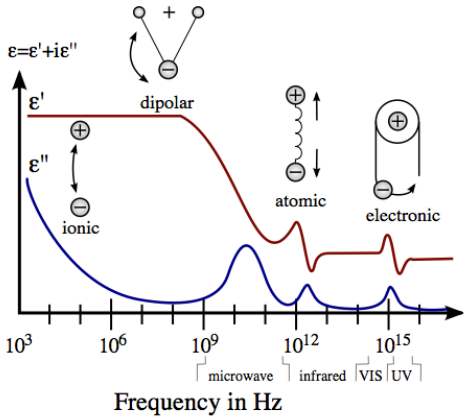


**Figure 2.17 :** A dielectric permittivity spectrum over a wide range of frequencies [107].

$\varepsilon$ (dielectric coefficient) informs that the polarizability of a material. Degree of polarizability is releated to density and size of dipoles which are accumulating in the material and oriented via external electrical field. Evidently, the greater the polarizability of the dielectric, the higher the dielectric coefficient.

Generally, dielectric coefficient decreases with an increase of the frequency and dielectric coefficient remains constant at high frequencies.

#### 2.6.2.1 The Types of dielectric mechanisms

Polarization can be derived from four different polarization mechanisms for a dielectric material. Electronic (or atomic) polarization occurs in all dielectric materials. The electrons surrounding each nucleus are shifted very slightly in the

direction of the positive electrode. As soon as the electric field is removed, the electrons and nuclei return to their original distributions and the polarization disappears. Contribution of electronic polarization to dielectric coefficient are always very low values (Figure 2.18).

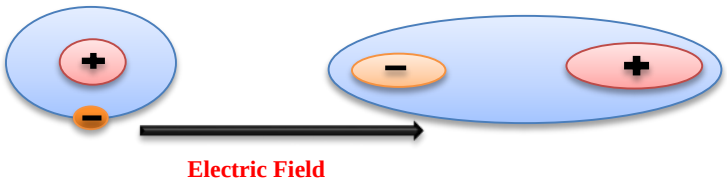


**Figure 2.18 :** Electronic Polarization.

Second polarization mechanism is ionic polarization which involves displacement of atoms or ions within a crystal structure when an electrical field is applied (Figure 2.19). This type of polarization typically occurs in ionic crystal elements such as NaCl, KCl, and LiBr. Third polarization of dielectric materials is orientation (dipolar) polarization. Orientation polarization contains nosymmetrical molecules. Nosymmetrical molecules have permanent electric dipoles. When there is a permanent dipole moment in the material, orientational polarization occurs. Materials have permanent dipole moment such as HCl and $H_2O$ and because of the charge distributions of these molecules are skewed, they will have a net permanent dipole moment. For instance, it is taken for a molecule of HCl, the chlorine atom will be net negative charge and the hydrogen atoms will be net positive charged because of the structure of dipolar molecule. The dipolar nature of the molecule should cause a dipole moment in the material, Under an electric field, however, the molecule will begin to rotate in order to align the molecule with the field, causing a net average dipole moment per molecule (Figure 2.19). However, in the absence of an electric field, the dipole moment is equilibrated by thermal agitation resulting in a net zero dipole moment per molecule (Figure 2.20).

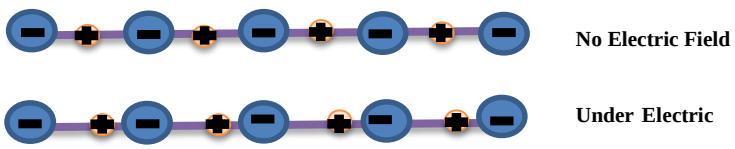


**Figure 2.19 :** The effect of an external electric field on an ionic material. The positive charges will flow with the field and the negative charges will flow against [72].

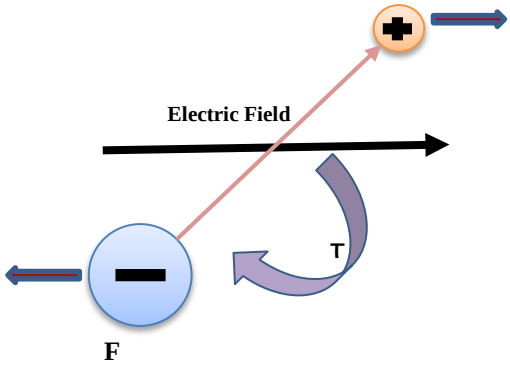


**Figure 2.20 :** The effect of an electric field on a typical dipolar molecule [72].

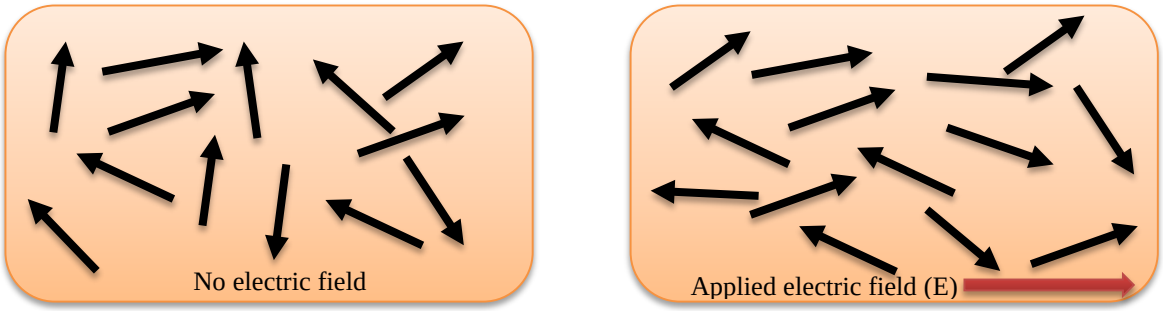


**Figure 2.21 :** The figure shows how thermally agitated molecules (left) can be made to produce a net dipole moment per ion in the material with an externally applied field (right) [72].

Another source of polarization is space charge (interfacial) polarization. It arises when there is a charge accumulation at an interface between two regions within a dielectric material because of an external field (Figure 2.22). Space charge polarization affects free charges and it is usually observed in amorphous or polycrystalline solids.

The total polarization (P) is the sum of all contributions from the various types of polarization:

$$\sum P = P_e + P_i + P_o + P_{sc} \qquad \textbf{(2.15)}$$

where $P_e$ is electronic polarization, $P_i$ is ionic polarization, $P_o$ is orientation polarization, $P_{sc}$ is space charge polarization.

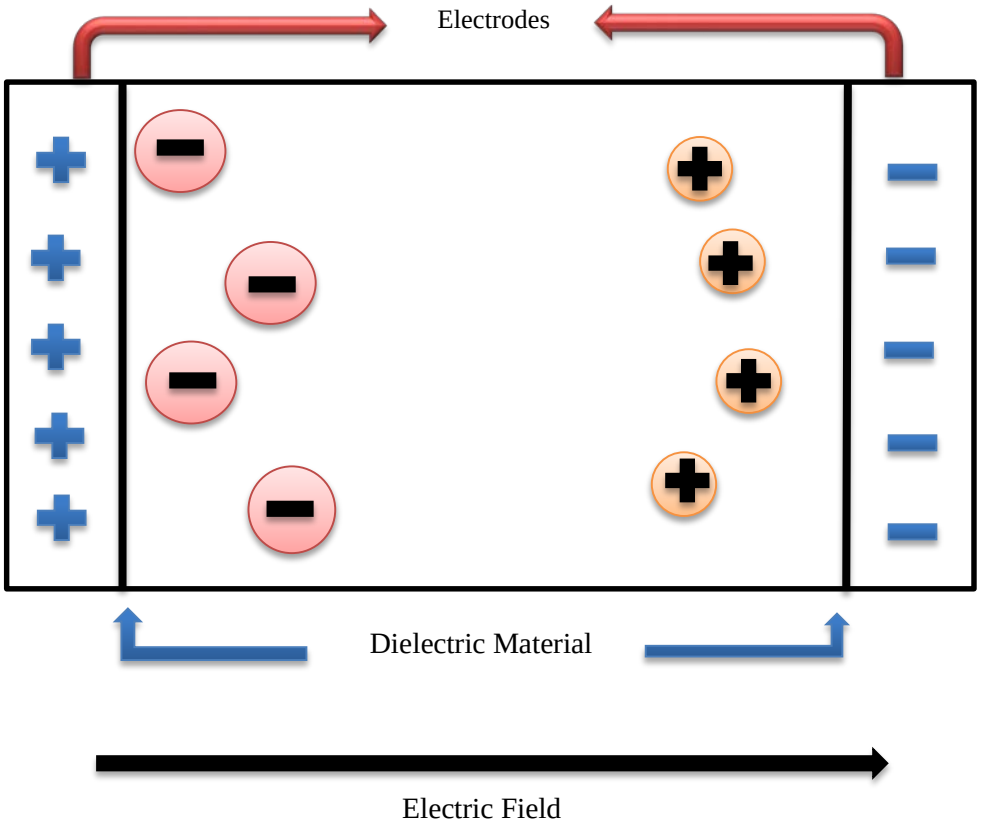


**Figure 2.22 :** Schematic of interfacial polarization [72].

### 2.6.3 Dielectric strength

Dielectric Strength is important dielectric property and which is the maximum electric field strength that it can withstand intrinsically without breaking down and allowing electrical current to pass [69].

If $\varepsilon_0'$ is the value at low frequency and $\varepsilon_s'$ is the value at high frequency;

Dielectric strength ($\Delta\varepsilon_{reel}'$) is

$$\Delta\varepsilon_{reel}' = \varepsilon_0' - \varepsilon_s' \qquad \textbf{(2.16)}$$

Thanks to this value; it is understood how much dielectric value hold in a material. Because this difference is only observed for dielectric materials.

Figure 2.23 is shown that real and imaginary parts of dielectric materials, which depend on angular frequency at semi-logarithmic scale.

This graph changes inform real dielectric components corresponding to the static value of materials, $\varepsilon_0'$ value in the low frequencies and $\varepsilon_s'$ value in the high frequencies.

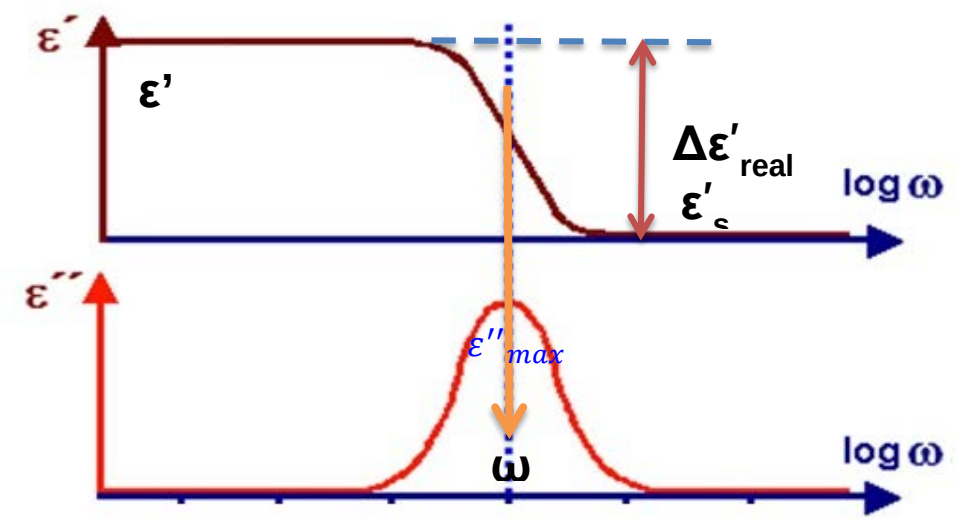


**Figure 2.23 :** Dielectric spectrum components based on frequency ($\varepsilon'$ and $\varepsilon''$ vs log ω).

Loss of energy level of materials corresponding to $\varepsilon''$, which represents the imaginary dielectric component. Two important parameters are determined for the materials from these changes. These are dielectric strength ($\Delta\varepsilon'_{reel}$) and dielectric relaxation time ($\tau$) [69].

### 2.6.4 Dielectric relaxation and dielectric relaxation time

It is a matter of polar orientation depends on internal structure of molecules and structure of dielectric molecules or molecular order. Relaxation time ($\tau$) is a measure of molecular movement. In other words, relaxation time can be expressed as a period of time as a result of making changes in the electric field to make the orientation of the dipole in that period. Relaxation frequency refers to the resonant frequency of the material. When the frequency of the electric field is smaller than the relaxation frequency, polarization is easily formed and it follows electric field. In this case the level of dielectric losses are negligible. If it is reached relaxation region as increasing frequency, polarization are forced to comply with the electric field and phase difference increases. In this case the losses are maximum. If it is continues to increase frequency, polarization does not occur and dielectric constant rapidly decreases. Dielectric loss does not occur in the absence of dielectric polarization. [69]

Critical frequency $(f_c)$ is the first max value of imaginary dielectric constant. The maximum angular relaxation time in the microwave region for materials is $\omega_{max}$ and also capacitance and resistance are $(C_P)$ and $(R_P)$, respectively

$$\omega_{max}.\tau = \omega_{max}.R_P.C_P = 1 \quad \textbf{(2.17)}$$

It varies proportionally with the value of 1. From this equation, it can be derived

$$2\pi f_c R_P C_P = 1 \quad \textbf{(2.18)}$$

Critical frequency value, parallel resistance and capacitance value of known materials are determined by critical frequency $(f_c)$;

$$f_c = \frac{1}{2\pi R_P C_P} \quad \textbf{(2.19)}$$

Dielectric relaxation time;

$$\tau = \frac{1}{2\pi f_c} = R_P.C_P \quad \textbf{(2.20)}$$

### 2.6.5 Complex dielectric constant

It was described equation which shows the complex dielectric constant related to frequency by Debye. The real $\varepsilon'(\omega)$ and the imaginary $\varepsilon''(\omega)$ parts of the complex dielectric constant is described as $\varepsilon^*(\omega)=\varepsilon'(\omega)-i\varepsilon''(\omega)$. The real $\varepsilon'(\omega)$ part of the dielectric constant is described as [76];

$$\varepsilon'(\omega) = \varepsilon_\infty + (\varepsilon_s - \varepsilon_\infty)\frac{1+(\omega\tau_o)^{1-\alpha}\sin\frac{1}{2}\alpha\pi}{1+2(\omega\tau_o)^{1-\alpha}\sin\frac{1}{2}\alpha\pi+(\omega\tau_o)^{2(1-\alpha)}} \quad \textbf{(2.21)}$$

$$\varepsilon''(\omega) = (\varepsilon_s - \varepsilon_\infty)\frac{(\omega\tau_o)^{1-\alpha}\cos\frac{1}{2}\alpha\pi}{1+2(\omega\tau_o)^{1-\alpha}\sin\frac{1}{2}\alpha\pi+(\omega\tau_o)^{2(1-\alpha)}} \quad \textbf{(2.22)}$$

Here, $\varepsilon_\infty$, $\varepsilon_s$ are high and low angular frequency dielectric constant, $\omega=2\pi$ times the frequency, and $\tau_0$ is a generalized relaxation time. The parameter $\alpha$ absorption coefficient changes from zero to one ($0 < \alpha \leq 1$). If $\alpha=0$, it corresponds to standard Debye type relaxation [76]. They are values different from zero and very close to zero as they are non-Debye type and nearly-Debye type relaxation, respectively [76]. The absorption parameter calculated from the Eq. (2.21).

The dielectric dispersion curves are described by the Cole-Cole relation [75],

$$\varepsilon^*(\omega) = \varepsilon_\infty + \frac{\varepsilon_s - \varepsilon_\infty}{1 + (i\omega\tau_o)^{1-\alpha}} \quad \textbf{(2.23)}$$

where $\varepsilon^*(\omega)$ is the complex dielectric constant, $\varepsilon_s$ is the limiting low-frequency dielectric constant and $\varepsilon_\infty$ the limiting high-frequency dielectric constant, $\tau_0$ is the average relaxation time, $\omega$ is the average angular frequency, $\alpha$ is the distribution parameter.

The dielectric strength $(\Delta\varepsilon)=\varepsilon_s - \varepsilon_\infty$, and all parameters except $\tau$ have been designated. $\tau$ is the characteristic or principal relaxation time, $\alpha$ $(0<\alpha<1)$ is an empirical parameter which is related to the width of the relaxation peak, and $\omega$ is the angular frequency. If the center of the semicircles lie $\varepsilon'$ axis, $\alpha$ is zero (Debye type) [75]. The relaxation phenomenon is analyzed by Cole-Cole plots. The plots indicate semi-circles and are passing through the origin. The center lies is located on the real axis which is explained by Debye type properties.

For a mono-dispersive relaxation process, one expects the circle center is located exactly on the $\varepsilon'$-axis, whereas for a poly-dispersive process, the circle center will be located below the $\varepsilon'$-axis. It is evident from these plots that the relaxation process differs from the mono-dispersive Debye type process (for which $\alpha = 0$) [75], and poly-dispersive situation non-Debye type process (for which $\alpha \neq 0$). The plots obey Cole-Cole type dispersion with a distribution of relaxation times.

### 2.6.6 Complex conductivity

The response of a conducting sample to an alternative current (AC) electrical field can be defined by the complex conductivity, $\sigma_{AC}(\omega)=\sigma'(\omega)+i\sigma''(\omega)$. Here, $\sigma'(\omega)$ and $\sigma''(\omega)$ are expressed as the real and the imaginary parts of the complex conductivity.

The AC conductivity dependence of frequency can be expressed by the following relation, as the empirical Jonscher's universal law [73,74],

$$\sigma_{AC}(\omega)=A\,\omega^s \quad \textbf{(2.24)}$$

where, A is a constant, $\omega$ is the angular frequency and s is the frequency exponent parameter which determines AC conduction with the value in the range of $0<s<1$. The values of angular frequency exponent s were calculated from the slope of the

logarithmic conductivity as a function of logarithmic angular frequency curve. It is obey the electrical conduction mechanism. In the Correlated barrier hopping (CBH) and Quantum mechanical tunneling (QMT) models, the frequency exponent s is ranged from 0.7–1 [73].

An equivalent series electrical impedance Z of Eq. (2.25) is written in the complex formulation as [73];

$$Z = Rs - j(\omega C_s)^{-1} \quad \textbf{(2.25)}$$

In this expression, $R_s$, and $C_s$, represent the series resistance and capacitance, respectively. The real and imaginary part of electrical impedance parameters are correlated by the Kramers–Kronig relations. Real part of impedance (Resistance) parameters expressed by the equivalent series resistance corresponding to Eq. (2.26) is a series resistance; Rs, angular frequency dependent as [73].

$$R_s = \sigma . \omega^{-1/2} \quad \textbf{(2.26)}$$

According to Kramers–Kronig relations AC conductivity studies the variation of Rs with angular frequency of ω. The Kramers–Kronig relations are the most suitable model [73].

The critical transition frequencies ω values were measured from the derivative of the measured the logarithm of the conductivity as a function the logarithm of the (angular) frequency ω.

### 2.6.7 Surface resistivity

Resistivity (ρ) relates to the material's electric properties. Resistivity is a characteristic of material and is not dependent on the dimensions of the measured material sample.

Four-point probe technique was employed during the in-plane conductivity measurements. The slope of (V-I ) plot gives the surface resistivity in Ohm-centimeter, when it is employed $\pi / \ln 2 = 4.5324$ coefficient.

The theory of measuring surface resistivity applies the formula,

$$\rho_s = 4.5324 (V/I). \quad \textbf{(2.27)}$$

ρs is the ohm-centimeter, V is the volts and I is the ampere. Linear increase in the V-I graph is fitted and surface resistivity is acquired from this fit. It is calculated slope and this calculated slope value gives surface resistivity values [45].

### 2.6.8 Electron paramagnetic resonance (EPR)

Electron Paramagnetic Resonance (EPR), also known as Electron Spin Resonance (ESR). The sample is held in a very strong magnetic field, while electromagnetic (EM) radiation is applied monochromatically in Figure 2.24 [108].It has widespread use in chemistry, biochemistry and physics applications.

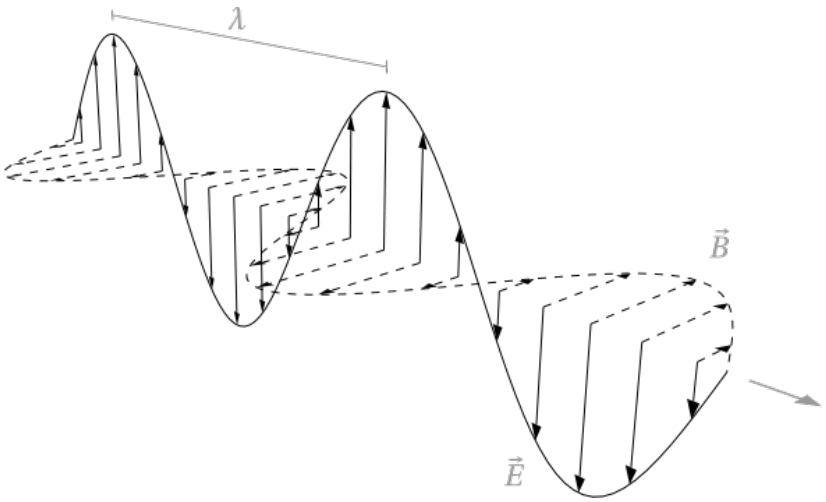


**Figure 2.24 :** Monochromatic electromagnetic beam [108].

This portion of EPR is analogous to simple spectroscopy, where absorbance by the sample of a single or range of wavelengths of EM radiation is monitored by the end user ie absorbance. The unpaired electrons can either occupy +1/2 or -1/2 $m_s$ value in Figure 2.25. From here either the magnetic field "$B_0$" is varied or the incident light is varied. Today most researchers adjust the EM radiation in the microwave region, the theory is the find the exact point where the electrons can jump from the less energetic $m_s$=-1/2 to $m_s$=+1/2. More electrons occupy the lower $m_s$ value [108].

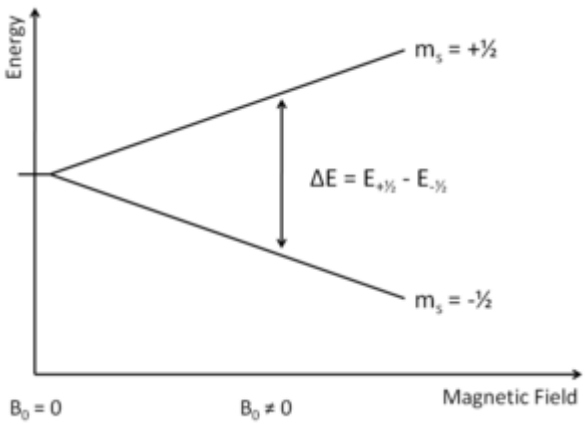


**Figure 2.25 :** Resonance of a free electron [108].

Overall, there is an absorption of energy. This absorbance value, when paired with the associated wavelength can be used in the equation to generate a graph of showing how absorption relates to frequency or magnetic field.

Electrons possess a property called “spin” (s), resulting in an angular momentum. Because the electron is charged, there is associated with the angular momentum a magnetic moment which points in the opposite direction to the angular momentum vector. In an external magnetic field, the spin precesses around the field direction at the Larmor frequency and thus a component of the magnetic moment is either parallel or anti-parallel to the field direction. If a microwave field of this frequency is applied to a spin containing sample, then the spins can change their direction relative to the magnetic field. This results in absorption of the microwave field, which may be measured. The energy of the transition will be affected by the local environment of the spins. Thus, EPR spectra can yield information about the structure and composition of a sample [109].

$$\Delta E = h\gamma = g\beta B_r \qquad \textbf{(2.28)}$$

g-factor was calculated from resonance conditions as seen in follows

$$g = \frac{h\gamma}{\beta B_r} \qquad \textbf{(2.29)}$$

where h is Planck constant, $\gamma$ the microwave frequency, $\beta$ the Bohr magnetron and $B_r$ is the resonance magnetic field.

# 3. EXPERIMENTAL PART

## 3.1 Materials

Aniline (99%, Aldrich), Ammonium persulfate (Fluka), Graphite (Aldrich), Boric acid (Fluka), 3-aminoacetophenon(Aldrich), 4-Pyridinecarboxaldehyde (Aldrich), Methanesulfonic acid(Fluka), Formic acid (Aldrich), Acetic acid (Aldrich), Propiolic acid (Aldrich), N-vinylcarbazole(Aldrich), 2-(Dimethylamino)ethylmethacrylate (Aldrich), Azobisisobutyronitrile (AIBN), NanoClay (Aldrich, particle size <25 μm, Graphite (GH) (Aldrich), Boron nitrite (BN) powder (Aldrich), $FeCl_2.4H_2O$ (Aldrich), $FeCl_3.6H_2O$ (Aldrich) and all the other chemicals were of analytical grade.

## 3.2 Instruments

FT-IR (Nicholet), Polarized Optical Microscope (POM) (Leica), H-NMR (Agilent VNMRS 500MHz), Scanning electron microscopy (FE-SEM) (FEI Quanta 250 FEG), DSC (Perkin Elmer), XRD, HP 4194A Impedance Analyzer, GPC (Viscotek, GPCmax)

## 3.3 Preparation of Doped PANI and Derivative and Investigation of Electrical Properties

### 3.3.1 Preparation of propiolic acid doped polyaniline

1.0 g of aniline and 0.75 g propiolic acid were added into 50 mL of water. To this solution, a 50 ml aqueous solution containing 3.0 g of ammonium persulfate was added dropwise (15–20 min. interval) at 0 °C. The reaction mixture was kept for 24 h at room temperature. The reaction mixture was filtered, washed with excess of water, and finally with ethanol. The sample was dried at room temperature under vacuum until constant weight was reached.

### 3.3.2 Preparation and polymerization of chalcone substituted aniline monomer

3-aminoacetophenone was reacted with aldehyde derivatives (pyridine aldehyde) to obtain chalcone substituted aniline derivative. Into a three-necked 500 mL flask equipped with magnetic stirring 1.35 g (0.01 mol) of 3-aminoacetophenone (0.1 mol) dissolved in 20 mL of ethanol and 0.048 g of NaOH (0.012 mol) dissolved in 5 mL of distilled water were placed. Then 1.07 g (0.01 mol) 4-pyridine carboxyldehyde in 20 mL ethanol was added dropwise at 10 $^{o}$C for 1 h. The mixture was stirred for 12 h at room temperature. The precipitated solid product was filtered, washed with excess of ice cold water, dried and recrystallized from ethanol to get yellow crystals. The monomer was dried under vacuum at room temperature.

#### 3.3.2.1 Polymerization of the monomer

This monomer (0.005 mol) was dissolved in 20 mL of ether and equivalen tamount of HBr in 10mLof ether was added to this mixture. Precipitated white product was filtered and dried under vacuum. The HBr salt of the monomer was dissolved in 50 mL of water and equivalent amount of ammonium persulfate in 50 mL of water as an initiator was added to the reaction mixture. Polymerization was performed at room temperature for 24 h. The black product was filtered and washed with excess of water and ethanol.

### 3.4 Preparation of PANI and Poly(thiophene) Composites

In this study, composites of PANI and polythiophene were prepared by using graphite, nano clay, magnetite and BN.

Spectroscopic characterization of the monomer and polymer by using FT-IR and H-NMR. Also, electrical characterization of the polymer was studied.

### 3.4.1 Preparation and electrical characterization of PANI-nano clay (NC) composites

Different weight percentage of nano clay (1%, 2%, 5%, 10% and 20%) in 20 mL of water were placed into ultrasonic bath at room temperature and sonicated for 5 h.

Then 1 g of aniline and 1 M of boric acid were dissolved. in 50 mL of water. This mixture was added into nano clay (NC) mixture. This solution was placed in an ice-bath and a 30 mL aqueous solution containing 2.42 g of ammonium persulfate was

added dropwise (15–20 min. interval) at 0 °C. The reaction mixture was kept for 24 h at room temperature.

The reaction mixture was filtered, washed with excess of water, and finally with ethanol. The sample was dried at room temperature under vacuum until constant weight was reached. Characterizations of the PANI-NC composites were investigated by FT-IR, SEM, XRD, and conductivity measurements.

### 3.4.2 Preparation and electrical characterization of PANI-Graphite (GH) composites

In this study, GH and PANI were prepared by using oxidative polymerization of aniline in the presence of different weight percentage of GH (2%, 5% and 10%). Different weight percentage of GH (2%, 5% and 10%) in 20 mL of water were placed into ultrasonic bath at room temperature and sonicated for 5 h. Then 1 g of aniline and 1 M of boric acid were dissolved in 50 mL of water. This mixture was added into GH mixture. This solution was placed in an ice-bath and a 30 mL aqueous solution containing 2.42 g of ammonium persulfate was added drop wise (15–20 min interval) at at 0°C. The reaction mixture was kept for 24 h at room temperature. The reaction mixture was filtered, washed with excess of water, and finally with ethanol. The sample was dried at room temperature under vacuum until constant weight was reached. The PANI doped GHs samples were characterized with impedance spectroscopy to determine their electrical parameters.

FT-IR measurements were recorded in the range of 400–4000 $cm^{-1}$ (KBr pellets) using a Perkin Elmer FT-IR Spectrometer. FEI Quanta 250 FEG scanning electron microscopy (FE-SEM) was used to observe the morphology of the PANI doped GHs composites. A HP 4194A Impedance Analyzer was employed for the IS measurements. The root mean square (RMS) amplitude of the signal was set to ~500 mV and the impedance parameters were measured at frequencies between 10 kHz and 15 MHz. Alternative current (AC) electric properties were analyzed from the impedance and dielectric values.

### 3.4.3 Structural, magnetical and electrical properties of magnetite doped polyaniline

#### 3.4.3.1 Synthesis of magnetite

The magnetic nanoparticles were synthesized by mixing a water solution of $FeCl_2.4H_2O$ (1.0 M) and $FeCl_3.6H_2O$ (1.5 M). The above mixture was poured in aqueous ammonium solution and the resulting solution was stirred for 3 h. Magnetite particles are precipitated out, filtered and thoroughly washed with excess distilled water.

#### 3.4.3.2 Preperation and characterization of poly (aniline)-magnetite composites

Composites of poly (aniline) and magnetite were prepared by using oxidative polymerization of aniline in the presence of different weight percentage of magnetite (2%, 5% and 10%). Different weight percentage of magnetite (2%, 5% and 10%) in 20 mL of water were placed into ultrasonic bath at room temperature and sonicated for 5 h. Then 1 g of aniline and 1 M of boric acid were dissolved in 50 mL of water. This mixture was added into magnetite containing mixture. This solution was placed in an ice-bath and a 30 ml aqueous solution containing 2.42 g of ammonium persulfate was added drop wise (15–20 min. interval) at 0°C. The reaction mixture was kept for 24 h at room temperature. The reaction mixture was filtered, washed with excess of water, and finally with ethanol. The sample was dried at room temperature under vacuum until constant weight was reached.

Characterization of PANI-Magnetite composites were recorded by Fourier transform infrared spectroscopy (FTIR) in the range of 400-4000 $cm^{-1}$ using Perkin Elmer FTIR Spectrometer. Field emission scanning electron microscope (FEI-Quanta FEG 250) was used to analysed the microstructure of the samples. The Powder EPR spectrum was recorded with a Bruker EMX X-band spectrometer (9.8 GHz) with 100 kHz magnetic field modulation. Dielectric measurements have been performed by using HP4194A impedance analyzer in frequency the range of 100Hz-10MHz. All measurements were performed at room temperature.

### 3.4.4 Preparation and characterization of Poly(thiophene)-Boron Nitride (BN) composites

Different weight percentage of boron nitride (BN) (1% and 2%) and thiophene were placed into 20 mL of chloroform and chemical polymerization was performed by using $FeCl_3$ as oxidant at room temperature for 48 h.

The Poly(thiophene) (TP) doped BNs samples were characterized with impedance spectroscopy to determine their electrical parameters. FT-IR measurements were recorded in the range of 400–4000 $cm^{-1}$ (KBr pellets) using a Perkin Elmer FTIR Spectrometer. FEI Quanta 250 FEG scanning electron microscopy (FE-SEM) was used to observe the morphology of the Poly(thiophene) (TP) doped BNs composites.A HP 4194A Impedance Analyzer was employed for the IS measurements. The root mean square (RMS) amplitude of the signal was set to ~500 mV and the impedance parameters were measured at logarithmic frequencies between 100 and 1M Hz. Alternative current (AC) electric properties were analyzed from the impedance and dielectric values.

## 3.5 Preparation of The Side Chain Hydrogen Bonded Liquid Crystalline Poly(N-vinylcarbazole)(NVC)-co-poly(2-(dimethylamino) ethylmethacrylate) (DMAEM)

### 3.5.1 Preparation of poly(N-vinylcarbazole)(NVC)-co-poly(2-(dimethylamino) ethylmethacrylate) (DMAEM)

Copolymers containing different (NVC) ratios (1%, 20% and 30 %NVC as mole) were prepared. Typical reaction procedure was given:

0.58 g (NVC) (3.0 mmol), 1.2 mL (7.12 mmol) of 2-(Dimethylamino) ethylmethacrylate and 2 mL of NMP as a solvent were placed into a three-necked 50mL flask equipped with magnetic stirring 0.01 g of AIBN in 1 mL of NMP was added to the mixture under $N_2$. Copolymerization reaction was performed at 70 $^oC$ for 10h. After reaction, highly viscous mixture was diluted with THF. The obtained copolymer was precipitated in cyclohexane. Homopolymerization of the 2-(Dimethylamino) ethylmethacrylate was also carried out in the same conditions. Characterizations of the copolymers were performed by spectroscopic methods by using FT-IR and H-NMR. Amine content of the copolymer was also determined by

using analytical methods. Molecular weights of the homopolymer and copolymers weredetermined by using GPC.

### 3.5.2 Synthesis of 8-(4-cyanobiphenyl-4'-oxy) octan-1-ol (LC8) as a mesogen

3 g (15 mmol) of 4'-hydroxy-4-biphenylcarbonitrile was in 200 mL of DMSO in the presence of 2 g (14.5 mmol ) of $K_2CO_3$ anhydrous as acid scavenger. 3.4 mL of ( 20 mmol) 8-chloro-1-octanol was added drop wise to a stirring mixture under nitrogen at 110 °C. The reaction mixture was heated at 110 °C for 3 hours. After this process, the reaction mixture was added drop wise to 400 mL of 10 % NaOH solution at room temperature and filtered. The resultant was dried at 40 °C in vacuum. It was re-crystallized from ethanol. White crystalline product was obtained and dried under vacuum (Yield: 52 %).

### 3.5.3 Preparation of the hydrogen bonded side-chain liquid crystal copolymer (HB-PLC)

The evaporation technique was used for preparing hydrogen bonded side chainliquid crystalline polymer. For this purpose, (LC8) as an H bond donor and (DMAEM) based homopolymer and copolymers as an H bond acceptor polymer are dissolved in the dimethylformamid (DMF). Slow solvent evaporation at room temperature causes phase separation of the HB-PLC.The resulting solid was dried undervacuum for 24 h.

### 3.5.4 Cell preparations

Before the construction of the cells, indiumtinoxide (ITO) covered glass Windows were treated with polyvinyl alcohol for planar alignment. Measurement cells were made up of two glass slides separated by Mylarsheetshaving ~5µm thicknesses. These cells were filled in capillary action with the samples at room temperature. The material was 8-(4-cyanobiphenyl-4'-oxy) octan-1-ol (LC8) and LC8+1%HB-PLC.LC8 was dissolved in DMMA and two samples were prepared; one of them contains pure LC8, the another one was filled with LC8+1%HB-PLC(w/w).

# 4. RESULTS AND DISCUSSION

## 4.1 Investigation of Electrical Properties of Doped PANI and Derivative

### 4.1.1 Investigation of dielectric properties of propiolic acid doped polyaniline

Aniline was polymerized in the presence of propiolic acid as dopant and ammonium persulfate as oxidant. The reaction mechanism was depicted in Figure 4.1.

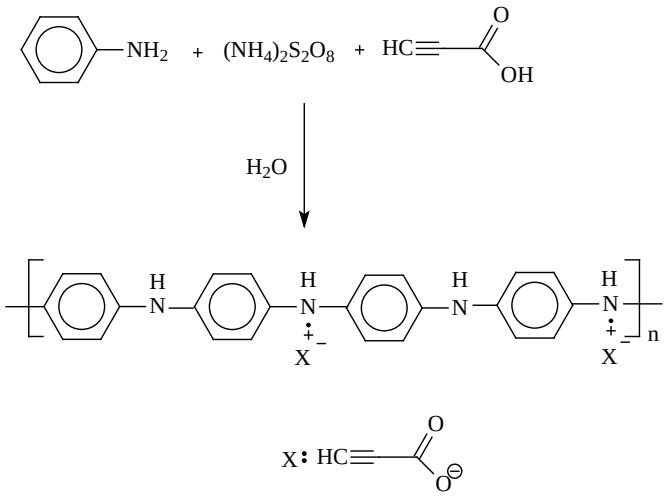


**Figure 4.1 :** Preparation of propiolic acid doped polyaniline.

The obtained polyaniline (PANI) was characterized by using chemical and physical methods as described below.

#### 4.1.1.1 Dielectric measurements

Alternative current (AC) impedance parameters; conductivity, dielectric constant, dissipation factor and impedance properties were analyzed from the parallel plate capacitor materials. The diameter and thickness of samples were measured by using the Mitutoyo micrometer. HP4194A Impedance.

Analyzer from Agilent was utilized during the measurements. The complex dielectric response of the PANI and doped PANI materials were considered at logarithmic frequencies between 100 and 15 M Hz. The Novotherm Temperature Control System (NTCS) of Novocontrol Technologies GmbH is enabled the monitoring of the

temperature in the 25 to 100 ºC range with an accuracy > 0.1 ºC. The temperature and frequency dependence of the real part of the impedance parameters was recorded by the automated WinDeta Novocontrol Software. The RMS amplitude of the device is ~500 mV.

### 4.1.1.2 Spectroscopic characterization of the PANI

There is no detectable splitting in PANI bands after doping. So the observed bands correspond to PANI absorptions only with a small shifts of some in FT-IR peaks of PANI. This indicates to the acids doping reactions occurred at the quinoid units in the polyaniline molecular chains while the benzoid units remained essentially unaffected [77].

Figure 4.2 shows a typical FT-IR spectrum of the PANI, the main chain characteristic bands at 1499 and 1576 $cm^{-1}$ was attributed to the C=N and C=C stretching modes for the quinoid and benzenoid rings. The bands at 1300 and 694 $cm^{-1}$ can be assigned to C-N stretching of the secondary aromatic amine and aromatic C-H out-of plane bending vibrations respectively. The band at 1142 and 800 $cm^{-1}$ due to the aromatic C-H in-plane bending and the out-of-plane deformation of C-H in the 1,4 disubstituted benzene ring. The band in the 3232 $cm^{-1}$ corresponds to secondary amine stretching (N-H) vibrations.

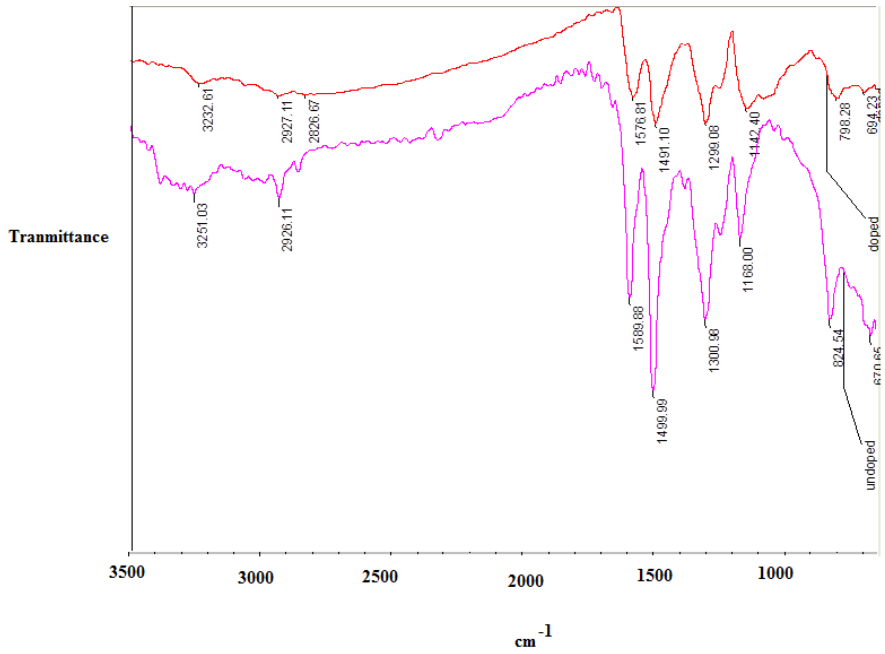


**Figure 4.2 :** FT-IR spectra of; --- doped PANI; --- undoped PANI.

### 4.1.1.3 Impedance properties

Impedance parameters were used to measure the response of the sample to the root mean square (rms) amplitude of the device response over the range of frequencies. The complex impedance describes for the sample, $Z^*(\omega) = Z' + jZ'' = R + jX$ where $\omega$ is the angular frequency, $Z^*(\omega)$ is the complex impedance, $Z'$ is the real part, $Z''$ is the imaginary part of the complex impedance, R is the resistance and X is the reactance the response to an alternating signal. The phase angle, $= \tan^{-1} (Z''/Z')$ include the complex impedance. Figure 4.3 shows the frequency evolution of the real part of impedance in semi-log graph for undoped and doped PANI in the frequency range of 100 Hz-15M Hz at different temperatures. Critical resonance frequency increases as temperature increases for undoped PANI as shown in Table 4.1. Doped PANI impedance level decreases significantly when compared with undoped PANI as shown in Figure 4.3b.

Here, critical resonance frequencies appear as the maximum peak, which approaches to higher values and maximum impedance values is at 40 ºC. The critical frequency value of doped PANI depending on temperature is given in Table 4.1.

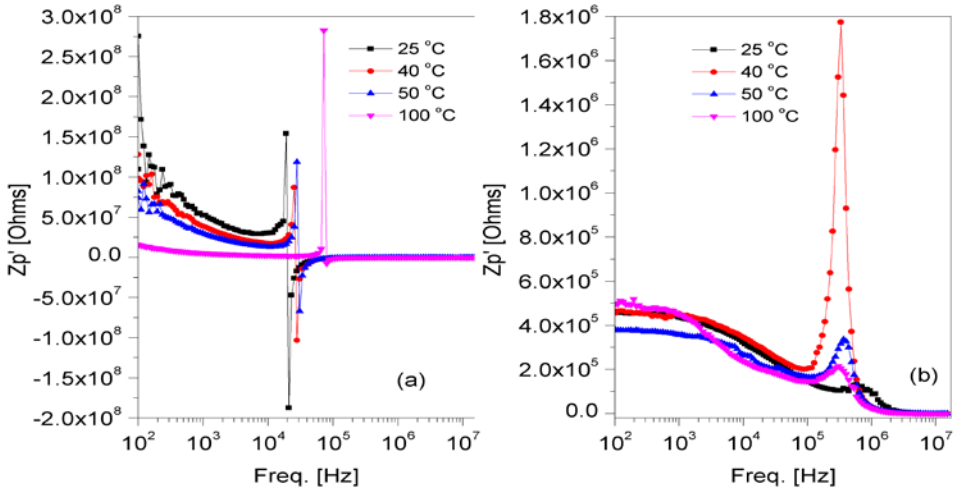


**Figure 4.3 :** The frequency evolution of the real part of parallel impedance (a), undoped PANI (b) doped PANI.

The impedance for undoped PANI has resonancy materials in the range frequency. This resonancy peaks behavior increases for temperatures. The impedance values decrease with the increase temperature for undoped PANI material. At the low frequency region, the highest value of the impedance has been recorded for room temperature measurements while its smallest value has been observed for doped

PANI for 50 ºC. The complex dielectric conductivity has been widely used for the ionic conduction effect for materials. The AC conductivity plane is plotted in the real part σ′ at different temperature in Figure 4.4.

**Table 4.1 :** The critical frequency and maximum peak frequency values for undoped and doped PANI, respectivelly.

| Temperature (˚C) | Undoped PANI Critical Frequency(Hz) | Doped PANI Critical Frequency (Hz) |
|---|---|---|
| 25 | 19821.3 | 696173.3 |
| 40 | 26285.8 | 338840.07 |
| 50 | 29427.7 | 337584.2 |
| 100 | 76005.5 | 297568.4 |

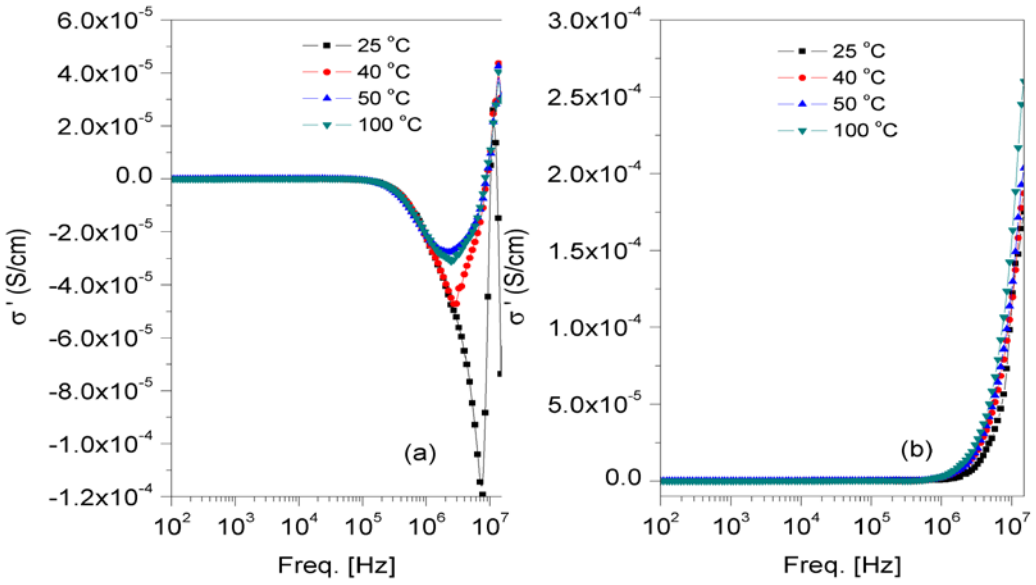


**Figure 4.4 :** The frequency dependency of the conductivity (σ′) in semi-log graph for undoped a doped PANI materials.

AC conductivity minimum peak frequencies decrease as temperature increases for undoped PANI, whereas such peaks did not appear for doped PANI, conductivity of which increased.

### 4.1.2 Preparation of chalcone substituted aniline and investigation of its impedance properties

The chalcone substituted aniline derivative was synthesized reaction between 3-aminoacetohenone and 4-pyridine carboxyalehyde in the presence of NaOH by using

Claissen-Smith method (Figure 4.5). The obtained monomer was characterized by using FTIR method.

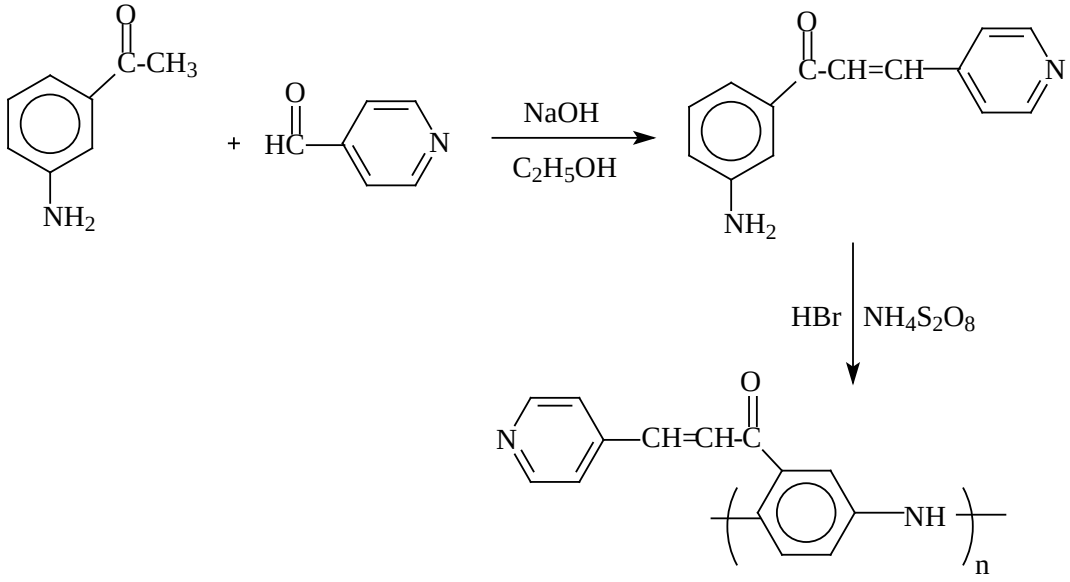


**Figure 4.5 :** Preparation of chalcone substituted polyaniline.

The obtained polymer was characterized by using FT-IR and physical methods. The α, β- unsaturated carbonyl group (C=C) appears at 1598 $cm^{-1}$. The IR band at 1669 $cm^{-1}$ suggesting the presence of (C=O) group. IR band at 3358 $cm^{-1}$ indicates presence of (N-H) group.

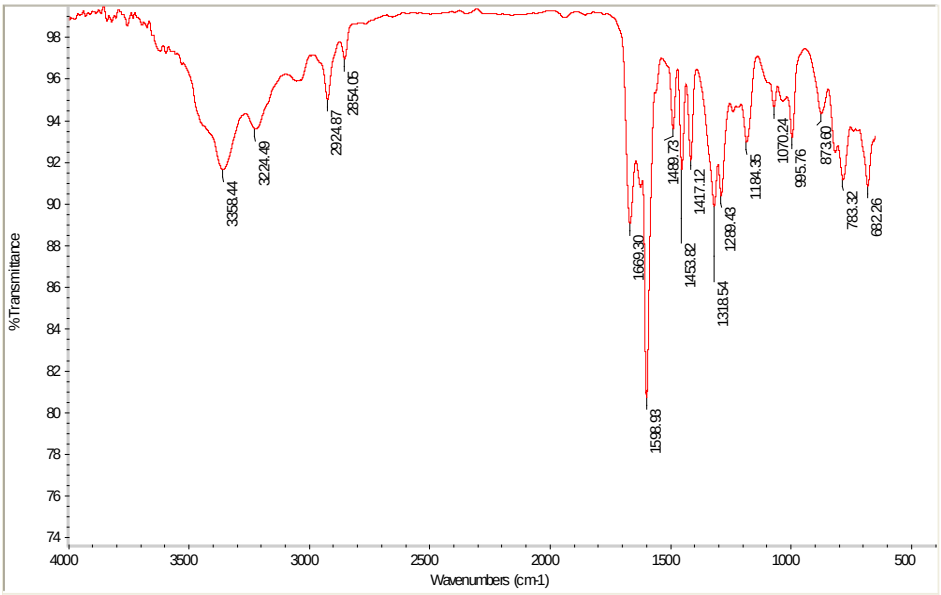


**Figure 4.6 :** FT-IR spectrum of chalcone substituted aniline.

The FT-IR spectrum of polymer (Figure 4.6) has been obtained for doped chalcone substituted PANI. The spectrum in the range 400-4000 $cm^{-1}$ was showing IR transmition due to the various vibrations involved. There is no detectable splitting in PANI (Figure 4.7) bands after doping by the used acids. The spectrum of PANI shows the major vibration bands: 1506 $cm^{-1}$ (stretching vibration of quinoid ring), around 1314 $cm^{-1}$ (stretching vibration of C-N), and around 820 $cm^{-1}$ (out-of-plane bending vibration of C-H on di-substituted rings).

Also, the polymer shows an absorption bands at 1632 and 1672 $cm^{-1}$ that is attributed to the unsaturated carbonyl groups in the chalcone unit.

**Figure 4.7 :** FT-IR spectrum of the chalcone substutied PANI.

The complex impedance $Z(\omega)$ is commonly used to separate the surface and bulk material properties. The complex impedance and its complex conjugate of $Z(\omega)$ for express the sample,

$$Z(\omega)= Z'(\omega)+ i\, Z''(\omega) = R(\omega)+i\, X\, (\omega) \quad \textbf{(4.1a)}$$

$$Z^{*}(\omega)= Z'(\omega)- i\, Z''(\omega) = R(\omega)+i\, X\, (\omega) \quad \textbf{(4.1b)}$$

respectively. In this Eq. 4.1, $\omega$ is the angular frequency, $Z(\omega)$ and $Z^{*}(\omega)$ are the complex impedance and its complex conjugate, respectively. $Z'(\omega)$ and $Z''(\omega)$ are the

real part, and the imaginary part of the complex impedance, respectively. R(ω) is the resistance and X(ω) is the reactance the response to an alternating current (AC). The magnitude of the complex conjugate impedance,

$$Z(\omega)x\ Z^{*}(\omega) = (Z'(\omega))^2 + (Z''(\omega))^2 \quad \textbf{(4.2)}$$

and the phase angle,

$$\theta=\tan^{-1}(Z''(\omega)/\ Z'(\omega)) \quad \textbf{(4.3)}$$

include the complex impedance.

Frequency dependency of electrical impedance for Cs-PANI can be seen from Figure 4.8 that a linear decrease is present with increasing frequency above $1.5x10^3$ Hz frequency region. In detail, frequency evolution of the impedance for chalcone exhibits similar behavior as conductive polymer materials regime.

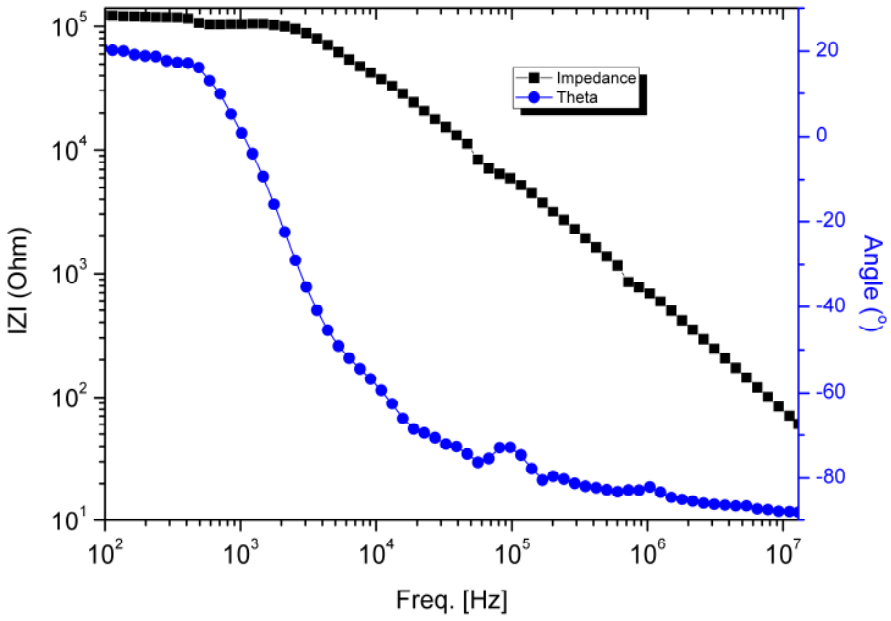


**Figure 4.8 :** The frequency evolution of the impedance (|Z|-*f* ) in log-log graph and the phase angle in semi-log graph for Cs-PANI.

The chalcone substituted aniline on the phase angle in the frequency range of 100 Hz to 13 MHz is shown in the Figure 4.8. The phase angle values positive region in the low frequency and it converts to the negative region in the high frequency regime of the Cs-PANI.

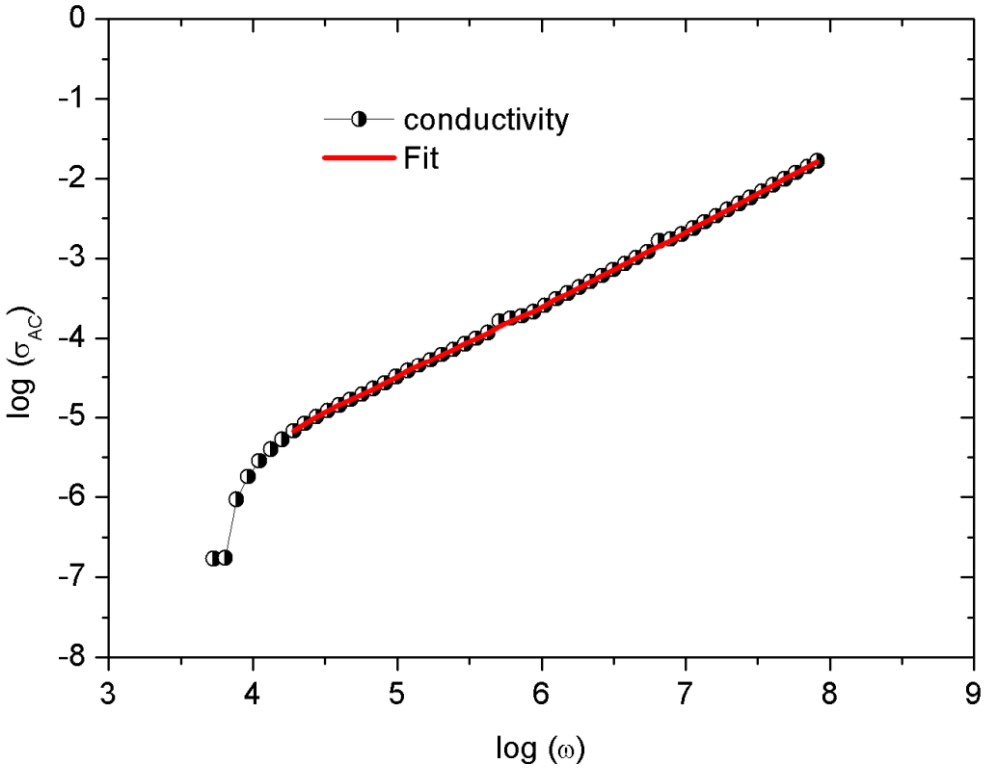


**Figure 4.9 :** Variation in logarithmic σAC as a function of logarithmic frequency (ω) for Cs-PANI.

The response of a conducting sample to an alternative current (AC) electrical field can be defined by the complex conductivity, $\sigma_{AC}(\omega)=\sigma'(\omega)+i\sigma''(\omega)$. Here, σ'(ω) and σ" (ω) are expressed as the real and the imaginary parts of the complex conductivity. Frequency dependency of the ac electrical conductivity for the Cs-PANI is shown in Figure 4.9 and AC conductivity linear increasing with increasing frequency.

The AC conductivity dependence of frequency can be expressed by the following relation, as the empirical Jonscher's universal law [78],

$$\sigma_{AC}(\omega)=A\,\omega^{s} \qquad \textbf{(4.4)}$$

where, A is a constant, ω is the angular frequency and s is the frequency exponent parameter which determines AC conduction with the value in the range of $0<s<1$. The angular frequency exponent values s were calculated from the slopes of Figure 4.9. It is obey the electrical conduction mechanism in of Cs-PANI sample. The values of angular frequency exponent s were calculated from the slope of the logarithmic conductivity as a function of logarithmic angular frequency curve. It works out to be 0.92. This value can be confirmed to the correlated barrier hopping and quantum mechanical tunneling (QMT) model. In the CBH and QMT models, the

frequency exponent s is ranged from 0.7–1 [79–81], which is in good agreement with the obtained result, as stated by Jonscher's universal law.

Figure 4.10 shows that the derivate $d\log\sigma_{AC}(\omega)/d\log\omega$ is a function of logarithmic angular frequency which con- firmed the dependence of $\sigma_{AC}$ (ω) in a conductive polymer chain, having three peaks of the values 5.58, 1.25, and 1.21. The critical transition frequencies ω, variable saturation region and angular frequency dependent slopes $d\log\sigma_{AC}$ (ω)/dlogω. The critical transition frequencies ω were measured from Figure 4.10 and given in Table 4.2.

An equivalent series electrical impedance Z of Eq. (4.1) is written in the complex formulation as [82];

$$Z = Rs - j(\omega Cs)^{-1} \quad \textbf{(4.5)}$$

In this expression, Rs, and Cs, represent the series resistance and capacitance, respectively. The real and imaginary part of electrical impedance parameters are correlated by the Kramers–Kronig relations. Real part of impedance (Resistance) parameters expressed by the equivalent series resistance corresponding to Eq. (4.6) is a series resistance; Rs, angular frequency dependent as [82].

$$R_s=\sigma.\ \omega^{-1/2} \quad \textbf{(4.6)}$$

According to Kramers–Kronig relations AC conductivity studies [83] the variation of Rs with angular frequency of ω which is shown in Figure 4.11.

The critical transition frequency calculated in Figure 4.10 correlated by the angular frequency dependency $R_s$ variations is given in Table 4.2. The Kramers–Kronig relations are the most suitable model [83,84] to characterize the impedance parameters of the new synthesized ionic polymeric materials as Cs-PANI.

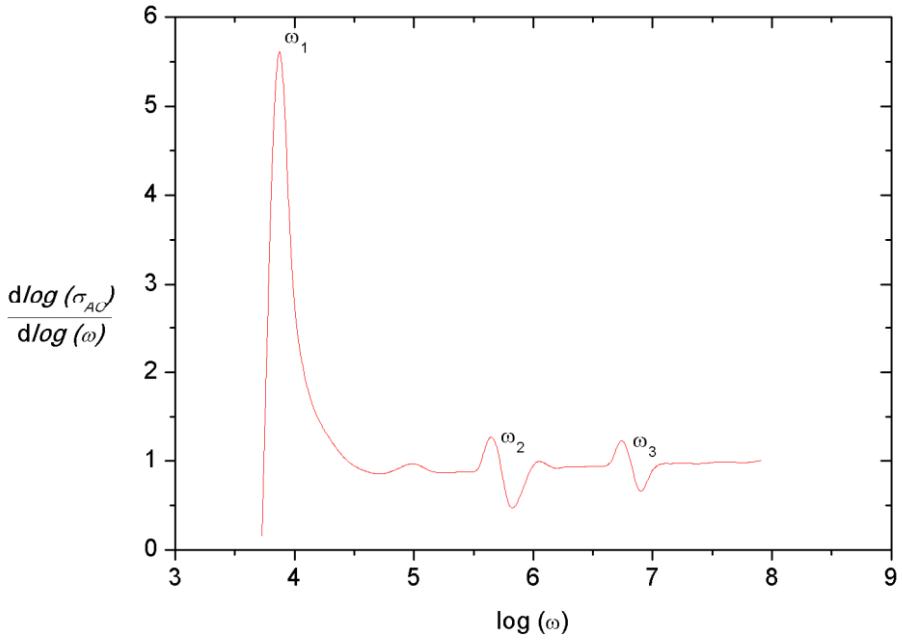


**Figure 4.10 :** The derivative of the measured the logarithm of the conductivity as a function the logarithm of the (angular) frequency ω.

**Table 4.2 :** The critical transition frequencies.

| Derivate Avarage | ω | ω | ω |
|---|---|---|---|
| Freq. [Hz] | 19821.3 | 696173.3 | 1041780 |

**Figure 4.11 :** Inverse frequency evolution of the equivalent series resistance ($Rs\text{-}f^{-1}$) in log–log graph for Cs-PANI.

## 4.2 Characterization of PANI and Polythiophene Composites

### 4.2.1 Preparation and electrical characterization of PANI- nano clay composites

Oxidative polymerization of aniline was investigated in the presence of Nanoclay with different weight percent- age, boric acid as dopant and ammonium persulfate (APS) (in 1.0:1.0 molar ratios) as initiator (Figure 4.12).

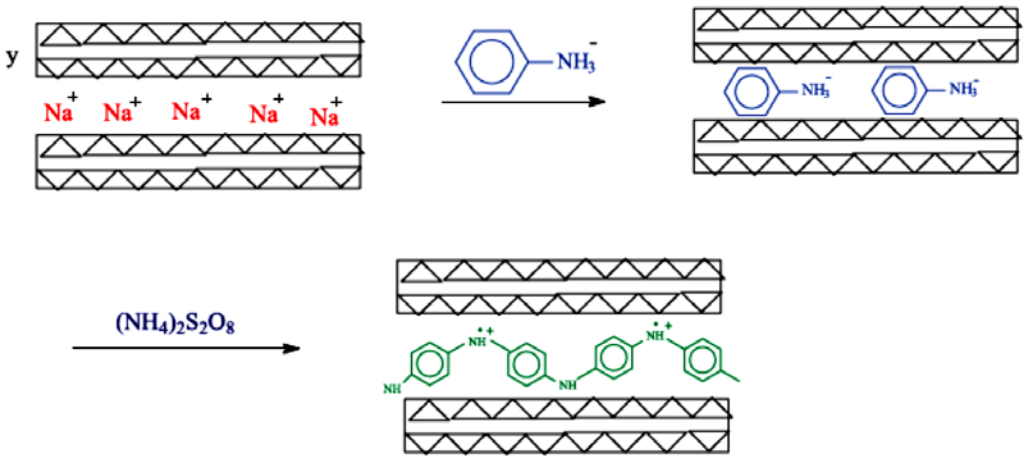


**Figure 4.12 :** Preparation of the PANI+NC composites.

Spectroscopic characterizations of the composites were performed by FT-IR. According to the FT-IR results (Figure 4.13); FTIR of PANI composite fibers exhibits absorption peaks due to the benzenoid ring of PANI at 1566, 1491, and 821 $cm^{-1}$. Peaks at 1566 and 1150 $cm^{-1}$ correspond to quinoid ring. The Si-O-Si stretching frequency of the clay matrix (1051 $cm^{-1}$ slightly shifted to 1040–1035 $cm^{-1}$) present in the composite confirms the retention of basic clay structure. The peaks at 1293 $cm^{-1}$ originate from the aromatic amine nitrogen (C-N stretching vibrations) asso- ciated with the oxidation or protonation states in PANI. In the composite there is slight shift to the frequency towards higher wave numbers and is suggested to be due to the Coulomb interaction between the positive nitrogen of the intercalated PANI and the partially negatively charged clay layers [84].

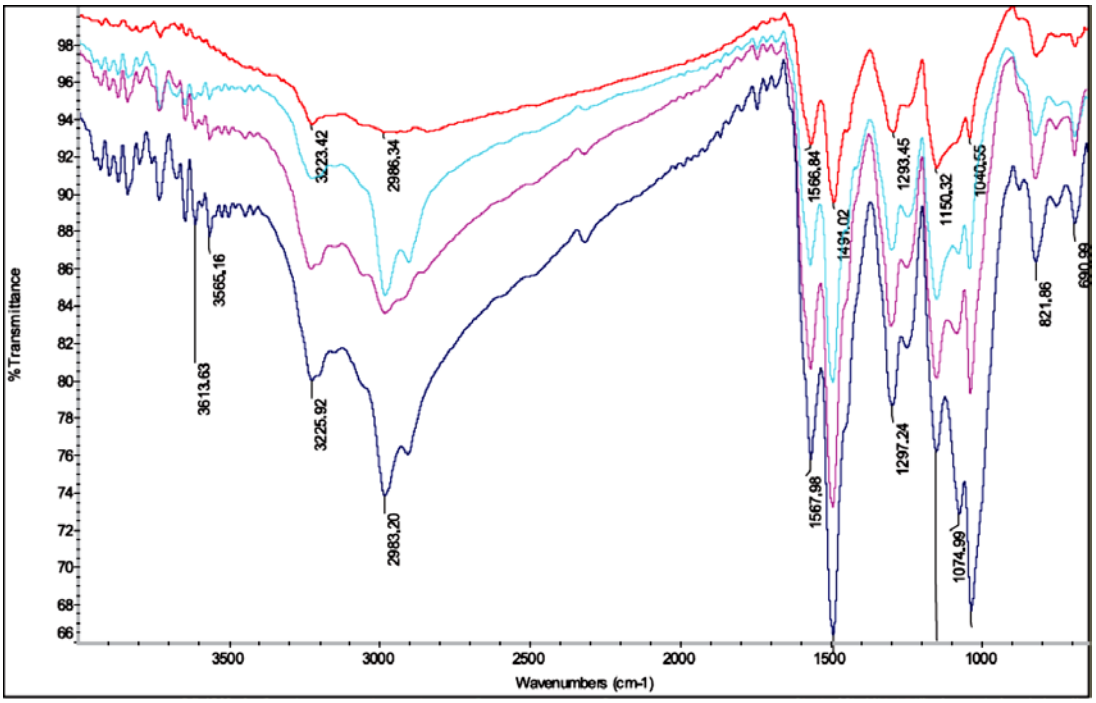


**Figure 4.13 :** FT-IR spectra of ---PANI, ---PANI+5%NC, ---PANI+10%NC, ---PANI+20%NC.

According to XRD results (Figure 4.14), the broad, amor- phous peak of 2θ (18 to 22°) in pure PANI was found in the PANI-clay composite. A sharp peak at 26.9° due to $SiO_2$ in clay was observed to be unchanged in the PANI-clay composite.

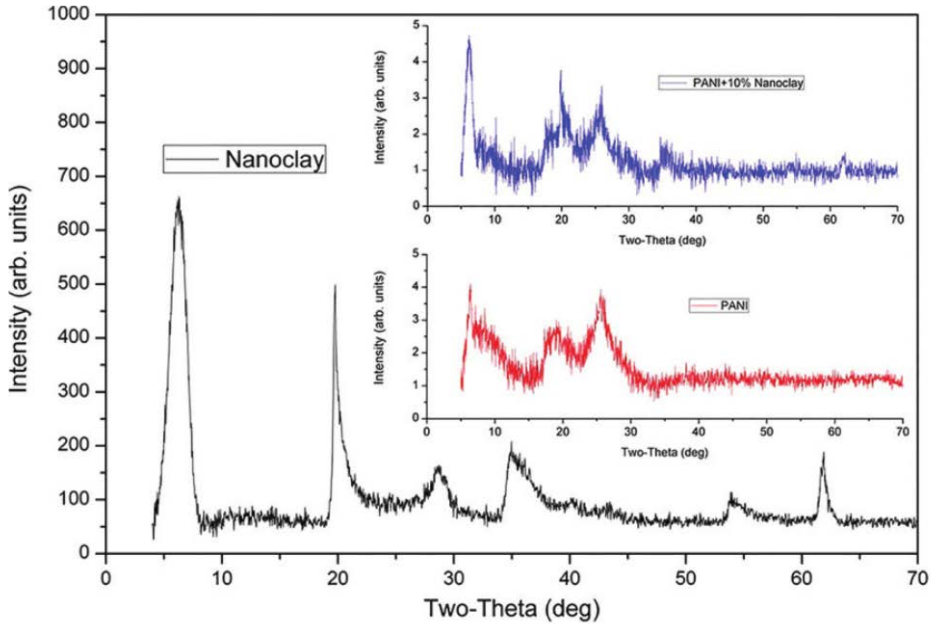


**Figure 4.14 :** X-ray diffraction patterns of nano clay(NC), PANI and PANI+10%NC.

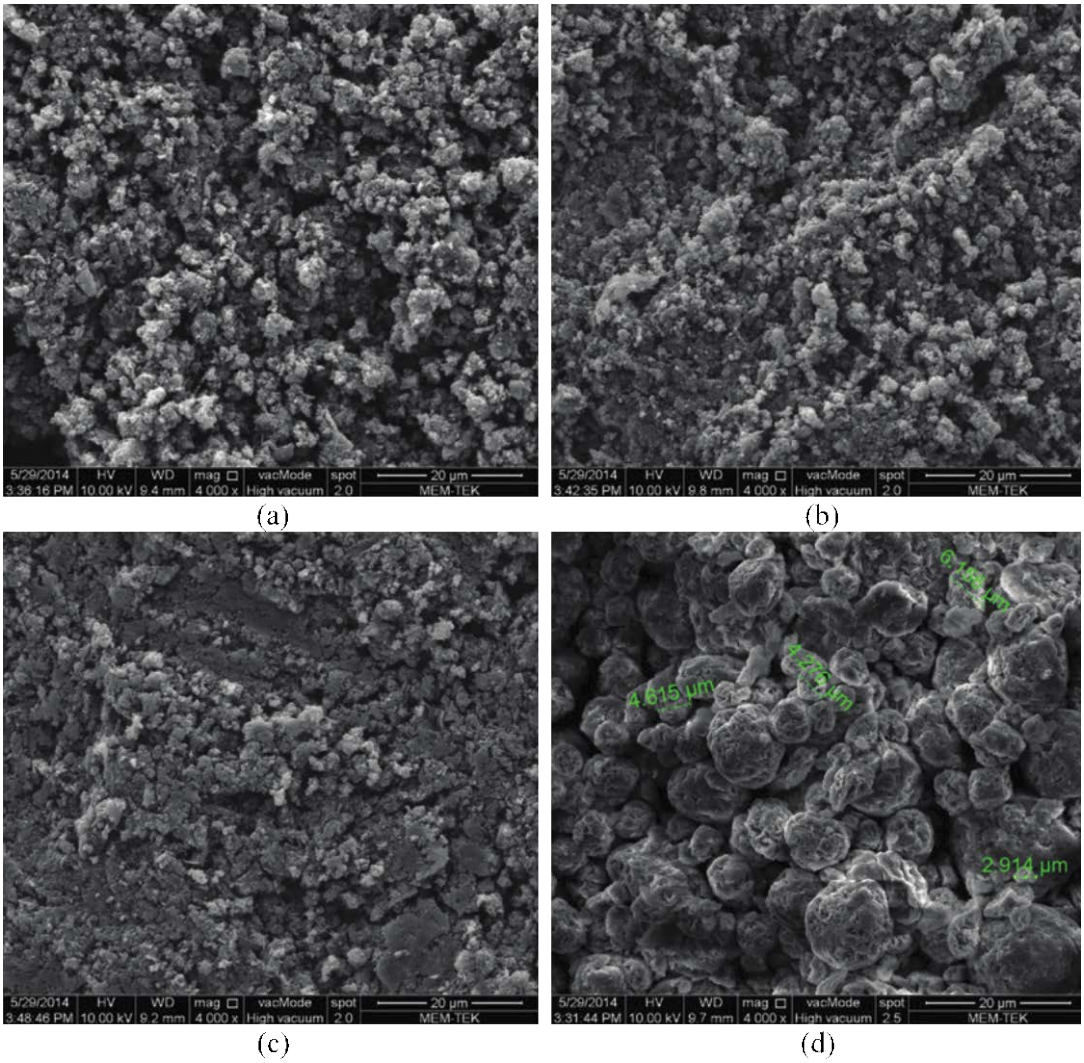


**Figure 4.15 :** SEM picture of a) PANI, b) PANI+5%NC, c) PANI+10%NC, and d) doped NC.

Figure 4.15 shows scanning electron micrographs (SEM) of PANI and PANI-NC composites. SEM revealed the typi- cal spherical granular morphology of PANI (Figure 4.15 a) and the formation of composites was clearly indicated in Figure 4.15b–4.15c. High resolution images of PANI-NC composites were similar to one another, but when the polymer proportion increases in the composites; its morphology was similar to that of PANI without NC.

The complex dielectric constant $\varepsilon$ is expressed in terms of the real $\varepsilon'$ and imaginary $\varepsilon''$ components, which represents the stored and dissipated energy components of the material, respectively. The dielectric constant is expressed as,

$$\varepsilon(\omega) = \varepsilon'(\omega) + i\varepsilon''(\omega) \qquad \textbf{(4.7)}$$

The real part of the dielectric constant $\varepsilon'$ of a material is the normalized permittivity

with respect to the permittivity of vacuum. It is also a measure of the amount of polar- ization in a material according to [85] and can be indirectly calculated from the following equation using the capacitance data,

$$\varepsilon' = C_p d/(\varepsilon_0 A) \quad \textbf{(4.8)}$$

where *Cp* is the parallel capacitance, *d* is the inter elec- trode distance, $\varepsilon_0$ is the permittivity of the free space and *A* is the sample area. The tan δ is given by

$$tan\delta = \frac{\varepsilon''}{\varepsilon'} \quad \textbf{(4.9)}$$

where $\delta = 90 - \varphi$ and $\varphi$ is the phase angle. Dissipation factor (tan δ) is also a typical dielectric parameter.

The dielectric strength (Δε) parameter is given in refrence [86] as

$$\Delta\varepsilon = \varepsilon_0 - \varepsilon_\infty \quad \textbf{(4.10)}$$

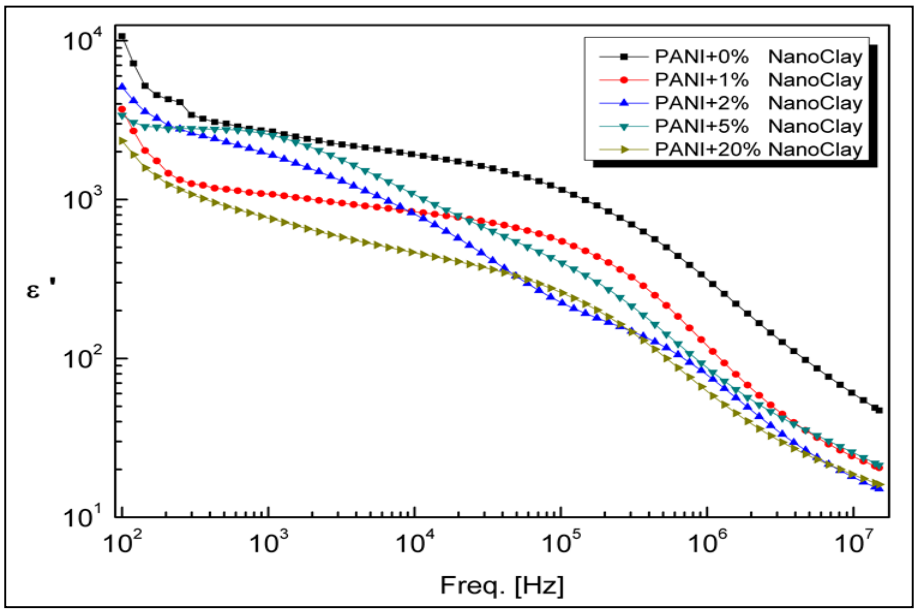


**Figure 4.16 :** Frequency dependency of the real part of dielectric constant of PANI+NC.

**Table 4.3 :** Maximum peak frequency values at dissipation plots, dielectric strength and surface resistivity.

| Samples | $f_{first.peak}$(Hz) | $f_{second.peak}$(Hz) | Δε | ρ(ohm.cm) |
|---|---|---|---|---|
| PANI | 146.90 | 3941763.30 | 10609.30 | 59578.35 |
| PANI+1%NC | 143.70 | 2301523.60 | 3683.20 | 106060.84 |
| PANI+2%NC | 122.80 | 2705710.80 | 5088.90 | 57885.32 |
| PANI+5%NC | <100.00 | 1140925.60 | 3373.00 | 345780.84 |
| PANI+20%NC | 136.10 | 1098794.70 | 2325.30 | 561462.61 |

where $\varepsilon_s$ and $\varepsilon_\infty$ are the low and high frequencies components of the real part of dielectric constant is shown in Figure 4.16 $\varepsilon_s$, $\varepsilon_\infty$ and Δε values at five different percentages (0%, 1%, 2%, 5%, 20%) nanoclay is given in the Table 4.3. It is also observed that the dielectric strength Δε decreases with increases the amount of the contribution of nanoclay. This result is consistent with the electrical behavior of the PANI+20%NC material.

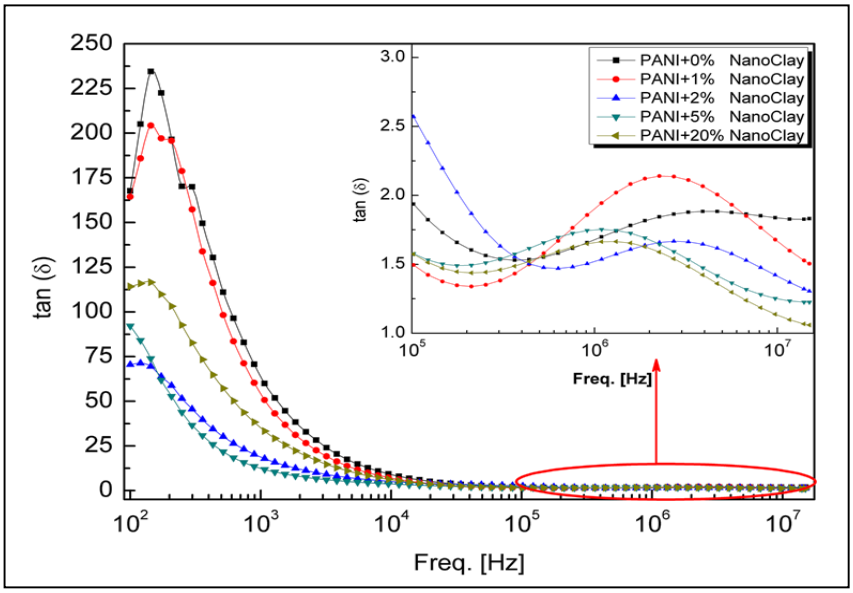


**Figure 4.17 :** Frequency dependence of the real part of dielectric constant of PANI+Nanoclay.

Frequency dependency of the ac dissipation factor/energy loss for PANI+NC is shown in Figure 4.17. According to dissipation factor plots, the materials present the first re- laxation times at low frequencies and second relaxation times at high frequencies. It is shown that lowest first and lowest second relaxation time is PANI+5%NC and PANI+20%NC, respectively. Relaxation frequencies values at five different nano clay are given in the Table 4.3.

Four-point probe technique was employed during the in-plane conductivity measurements, which were designed according to the property of the PANI+NC. The current source range which we have chosen for PANI+NC starts from $1 \times 10^{-6}$ to $100 \times 10^{-6}$ Amperes. The slope of (V-I ) plot gives us the surface resistivity in Ohm-centimeter, when we employ $\pi$ / ln 2 = 4.5324 coefficient. The theory of measuring surface resistivity applies the formula, $\rho_s$ = 4.5324 (V/I). $\rho_s$ is the ohm-centimeter, $V$ is the volts and $I$ is the ampere. Linear increase in the *V-I* graph is fitted and surface resistivity is acquired from this fit. We have calculated slope, surface resistivity values are given in the Table 4.3. The surface resistivity value exhibits high resistance new materials. This result is consistent with the electrical behavior of the PANI+20%NC material.

### 4.2.2 Preparation and electrical characterization of PANI- GH composites

PANI + GH composites were prepared by using oxidative polymerization of aniline in the presence of different weight percentage of GH (2%, 5% and 10%) and ammonium persulfate as oxidant (Figure 4.18).

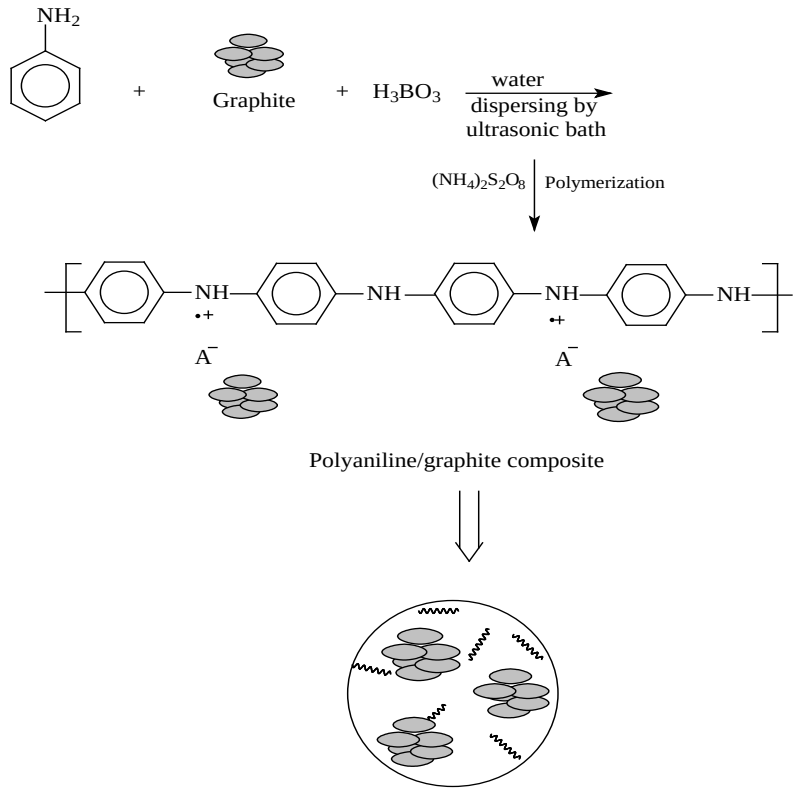


**Figure 4.18 :** Preparation of the Polyaniline/graphite composite**.**

Spectroscopic characterizations of the composites of the PANI + GH were investigated of the GH 10% by FT-IR in Figure 4.19.

Spectroscopic characterizations of the composites were performed by FT-IR. The main characteristic bands of doped polyaniline are assigned as follows: the bands at 1580 and 1495 $cm^{-1}$ are attributable to C=N and C=C stretching mode for the quinoid and benzenoid rings. The band at about 1141 $cm^{-1}$ is assigned to a plane bending vibration of C–H (mode of N=Q=N, Q=N +H–B and B–N +H–B), which is formed during protonation.

Curve in Figure 4.19 indicates that the main characteristic bands of doped PANI and GH all appear in FT-IR spectra of polyaniline/graphite composite. However, the incorporation of graphite particles leads to the shift of some bands of PANI. The bands at 1551 and 1231 $cm^{-1}$, corresponding to the stretching mode of C=N and C–N, all shifted to lower wavenumbers.

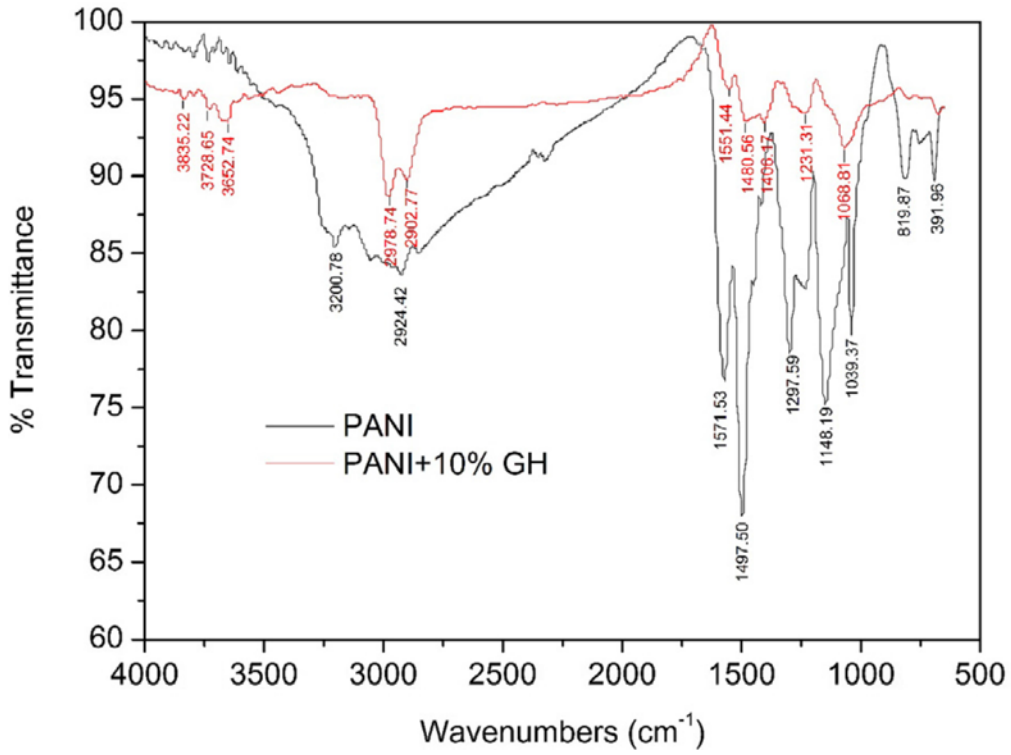


**Figure 4.19 :** FT-IR spectra of boric acid doped PANI and PANI + 10% GH composite.

The SEM images of the PANI (Figure 4.20a), the graphite (Figure 4.20b) and synthesized PANI + GH are shown in (Figure 4.20 c and d). The particle size of PANI is about ~200 nm. The composites show a uniform distribution of small

particles in graphite and PANI matrix (Figure 4.20 c and d); the graphite dispersed in PANI matrix and the PANI also embedded in the graphite are clearly observed.

Furthermore, increasing quantity of the graphite powders are distributed quite uniformly within the PANI matrix. Also, Figure 4.20 (c and d) demonstrates a well coating of the graphite and particle size of composites larger than pure PANI.

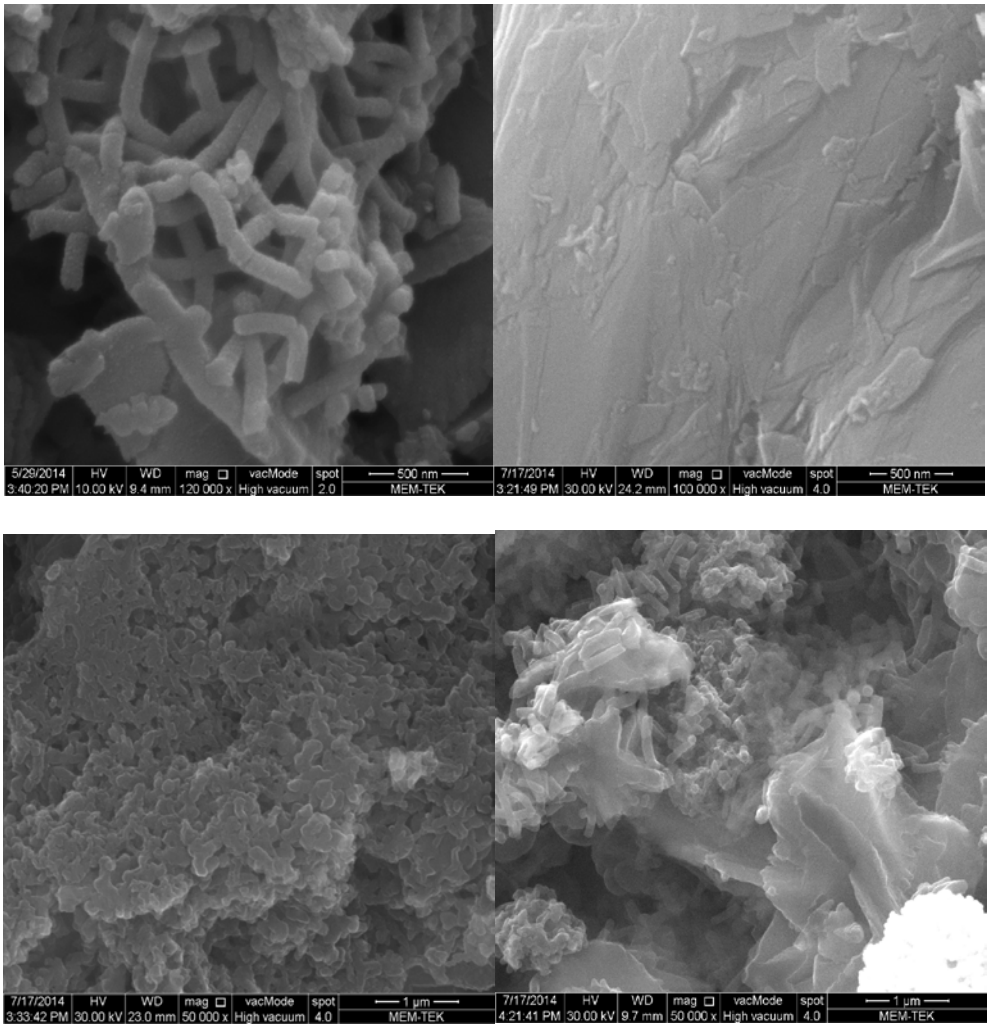


**Figure 4.20 :** SEM images of (a) PANI, (b) GH, (c) PANI + 2% GH, and (d) PANI + 10% GH, respectively.

Impedance properties were used to measure the response of the PANI+GH to the root mean square (rms) amplitude of the device response over the range of frequencies. The complex impedance describes for the sample, $Z^*(\omega) = Z' + jZ'' = R + jX$. where ω is the angular frequency, Z*(ω) is the complex impedance, Z′(ω) is the real part, $Z''(\omega)$ is the imaginary part of the impedance the response to an alternating signal.

Figure 4.21 shows the frequency evolution of the real part of the impedance Z′(ω) in log-log graph for PANI and different weight percentage of PANI doped 2%, 5% and 10% GH in the frequency range of 10 kHz-15 MHz. The real part of the impedance/ Z′(ω) for PANI loaded GHs have nearly linear decrease with the frequency. The real part of the impedance values decrease within the all frequency range and different weight percentage of PANI doped 2%, 5% and 10% GH. At the low frequency region, the largest value of the real part of impedance has been recorded for 10%GH+PANI while its smallest value has been observed for 2%GH+PANI.

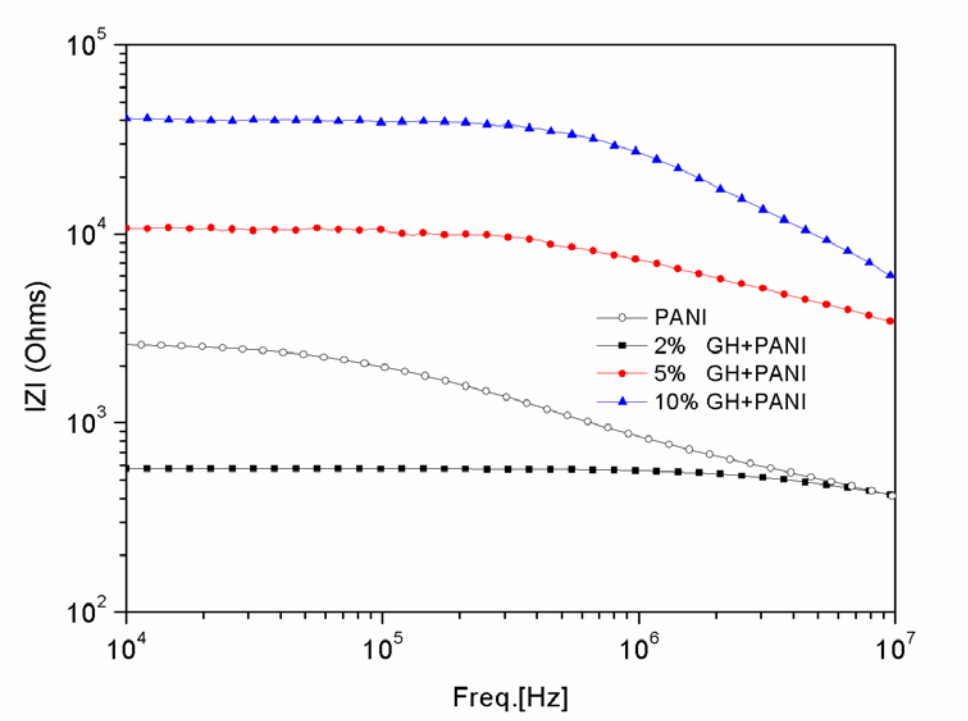


**Figure 4.21 :** Frequency variation of the real part of the impedance for PANI and PANI with different GH concentrations.

The frequency evolution of the imaginary part of the impedance/ Z″(ω) values for PANI with different GH concentrations has been showed in Figure 4.22 (a,b,c). The Z″(ω) for PANI doped 2%, 5% and 10% GH have linear decrease with the increasing frequency. The critical frequencies for PANI doped 2%, 5% and 10% GH have been determined 9043852.8 Hz (in Figure 4.22a), 552280.92 Hz (in Figure 4.22b), and 309130 Hz (in Figure 4.22c) Hz, respectively. The critical frequency values have been decreased with doping concentration GH. The conductive properties of graphite have decreased of the critical frequency its use as between semiconductor and metallic properties organic materials.

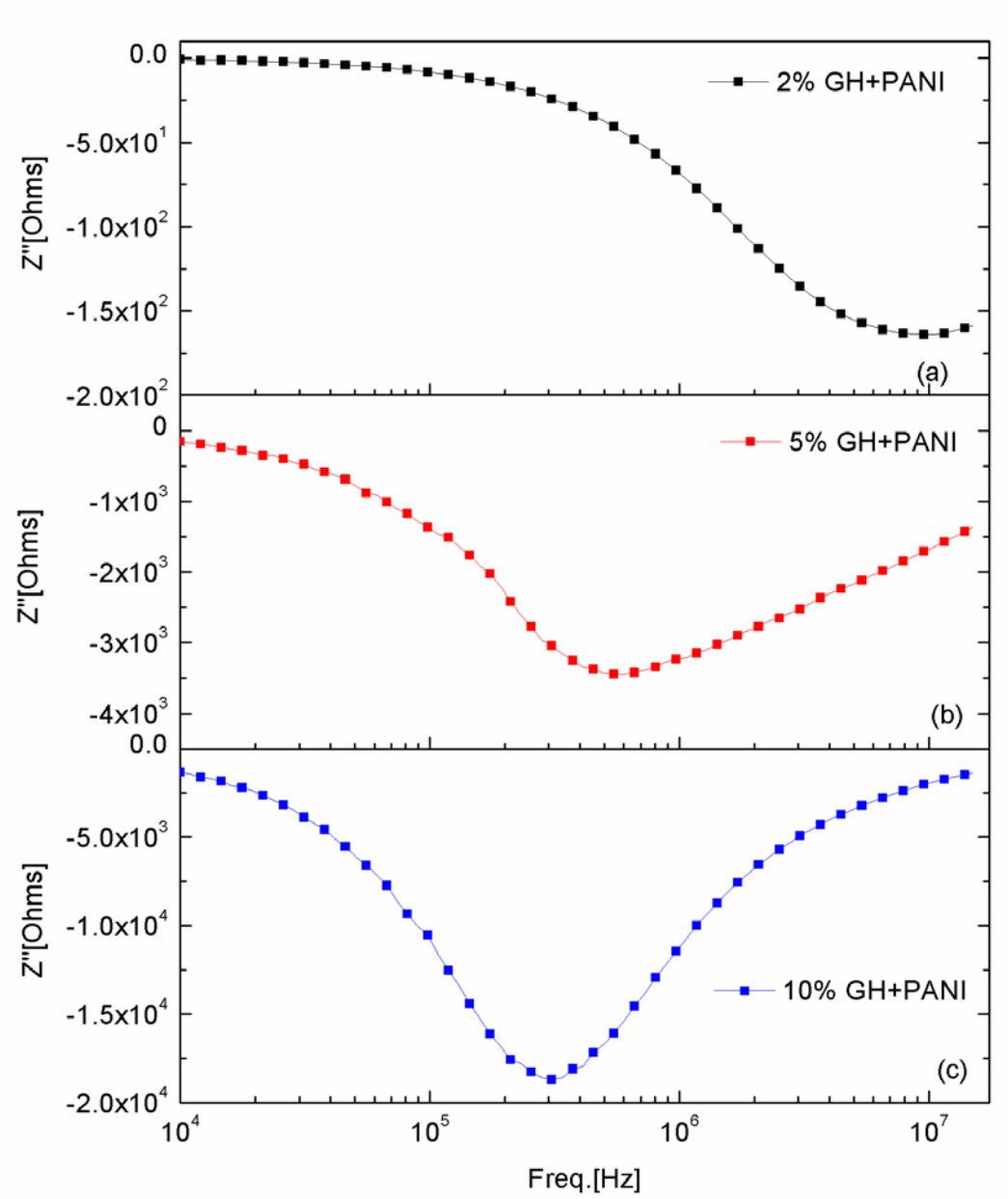


**Figure 4.22 :** Frequency variation of the imaginary part of the impedance; a) 2 % GH+PANI b) 5% GH+PANI, c) 10% GH+PANI.

The real $\varepsilon'(\omega)$ and the imaginary $\varepsilon''(\omega)$ parts of the complex dielectric constant is described as $\varepsilon^*(\omega)=\varepsilon'(\omega)-i\varepsilon''(\omega)$. The real $\varepsilon'(\omega)$ part of the dielectric constant is described as [11];

$$\varepsilon'(\omega) = \varepsilon_\infty + (\varepsilon_s - \varepsilon_\infty)\frac{1+(\omega\tau_o)^{1-\alpha}\sin\frac{1}{2}\alpha\pi}{1+2(\omega\tau_o)^{1-\alpha}\sin\frac{1}{2}\alpha\pi+(\omega\tau_o)^{2(1-\alpha)}} \qquad \textbf{(4.11)}$$

Here, $\varepsilon_\infty$, $\varepsilon_s$ are high and low angular frequency dielectric constant is shown in Figure 4.23, $\omega=2\pi$ times the frequency, and $\tau_0$ is a generalized relaxation time. The parameter α absorption coefficient changes from zero to one ($0 < \alpha \leq 1$).

If α=0, it corresponds to standard Debye type relaxation [88]. They are values different from zero and very close to zero as they are non-Debye type and nearly-Debye type relaxation, respectively [88,89]. The absorption parameter calculated from the Eq. (4.11). To analyze the dielectric relaxation type of PANI and PANI + GH, a absorption coefficient has been also calculated by the fitted dispersion curves given in Figure 4.23. The fitting functions of these curves, determined by Origin Lab. 8.5 program, are represented by Eq. (4.11). With this program, according to the raw data of Figure 4.23 (Adj.R-Square 0.99) was calculated directly constants. We have calculated $\tau_0$ relaxation time and α absorption coefficient from Eq. (4.11) and they are fitted by the results given in Figure 4.23. The absorption coefficient effects works of the PANI doped GH samples showed nearly-Debye type process. The relaxation times value of the real part of the dielectric constant dependent angular frequency value is calculated from Eq. (4.11). The calculated $\tau_0$ and a value are given in Table 4.3.

The dielectric strength; $\Delta\varepsilon$ parameter is given as [90],

$$\Delta\varepsilon = \varepsilon_0 - \varepsilon_\infty \qquad \textbf{(4.12)}$$

$\varepsilon_s$, $\varepsilon_\infty$ and $\Delta\varepsilon$ values for pure PANI and different percentages (2%, 5%, 10%) graphite are given in the Table 4.4. It is also observed that the dielectric strength decreases with increases the amount of the contribution of graphite. Dielectric strength value for pure PANI is ~18. This value has reached to the highest level of 2% GH. But, dielectric strength value has decreased to the lowest level when the doped 10% GH. In this case, it is understood to decreasing dielectric behaviors with increasing percentages graphite.

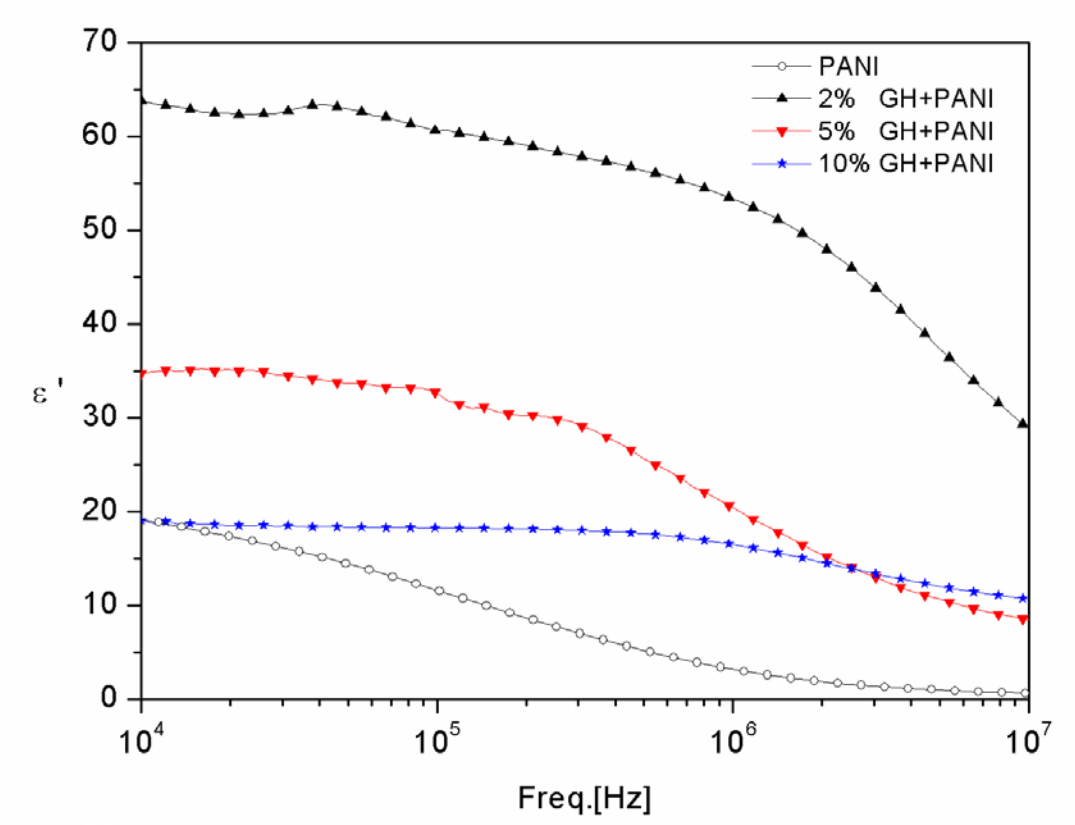


**Figure 4.23 :** Frequency variation of the imaginary part of the impedance; (a) PANI + 2%GH (b) PANI + 5% GH, (c) PANI + 10% GH.

**Table 4.4 :** Dielectric parameters of PANI and PANI doped GH .

| Parameters | PANI | 2%GH+PANI | 5%GH+PANI | 10%GH+PANI |
|---|---|---|---|---|
| α | 0.19 | 0.18 | 0.17 | 0.14 |
| $\tau_0$ | $6.39\times10^{-6}$ | $5.29\times10^{-7}$ | $1.20\times10^{-6}$ | $6.08\times10^{-7}$ |
| $\varepsilon_S$ | 19.30 | 63.50 | 34.73 | 19.02 |
| $\varepsilon_\infty$ | 0.60 | 29.33 | 8.51 | 10.70 |
| $\Delta\varepsilon$ | 18.70 | 34.17 | 26.22 | 8.32 |

The AC conductivity dependence of frequency can be expressed by the following relation, as the empirical Jonscher's universal law [91],

$$\sigma_{AC}(\omega)=A\,\omega^{s} \qquad \textbf{(4.13)}$$

where, A is a constant, ω is the angular frequency and s is the frequency exponent parameter which determines AC conduction mechanisms. The angular frequency exponent values *s* were calculated from the slopes of Figure 4.24.

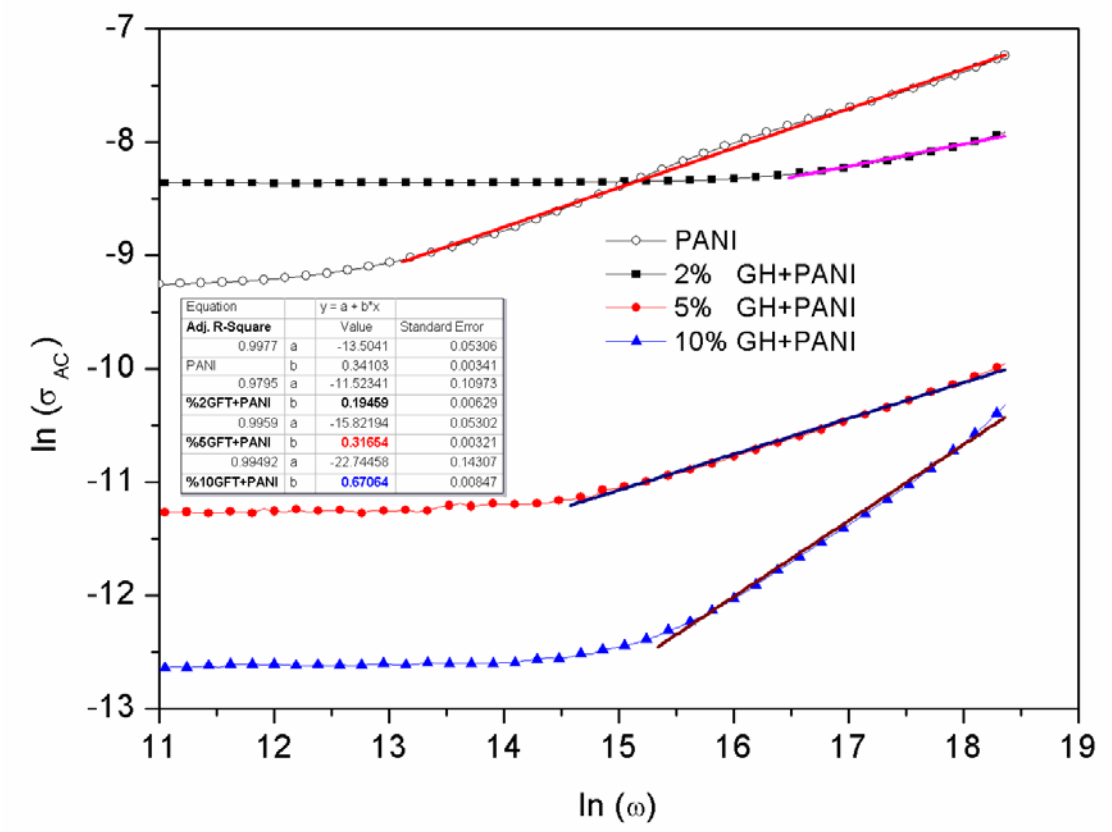


**Figure 4.24 :** AC conductivity for PANI and PANI with different GH concentrations.

The variations of ln $\sigma_{AC}$ with angular frequency have been given in Figure 4.24 for PANI doped GH.

**Table 4.5 :** "s" parameter of the samples.

| s parameter | PANI | 2%GH+PANI | 5%GH+PANI | 10%GH+PANI |
|---|---|---|---|---|
| Low frequency | 0.015 | 0 | 0 | 0 |
| High frequency | 0.341 | 0.19 | 0.31 | 0.67 |

The *s* parameters can be interpreted by different power laws for frequency dependent conductivity; for dc conductivity s parameter value is 0 [92] and for Correlated Barrier Hoping (CBH) Mechanism values 0<s<1 [93]. According to the values of exponent "s" varying from 0 to 0.7 are shown in the Table 4.5. Pure PANI shows nearly dc conductivity behaviors in the low frequency regions and CBH Mechanism behaviors in the high frequency regions. PANI doped GH all samples composites display dc conductivity behaviors in the low frequency regions and CBH Mechanism behaviors in the high frequency regions, respectively. The frequencies, at which the transition from dc conductivity to CBH occurs, have been listed in Table 4.4 for

PANI and PANI doped different percentages GHs. PANI different weight percentage of graphite doping was provided to direct current mechanism in low frequency region.

### 4.2.3 Structural, magnetical and electrical properties of magnetite doped polyaniline

#### 4.2.3.1 Preparation of magnetite

The magnetic nanoparticles were sprepared starting from of $FeCl_2.4H_2O$ (1.0 M) and $FeCl_3.6H_2O$ (1.5 M). Obtained magnetite nanoparticles were used to prepare PANI-magnetite composites.

#### 4.2.3.2 FTIR and SEM Analyses

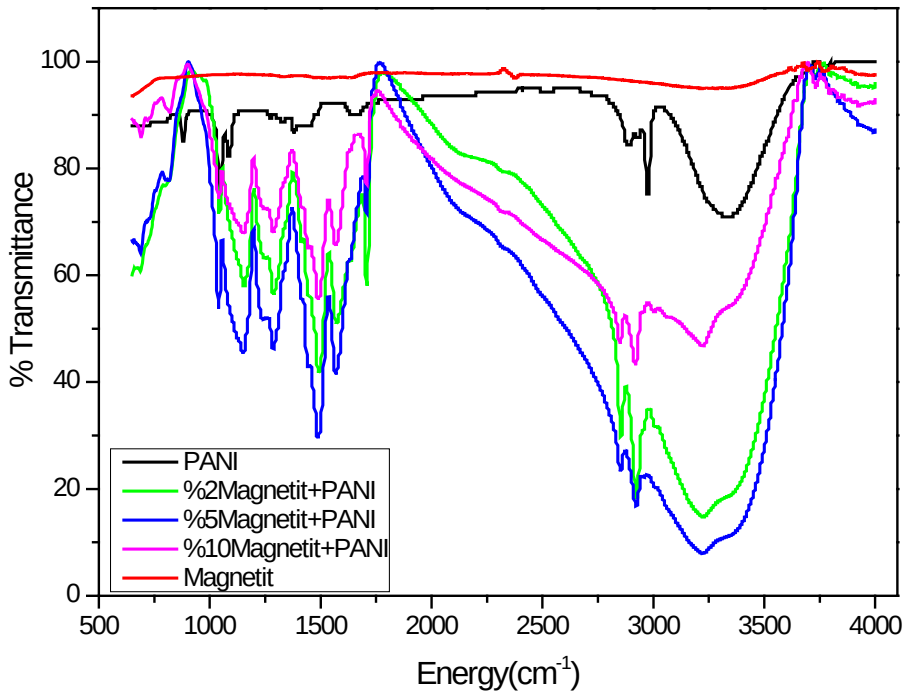


**Figure 4.25 :** FTIR spectrum of PANI-Magnetite Composites.

FTIR spectra of magnetite and PANI are shown in Figure 4.25 The main characteristic bands for PANI are assigned as follows: the bands at 1568 and 1497 $cm^{-1}$ can be ascribed to the C=C stretching vibration of the quinoid (Q) and benzenoid rings, respectively. The band at 1297 $cm^{-1}$ results from the stretching vibration of C–N. The band at 1148 $cm^{-1}$ is associated with the vibrational mode of

N=Q=N in the doped PANI chains, while the band at 819 $cm^{-1}$ corresponds to the out-of-plane blending of C–H in the substituted benzenoid ring. It can be noticed that the characteristic band of PANI at around 1691 $cm^{-1}$ assigned to the C-O stretching vibration can be easily observed. From the FTIR spectra of composites in the Figure 4.25, it is shown that all the characteristic bands of PANI are present and these bands are found to be shifted slightly, when compared with those of pure PANI.

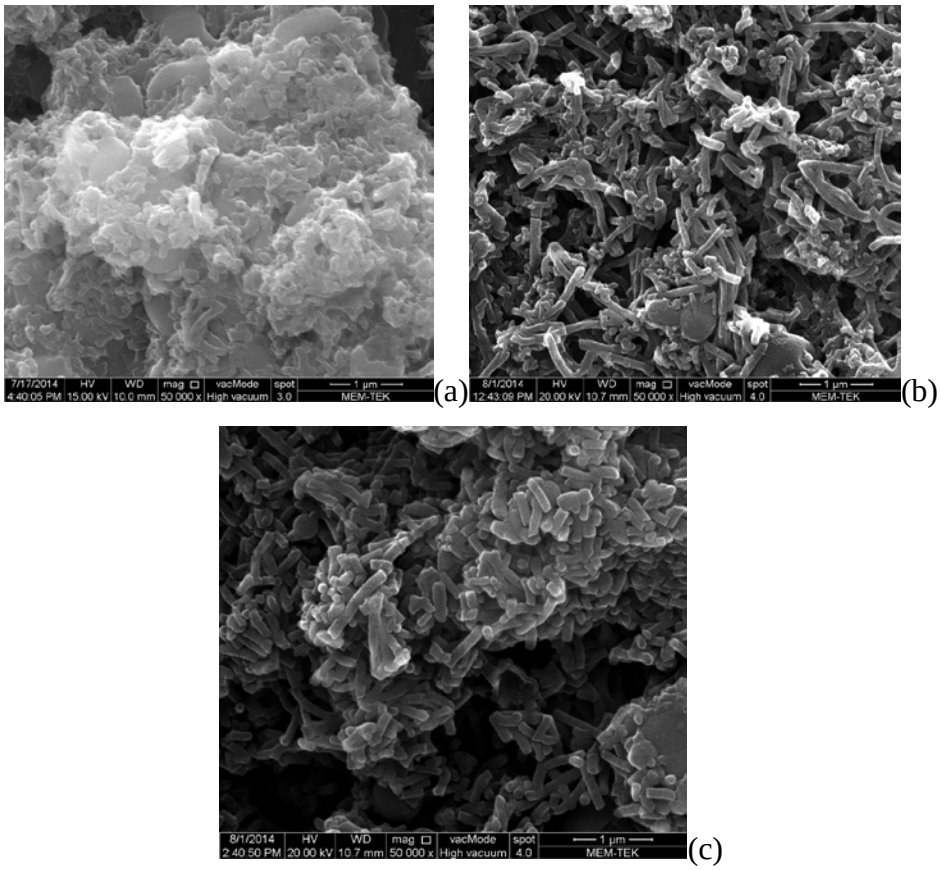


**Figure 4.26 :** SEM images of a) pure PANI, b) PANI+ 2% Magnetite and c) PANI+ 10% Magnetite composites.

The synthesized surfactant can control the morphology of PANI and doped magnetite particles. Fig 4.26 gives typical SEM images of the resulting pure PANI and PANI-Magnetite rods. PANI-Magnetite composites have a unique rods structure. It is clear that a great number of magnetite nanoparticles adsorbed on the surface of the PANI rods. Also, magnetite nanoparticles are observed to be fairly well dispersed in the PANI matrix. It can be seen in Fig 4.26(a) that pure PANI aggregates to form like large clusters. Magnetite particles doping rates increased weight to weight in the

PANI which are in the rod structures spread homogenous on the surface (Fig 4.26b, Fig 4.26c).

### 4.2.3.3 Magnetical measurements -EPR study

Magnetite is the most abundant magnetic mineral on the earth. Chemical formula is written as $FeO.Fe_2O_3$ ($Fe_3O_4$). In crystal structure, magnetic moments of $Fe^{3+}$ ions (S = 5/2), which have the same magnitudes, are aligned anti-parallel, so net magnetic moment drops to zero. Therefore the magnetic moment of the unit cell only comes from the $Fe^{2+}$ ions (S = 2).

g-factor was calculated from resonance conditions as seen in follows:

$$g = \frac{h\gamma}{\beta B_r} \qquad \textbf{(4.14)}$$

Where h is Planck constant, $\gamma$ the microwave frequency, $\beta$ the Bohr magnetron and $B_r$ is the resonance magnetic field.

**Table 4.6 :** g- factor values of the PANI, Magnetite and Poly(aniline) – magnetite composites with different magnetite concentrations.

| Samples | g parameter |
|---|---|
| PANI | 2.005 [18] |
| PANI+2%NC | 2.2277 |
| PANI+5%NC | 2.1452 |
| PANI+10%NC | 2.2333 |
| Magnetite | 2.3248 |

Figure 4.27 shows the powder EPR spectrum of magnetite complex recorded in the 0–8000 G range at the room temperature. The spectra have a very broad line belonging $Fe^{2+}$ ions (S = 2), which is caused by exchange interactions between unpaired electron spins and spin-orbital interactions. The g-factor values of magnetite in complex are lower. The narrow intensive peak in spectra is free radical signal from organic molecules. This lowering can be due to the decreasing of magnetic anisotropy.

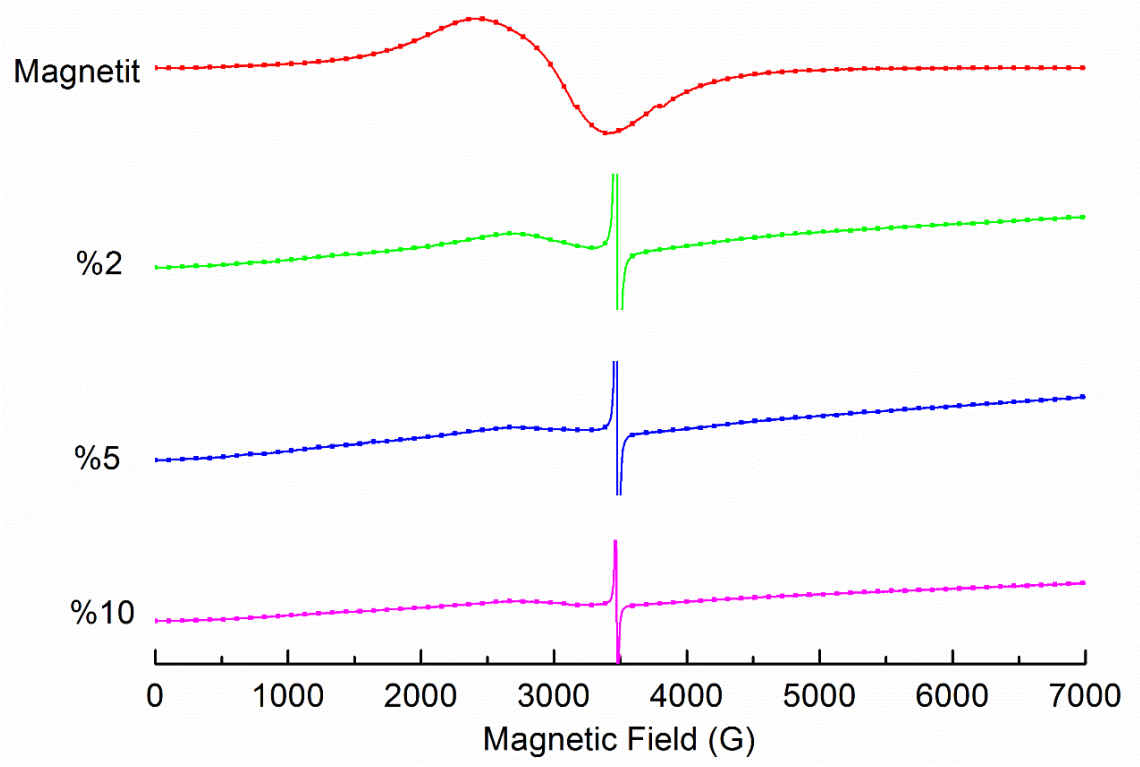


**Figure 4.27 :** The powder EPR spectrum of PANI, Magnetite and Poly(aniline)–magnetite composites with different magnetite concentrations.

#### 4.2.3.4 Electrical measurements

The complex dielectric constant ε is consist of two parts where real ε′ and imaginary ε″ components.

$$\varepsilon^*(\omega) = \varepsilon'(\omega) - i\varepsilon''(\omega) \qquad \textbf{(4.15)}$$

The real part ε′ is expressed by the following equation,

$$\varepsilon'(\omega) = \varepsilon_\infty + (\varepsilon_s - \varepsilon_\infty)\frac{1+(\omega\tau_o)^{1-\alpha}\sin\frac{1}{2}\alpha\pi}{1+2(\omega\tau_o)^{1-\alpha}\sin\frac{1}{2}\alpha\pi+(\omega\tau_o)^{2(1-\alpha)}} \qquad \textbf{(4.16)}$$

Here, $\varepsilon_\infty$, $\varepsilon_s$ are high and low frequency dielectric constant are given in Table 4.7 $\tau$ is the relaxation time and α is the absorption coefficient changes from zero to one ($0 < \alpha \leq 1$).

**Table 4.7 :** Dielectric parameters of PANI, magnetite and Poly(aniline) – magnetite composites with different magnetite concentrations.

| Parameter | PANI | Magnetite | 2%Mag+PANI | 5%Mag+PANI | 10%Mag+PANI |
|---|---|---|---|---|---|
| $\alpha$ | 0.57 | 0.13 | 0.49 | 0.44 | 0.42 |
| $\tau_0$ | $1.56658E^{-5}$ | $6.58451E^{-4}$ | $2.76964E^{-5}$ | $3.53875E^{-4}$ | 0.00134 |
| $\varepsilon_S$ | 37.90 | 1049.9 | 19.99 | 426.7 | 3826.6 |
| $\varepsilon_\infty$ | 0.47 | 7.99 | 8.51 | 1.31 | 4.79 |
| $\Delta\varepsilon$ | 37.43 | 1041.91 | 19.25 | 425.39 | 3821.81 |

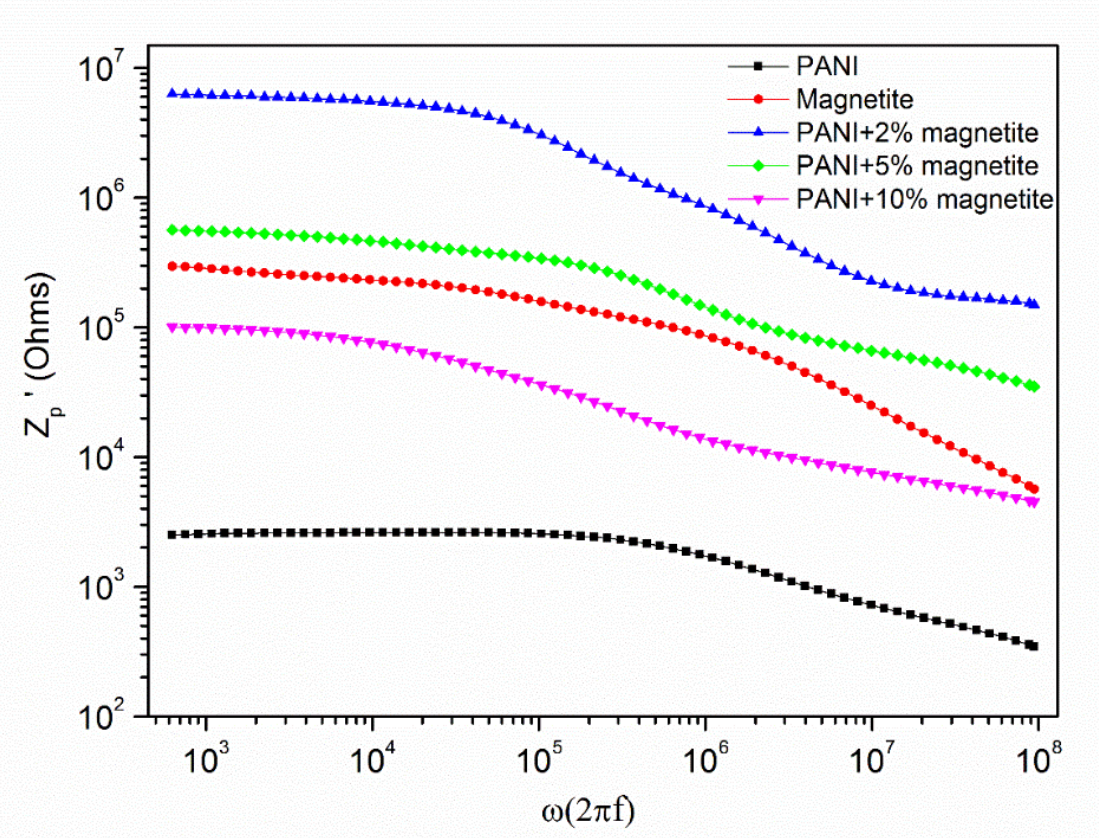


**Figure 4.28 :** Frequency variation of the impedance for PANI, Magnetite and Poly(aniline) – magnetite composites with different magnetite concentrations.

Fig 4.28 illustrates the variation of the impedance $Z_p'$ as dependence of the angular frequency in the logarithmic scale for undoped PANI, magnetite and different weight percentage of magnetite doped 2%, 5% and 10% PANI – magnetite composites. The impedance of magnetite ($Fe_3O_4$) is higher than PANI. PANI has the smallest Z value because of its semiconducting behaviour. It is observed that the impedance values decrease with the increasing the amount of magnetite in the PANI matrix. In this

case, the semiconductor behavior is deteriorated by the doping magnetite. Therefore, conductivity increases.

The reel part of the dielectric constant ε′ as a function of frequency is shown in Fig 4.29. For all compositions, the dielectric constant ε′ decrease with the increasing frequency but increase with the increasing the weight percentage of magnetite due to the oxide structure of magnetite. Therefore, it contributes the increasing of the dielectric strength (***Δε***) of the material. Thereby, it allows the use of electronic devices in applications that require mechanical strength. Dielectric parameters ε′, ε″ and ***Δε*** are given in Table 4.6.

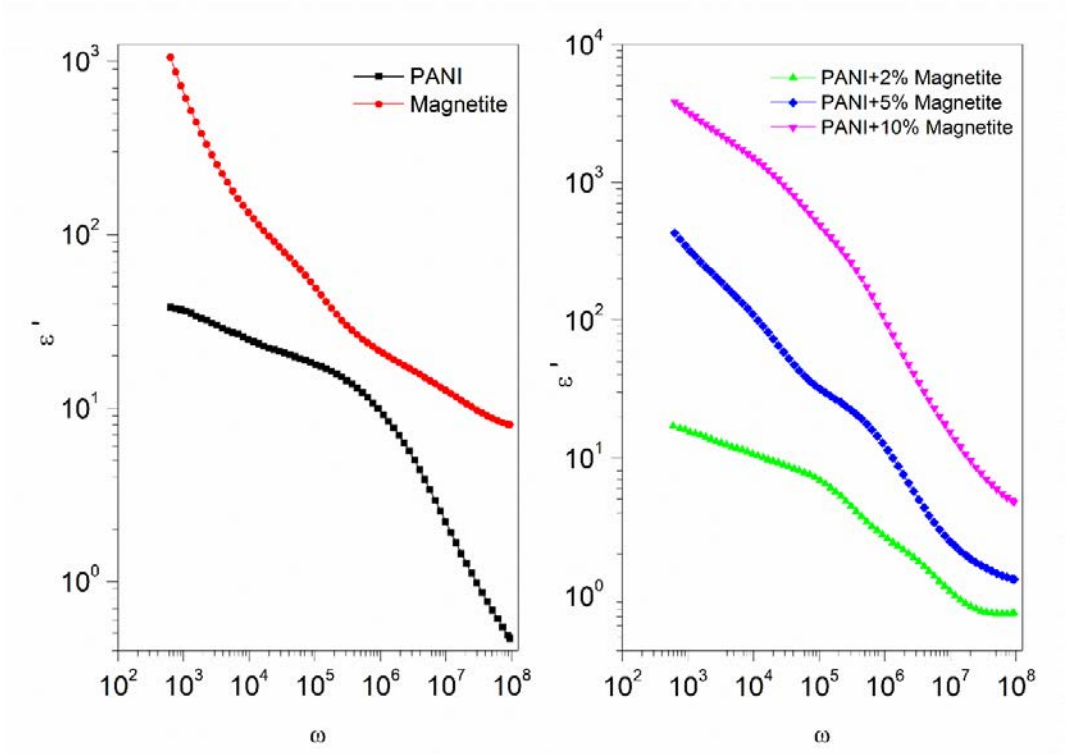


**Figure 4.29 :** Frequency variation of the real part of dielectric constant for PANI, Magnetite and PANI– magnetite composites with different magnetite concentrations.

In Figure 4.30, the imaginary part ε″ has a linear decrease with the increasing frequency that shows similar behavior as the real part ε′. The energy loss (ε″) increases with increasing the amount of magnetite. The reason of increasing the energy loss is due to free electrons in the PANI-magnetite composite. Because, $Fe^{2+}$ and $Fe^{3+}$ ions are contribute to the ionic conductivity. This increase can be seen in Fig 4.31 as obvious.

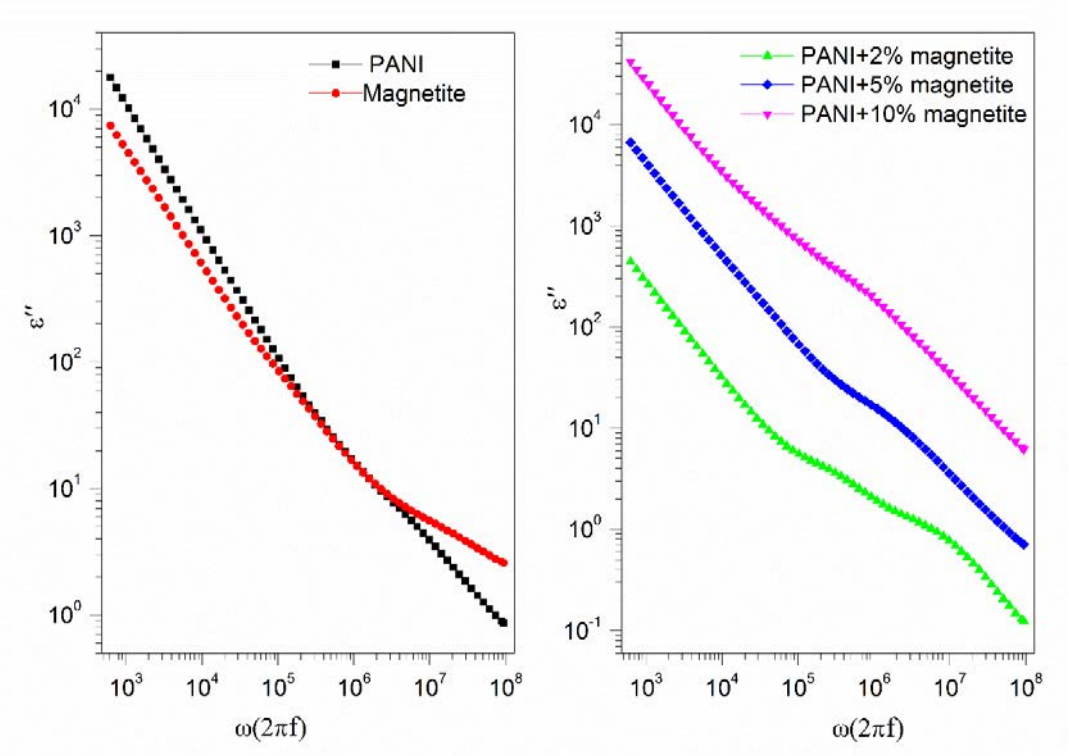


**Figure 4.30 :** Frequency variation of the imaginary part of dielectric constant for PANI, Magnetite and Poly(aniline) – magnetite composites with different magnetite concentrations.

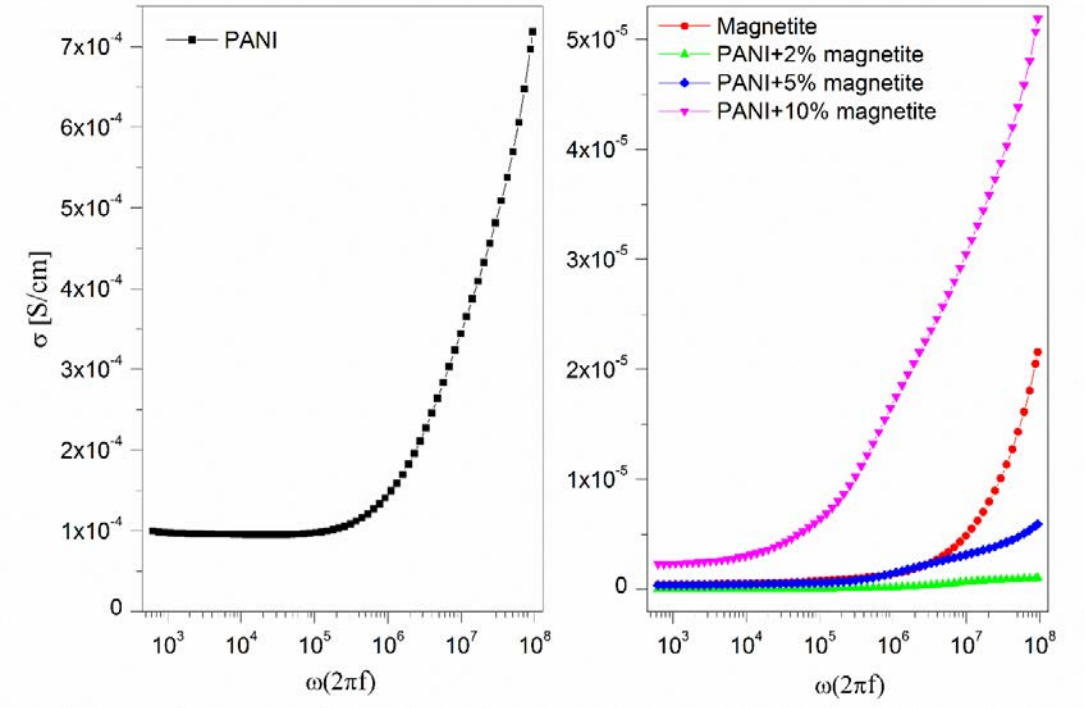


**Figure 4.31 :** Variation of $\sigma_{AC}$ as a function of logarithmic frequency (ω) for PANI, Magnetite and Poly(aniline) – magnetite composites with different magnetit concentrations.

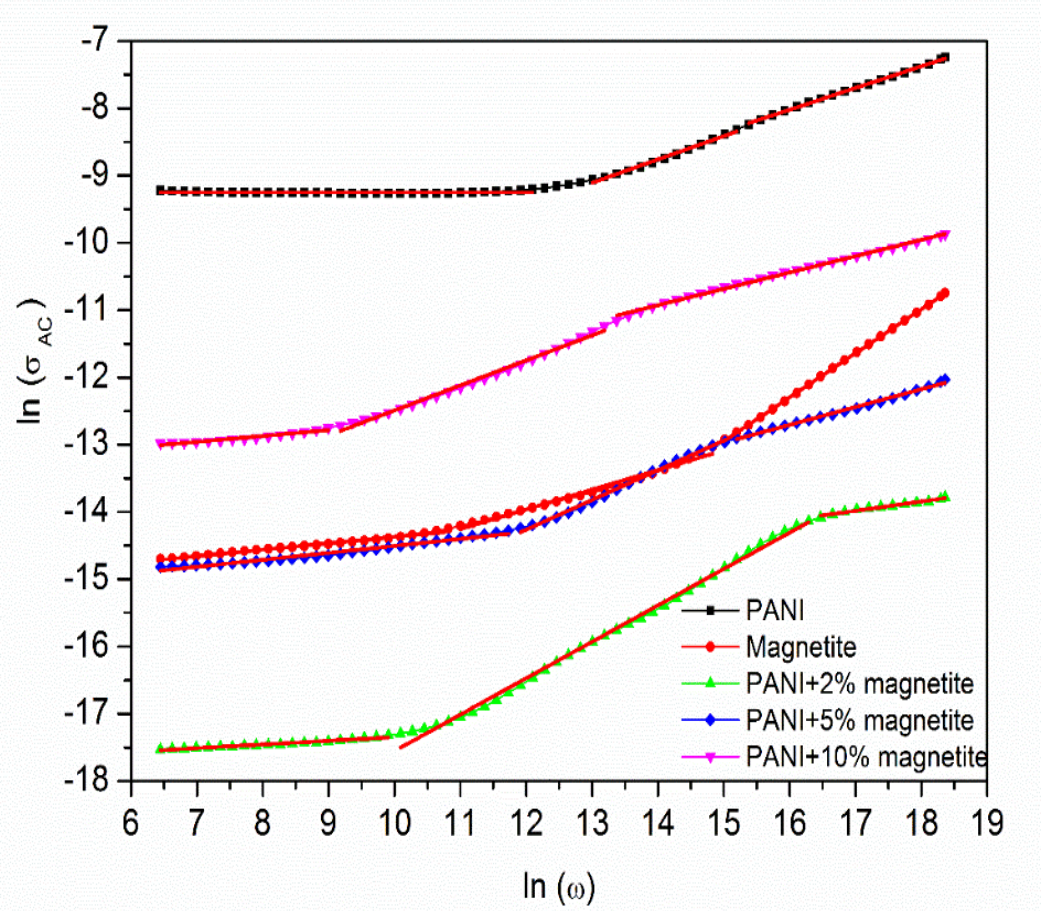


**Figure 4.32 :** Variation of σAC as a function of angular frequency for PANI, Magnetite and Poly(aniline) – magnetite composites with different magnetite concentrations.

The frequency dependence of the total conductivity is defined by the following relation [95],

$$\sigma_T = \sigma_{DC} + \sigma_{AC} = \sigma_{DC} + A\omega^s \qquad \textbf{(4.16)}$$

where, A is a constant, $\omega$ is the angular frequency and s is the frequency exponent parameter which determines AC conduction mechanisms.

Fig 4.32 shows the relation between lnσ and ln $\omega$ for different weight percentage of PANI +magnetite composites. The values of *s* parameters determined from the slopes of the curves are given in Table 4.8. All samples show the DC conductivity behavior at low frequencies (first region). For second region, s parameter varies in the range of 0.29 to 0.54 and these values indicate that it is compatible with the correlated barrier hopping (CBH) model [96] of the AC conduction mechanism in this region.

**Table 4.8 :** s parameter of the PANI, Magnetite and PANI – magnetite composites with different magnetite concentrations.

| wt% magnetite | s parameter (1.region) | $f_1$ (Hz) | s parameter (2.region) | $f_2$ (Hz) | s parameter (3.region) |
|---|---|---|---|---|---|
| Magnetite | 0.096 | 9540 | 0.293 | 438870 | 0.655 |
| PANI | $1.5x10^{-4}$ | 70880 | 0.347 | 631980 | 0.323 |
| 2%Magnetite+PANI | 0.055 | 3834 | 0.541 | $1.887x10^{6}$ | 0.138 |
| 5%Magnetite+PANI | 0.104 | 23738 | 0.441 | 438942 | 0.265 |
| 10%Magnetite+PANI | 0.087 | 1539 | 0.372 | 85060.9 | 0.243 |

Fig 4.33 illustrates the dissipation factor/energy loss of PANI, magnetite and PANI+Magnetite composites. These curves give the information about the relaxation frequencies of the materials.

At low frequencies, the dissipation factor values are decreasing exponentially with increasing frequency for all samples. Besides, the loss tangent peak values increase with increasing the amount of magnetite in the PANI matrix at higher frequencies ( >80000 Hz). The dielectric loss factor declined nearly exponential and the dipole contributed the polarization was able to orient themselves with electrical field at higher frequency. Values of the relaxation frequencies are given in Table 4.9.

**Table 4.9 :** The loss tangent peak values of PANI, Magnetite and Poly(aniline) – magnetite composites with different magnetit concentrations.

| Samples | $f_{\text{first.peak}}$(Hz) | $f_{\text{second.peak}}$(Hz) |
|---|---|---|
| PANI | 150 | - |
| PANI+1%NC | 172.8 | 28500 |
| PANI+2%NC | 59067 | 1092654 |
| PANI+5%NC | 5520 | 631980 |
| PANI+20%NC | - | 758754 |

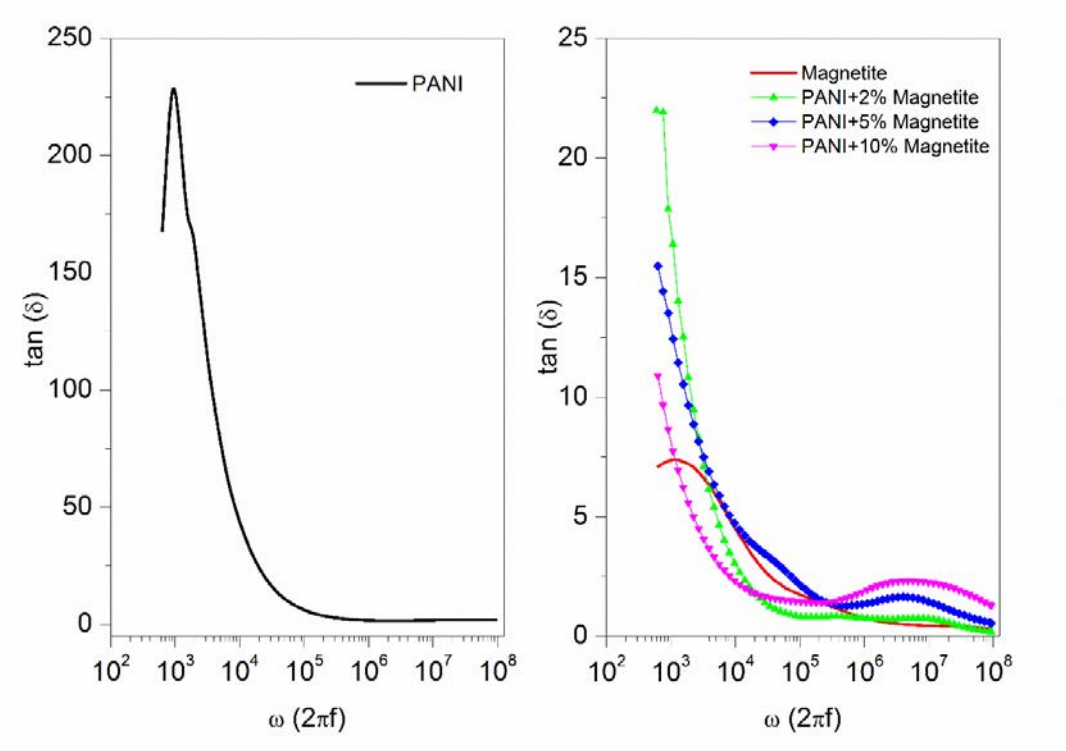


**Figure 4.33 :** Frequency dependency of the dissipation factor of PANI, Magnetite and Poly(aniline) – magnetite composites with different magnetit concentrations.

### 4.2.4 Preparation and characterization of poly (Thiophene)-Boron Nitride composites

Poly(thiophene)-TP/BN3 composites were prepared by using oxidative polymerization of thiophene in the presence of different weight percentage of BN3 (1% and 2%) and anhydro $FeCl_3$ as oxidant and chloroform as solvent . Spectroscopic characterizations of the composites of the poly(thiophene)-BN3 were investigated by FT-IR (Figure 4.34). In this study, TP and TP/BN3 composites were prepared by using oxidative polymerization of thiophene in the presence of different weight percentage of BN3 (1% and 2%). Spectroscopic characterizations of the composites of the poly (thiophene)-BN3 were investigated by FT-IR (Figure 4.34).

Two medium bands at 1488 and 1430 $cm^{-1}$ are assigned to stretching vibrational modes of the thiophene ring [97]. The peaks at 1366, and 1512 $cm^{-1}$ originate from BNs and in the poly(thiophene)/BN3 composite, the main peaks belongs poly(thiophene) such as 1292 $cm^{-1}$ aromatic C=S stretching absorption and 1034 Aromatic C=S stretching absorption combine and a new peak was observed at about 1366 $cm^{-1}$

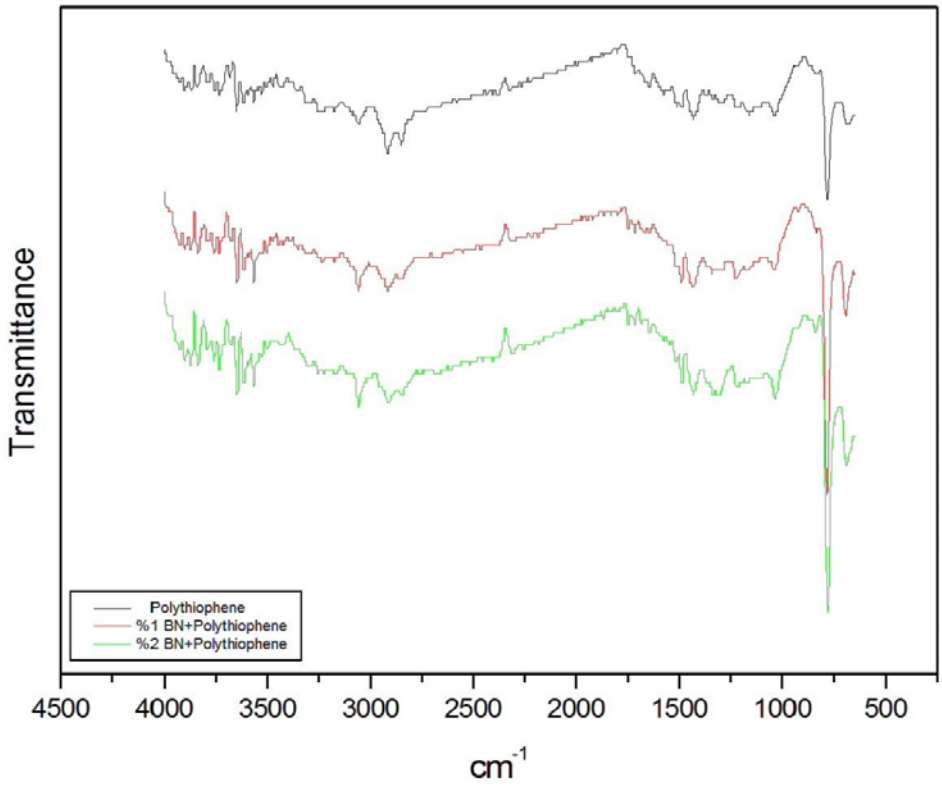


**Figure 4.34 :** FT-IR spectra of Poly(Thiophene)-BN3 Composites.

As shown in Figure 4.35a, the FE-SEM image of poly (Thiophene)/1% BN3 roughly indicated that porous structure of the composite was appeared. Increasing BN amount in Fig 4.35b, porousness of the composite are filled with BN3.

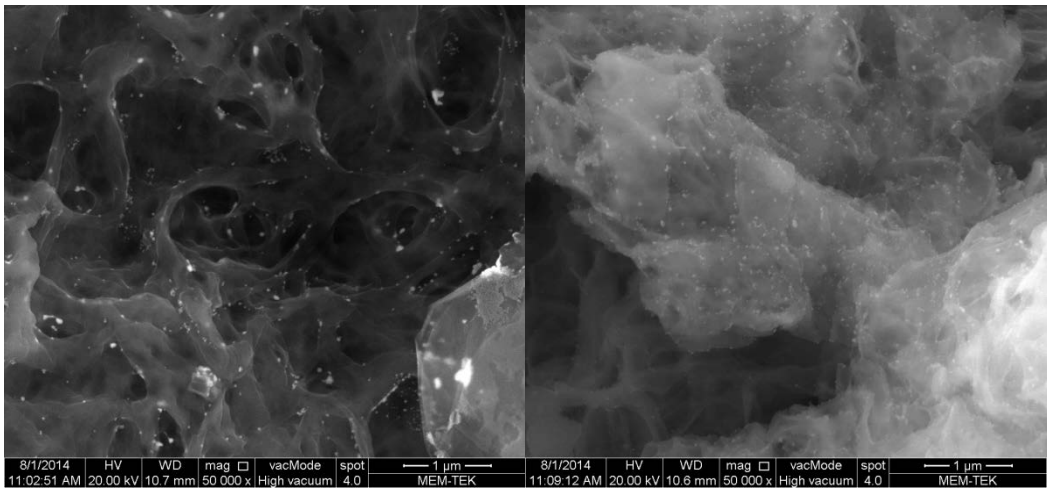


a) %1BN3+ Poly(thiophene) b) %2BN3+ Poly(thiophene)

**Figure 4.35 :** SEM images of a) %1 BN3+TP, b) %2BN3+TP.

The complex impedance $Z(\omega)$ is commonly used to separate the surface and bulk material properties [98]. The complex impedance for express the sample,

$$Z(\omega) = Z'(\omega) + iZ''(\omega) \quad \textbf{(4.17)}$$

$\omega$ is the angular frequency, $Z(\omega)$ and $Z^*(\omega)$ are the complex impedance and its complex conjugate, respectively. $Z'(\omega)$ and $Z''(\omega)$ are the real part, and the imaginary part of the complex impedance the response to an AC, respectively.

As shown in Figure 4.36, at low frequency the real impedance of %0 BN3+Poly(thiophene) sample is $4.39 \times 10^7$ Ω. Nevertheless real impedance of %1 BN3+Poly(thiophene) and %2 BN3+Poly(thiophene) values have decreased as 186980 Ω, 68147 Ω, respectively. This situation can explain, as the pores are filled with BN3 as shown in SEM image (in Fig 4.35) and by observing of decreases of impedance; these BN3 dipoles have contributed conductivity.

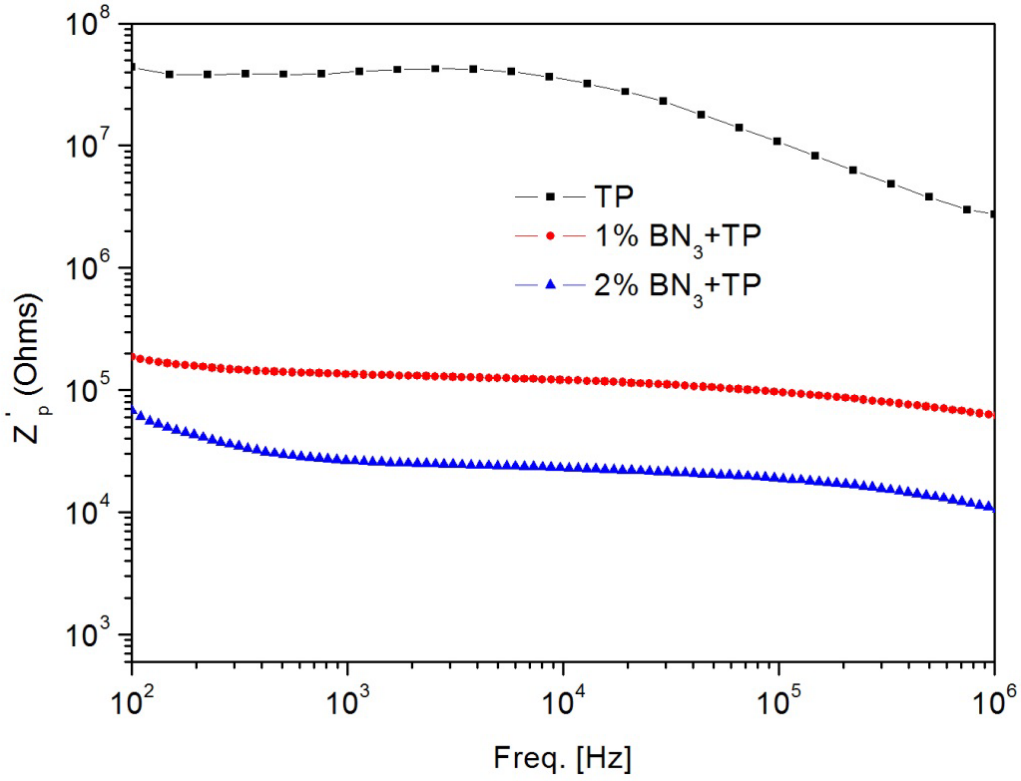


**Figure 4.36 :** Frequency variation of the real part of the impedance for Poly(thiophene) with different BN3 concentrations.

Thanks to this situation these samples can be contributed less draws current circuit applications. Impedance value reduce from $10^7$ Ω to about $10^4$ Ω with contribution of 2% BN3 and $10^3$ times improvement is seen.

As seen that in Fig 4.37, the imaginary part of impedance is shown that amount of energy loss. It is not observed critical frequency at AC frequencies (Fig 4.37a). These samples can be named that semiconductor polymer due to not observing critical frequency at measuring AC frequency because of strong loss energy properties of doped BN3 as dielectric material.

At Fig 4.37b and Fig 4.37c the critical frequency values of %1 BN3 and %2 BN3 are 1586.3 Hz and 4525.9 Hz, respectively. Also critical frequency peak decreases with increasing amount of BN3 as dielectric material. This result is shown that loss energy decreases. Vibration frequency of dipoles has increased as shrinking of peak.

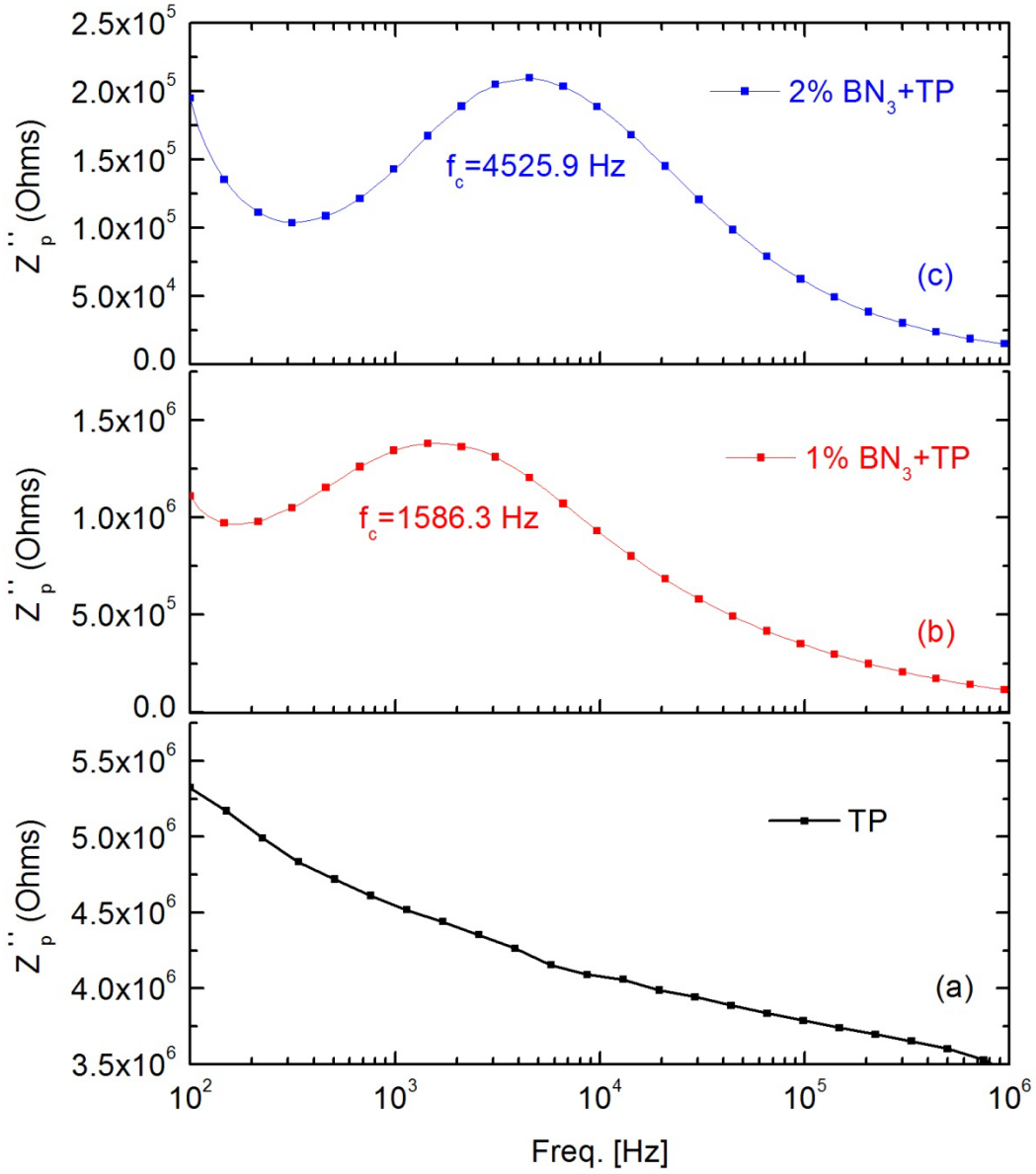


**Figure 4.37 :** Frequency variation of the imaginary part of the impedance for Poly(thiophene)/BN3 Composites; a) TP, b) %1BN3, and c) 2%BN3.

The real and the imaginary parts of the complex dielectric constants are described as. The complex conjugates of dielectric constant successive can be written as [99]:

$$\varepsilon^*(\omega) = \varepsilon'(\omega) - i\varepsilon''(\omega) = \varepsilon_\infty + \frac{\varepsilon_s - \varepsilon_\infty}{1 + (i\omega\tau)^{1-\alpha}} \quad \textbf{(4.18)}$$

Here, $\varepsilon^*(w)$ is the complex relative dielectric constant $\varepsilon_\infty$, $\varepsilon_s$ are high and low frequency dielectric permittivity, $\omega=2\pi$ times the frequency, and $\tau_0$ is a generalized relaxation time. The parameter α absorption coefficient changes from zero to one ($0 < \alpha \leq 1$)and this depends on doping $BN_3$. If $\alpha = 0$, it corresponds to standard Debye type relation. The α parameter calculated from the Eq. 4.19 and it has values different from zero as it is non-Debye type relation [100]:

$$\varepsilon'(\omega) = \varepsilon_\infty + (\varepsilon_s - \varepsilon_\infty)\frac{1 + (\omega\tau_o)^{1-\alpha}\sin\frac{1}{2}\alpha\pi}{1 + 2(\omega\tau_o)^{1-\alpha}\sin\frac{1}{2}\alpha\pi + (\omega\tau_o)^{2(1-\alpha)}} \quad \textbf{(4.19)}$$

It is calculated $\tau_0$ relaxation time and α absorption coefficient from equation (4.19) and they are fitted by the results given in Figure 4.39. The calculated $\tau_0$ and α value are given in Table 4.10. The absorption coefficient effects works of the Poly(thiophene) sample showed non-Debye type process and then this values are firstly decreasing to the standard Debye type with the BN3 doping amount. This works of the BN3/TP samples showed absorption coefficient effects which are non-Debye type process with the real part of the dielectric parameters. The increase in the relaxation times value of the real part of the dielectric constant equation is caused from doping dependency of high energy loss and strong dielectric BN3 materials.

**Table 4.10 :** Absorption coefficient α relaxation time $\tau_0$ (with the fitting and Adj. R-Square 0.99) of Poly (thiophene) with different concentrations BN3.

| Samples | $\alpha$ | $\tau_0$ |
|---|---|---|
| TP | 0.55 | $6.04\times10^{-5}$ |
| 1%$BN_3$ +TP | 172.8 | $3.95\times10^{-4}$ |
| 2%$BN_3$ +TP | 59067 | $6.65\times10^{-4}$ |

The dielectric relaxation strength Δε is the difference between the dielectric values at low and high frequencies. In the dielectric spectroscopy technique, the dielectric relaxation strength Δε is expressed as [101];

$$\Delta\varepsilon = \varepsilon_s - \varepsilon_\infty \quad \textbf{(4.20)}$$

where $\varepsilon_s$ and $\varepsilon_\infty$ are the low and high frequencies components of the real part of dielectric constant.

Figure 4.38 is shown that the changes of reel dielectric constant of samples based on frequency and measured value are 2,66 and 1,72 at low frequency and high frequency, respectively and the dielectric strength of Poly(thiophene) is 0.94. Dielectric constant of %1 BN3+Poly (thiophene) is 10422 and 10.13 at low frequency and at high frequency, respectively and the dielectric strength of %1 BN3+ Poly(thiophene) increased as 1411.87 with less doping BN3. For %2 BN3+Poly(thiophene); dielectric constant of %2 BN3+Poly(thiophene) is 45771 and 60.2 at low frequency and at high frequency, respectively and the dielectric strength of %2 BN3+Poly(thiophene) increased as 45710.8. As a result; thanks to contribution of BN3, these samples has effective dielectric strength and it is clear that this effective dielectric strength provide structural strength to samples.

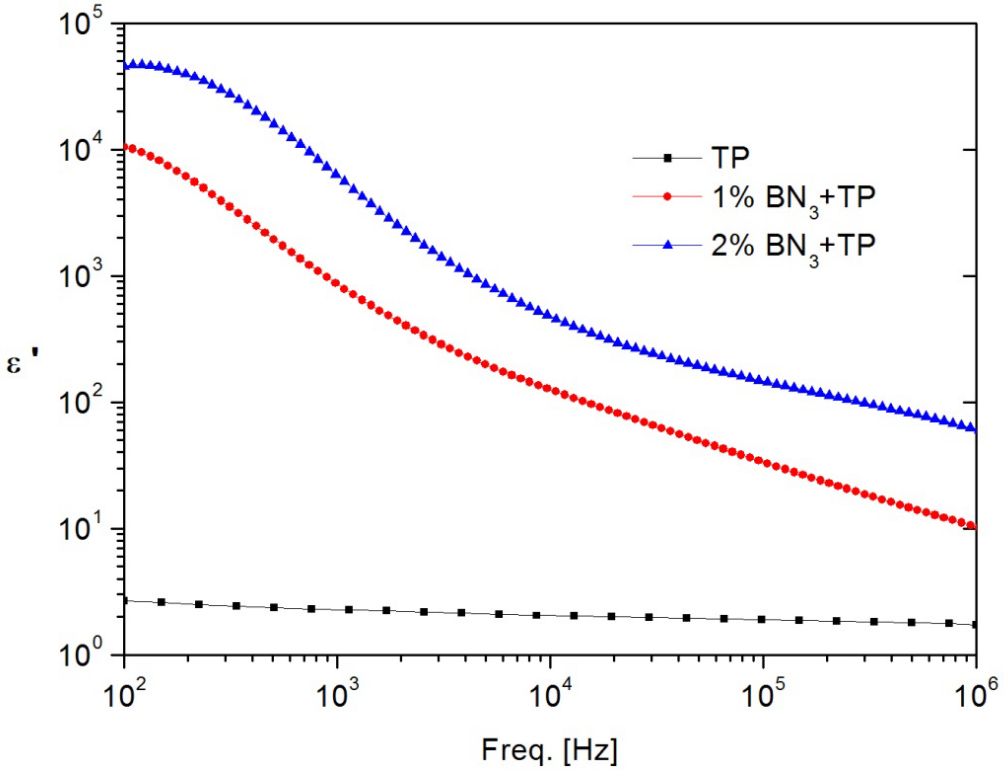


**Figure 4.38 :** Frequency evolution of the real part of dielectric constant for Poly(thiophene) with different BN3 concentrations.

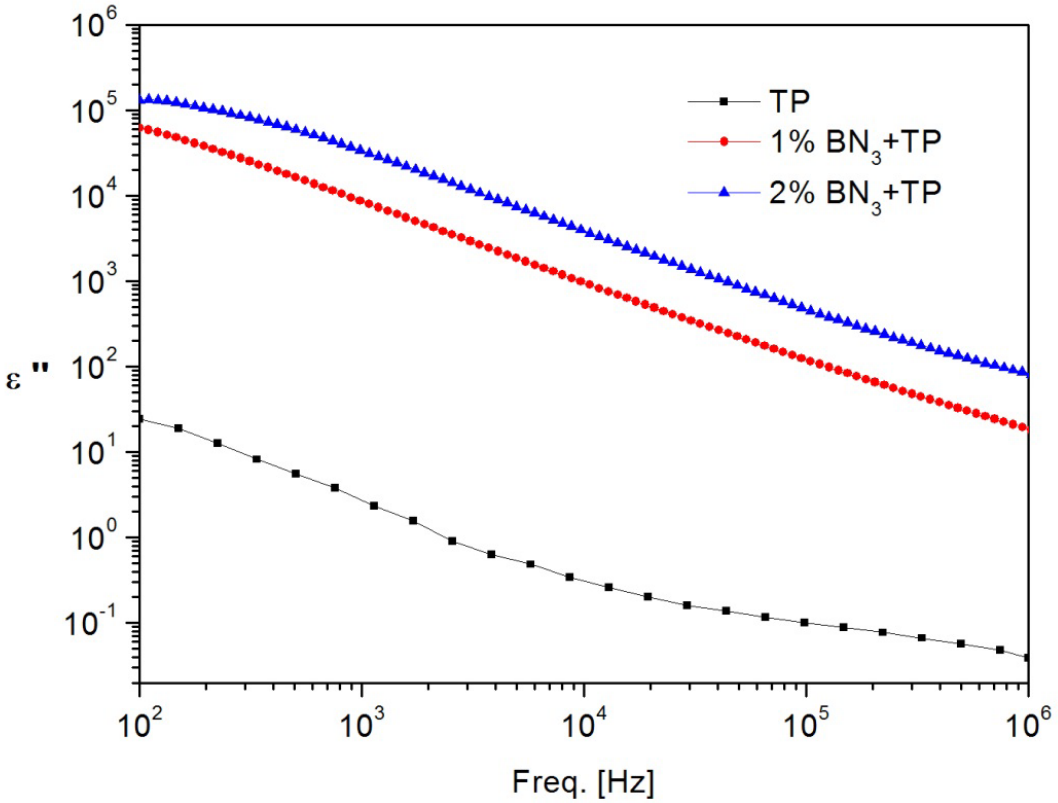


**Figure 4.39 :** Frequency evolution of the imaginary part of dielectric constant for Poly(thiophene) with different BN3 concentrations.

**Table 4.11 :** The imaginer part of the dielectric constant of the samples.

| | TP | %1$BN_3$+TP | %1$BN_3$+TP |
|---|---|---|---|
| Low frequency | 24.56 | 61966 | 131040 |
| High frequency | 0.04 | 18.2 | 81.4 |

In Figure 4.39 is shown that the changes of the imaginary part of the dielectric constant of samples based on frequency. By increasing amount of BN3, strength and imaginary part of energy storage is increased. As a result of this, it is gained the ability to facilitate transfer of energy. The changes of imaginary dielectric constants by contribution of BN3 is seen Table 4.11.

## 4.3 Characterization of The Side Chain Hydrogen Bonded Liquid Crystalline Poly(N-vinylcarbazole)(NVC)-co-poly(2-(dimethylamino)ethylmethacrylate) (DMAEM)

In this study, N-vinyl carbazole and 2-(Dimethylamino) ethyl methacrylate copolymer has been prepared as three composition depending on monomers ratio by free radical polymerization method. The amine content of the copolymer C3 was

calculated as 2.15 mmol amine/g copolymer. Polymerization conditions and the results are summarized in Table 4.12.

**Table 4.12 :** Synthesis of homopolymer and copolymers.

| Code | Composition of DMAEM (mole%) | Composition of NVC (mole%) | $M_n$ | $M_w$ / $M_n$ |
|---|---|---|---|---|
| HB-P | 100 | 0 | 16390 | 2.71 |
| C1 | 99 | 1 | 28335 | 2.22 |
| C2 | 80 | 20 | 16454 | 2.96 |
| C3 | 70 | 30 | 15867 | 3.13 |

[a]: Solvent : NMP, temperature: 70 $^0$C, time: 10 h.

The copolymer was used as hydrogen acceptor and the LC8 mesogen group as hydrogen donor.

### 4.3.1 Synthesis of hydrogen bond donor (LC8)

8-(4-Cyanobiphenyl-4'-oxy) octan-1-ol (LC8) and 11-(4-Cyanobiphenyl-4'-oxy) undecan-1-ol (LC11) were synthesized according to the synthetic route illustrated in Figure 4.40.

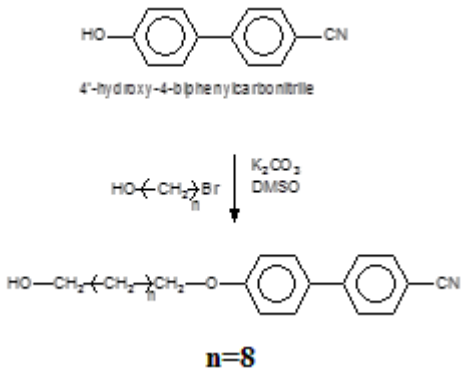


**Figure 4.40 :** Synthesis of hydrogen bond donor.

Spectral characterization of the LC8 was investigated by using FT-IR and H-NMR methods.

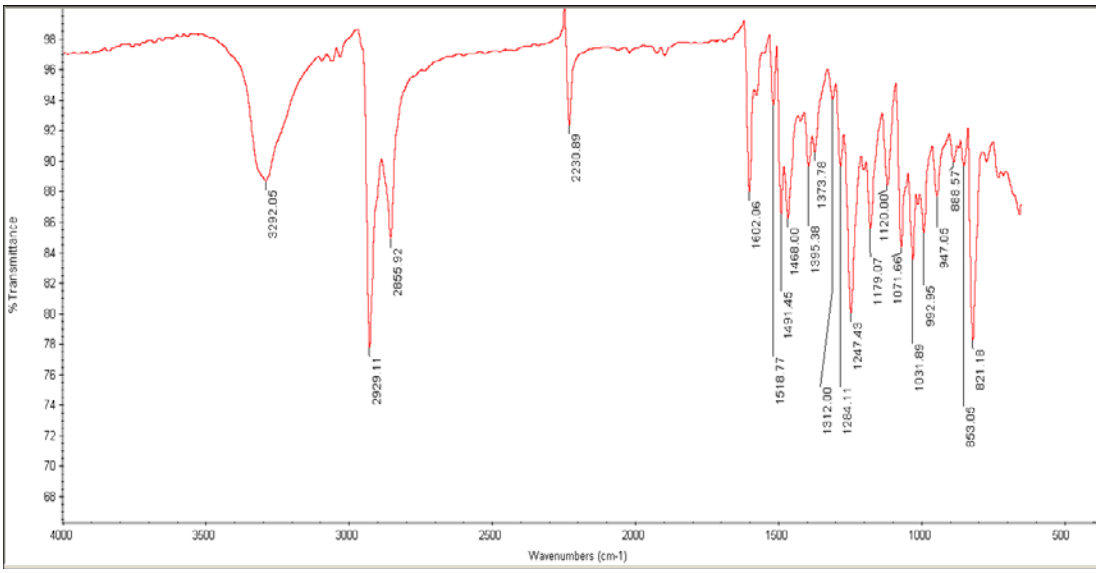


**Figure 4.41 :** FT-IR spectra of LC8.

FT-IR ($cm^{-1}$): 3500-3224 (OH, aliphatic), 2956- 2852 (CH, aliphatic), 2235 (CN), 1251, 1051 (C-O-C).

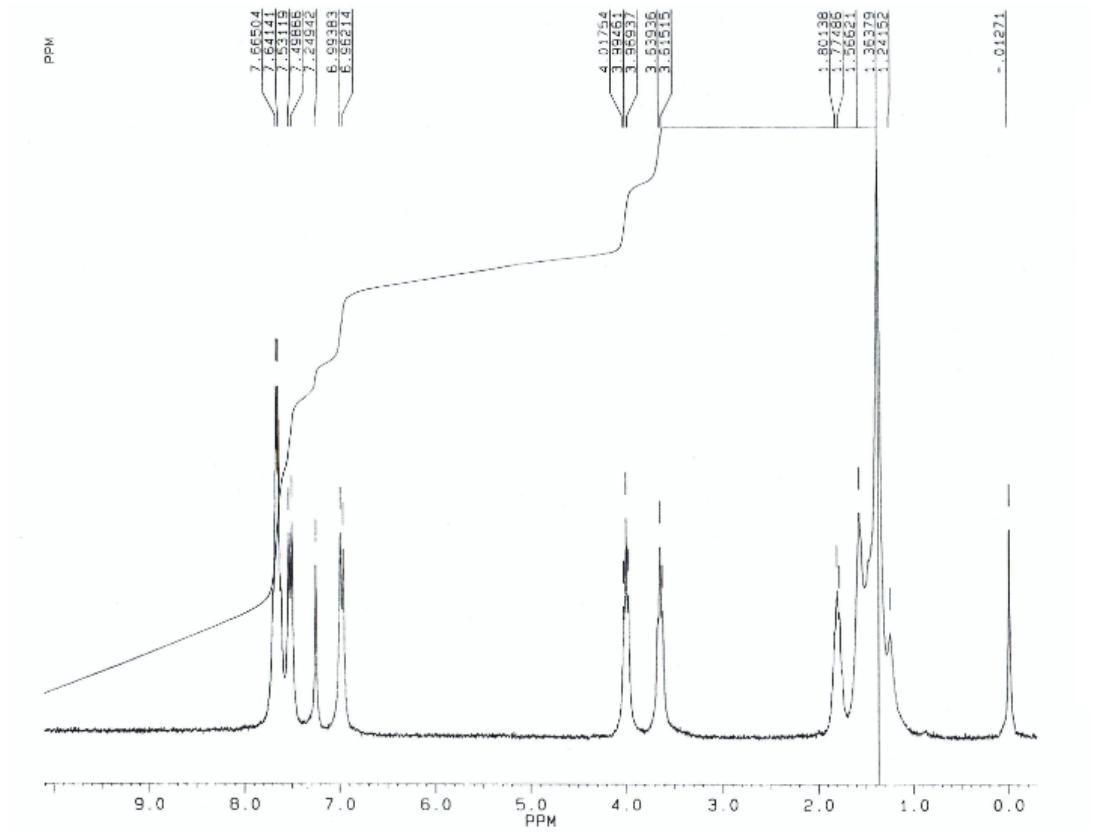


**Figure 4.42 :** 1H-NMR spectrum of the LC8.

$^1H$ NMR (50 MHz,$CDCl_3$): δ (ppm): 6.9–7.0 (m, 4H, aromatic), 3.9–4.0 (t, 2H, $CH_2$-O), 1.3–1.8 (m, 12H, -$(CH_2)_6$).

The obtained copolymer has been interacted with mesogen (LC8) to obtain hydrogen bonded side-chain liquid crystal copolymer.

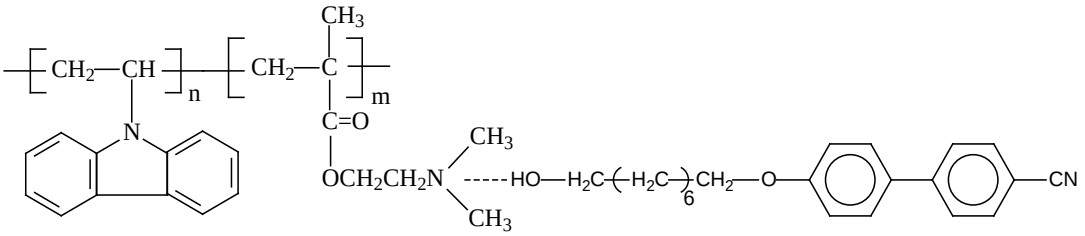

**Figure 4.43 :** Preparation of the side chain liquid crystal copolymer.

The structures of the copolymers and hydrogen bonded side chain liquid crystalline copolymers were also characterized using 1H-NMR spectroscopy and the results confirmed the synthesis of polymers (Figure 4.44). The peaks among the 2.57-2.70 ppm and 7.7-7.0 ppm correspond to the protons ($CH_3$-N and $COOCH_2$) of the 2-(Dimethylamino)ethyl methacrylate units and aromatic protons of the vinyl carbazole and 8-(4-cyanobiphenyl-4'- oxy)octan-1-ol units, respectively.

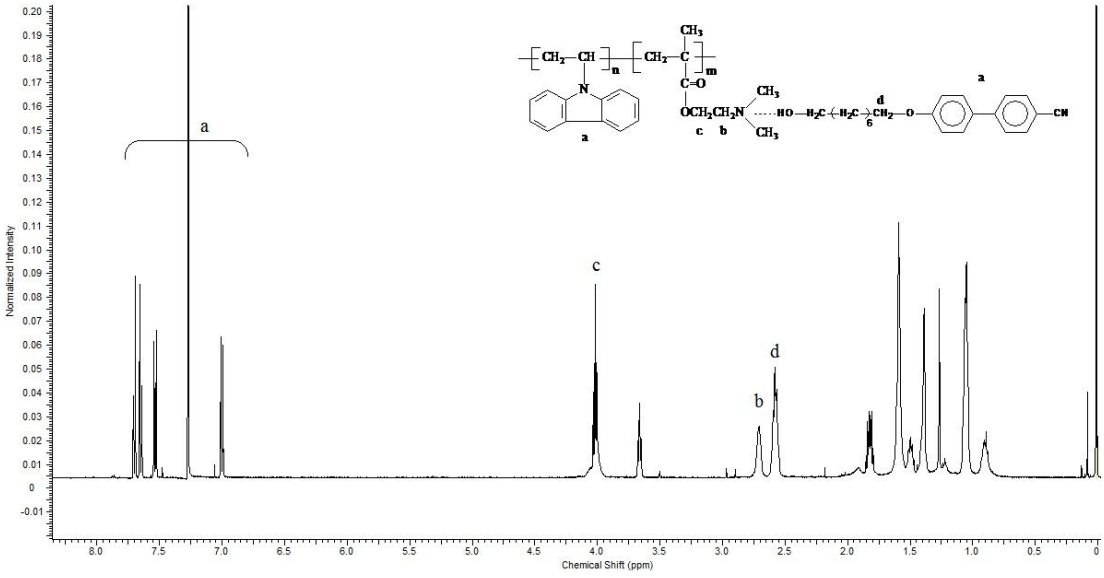


**Figure 4.44 :** The H-NMR Spectrum of side chain liquid crystal copolymer C3-LC8.

The IR spectra of the H-acceptor copolymer C3 and its H-bonded complexes C3-LC8 shown in Figure 4.45, are compared in order to analyze the formation of H-bond. The broad spectral shape in the O–H stretching region at about 3300 $cm^{-1}$ should be an evidence for hydrogen- bonds through the hydroxyl group in the LC8.

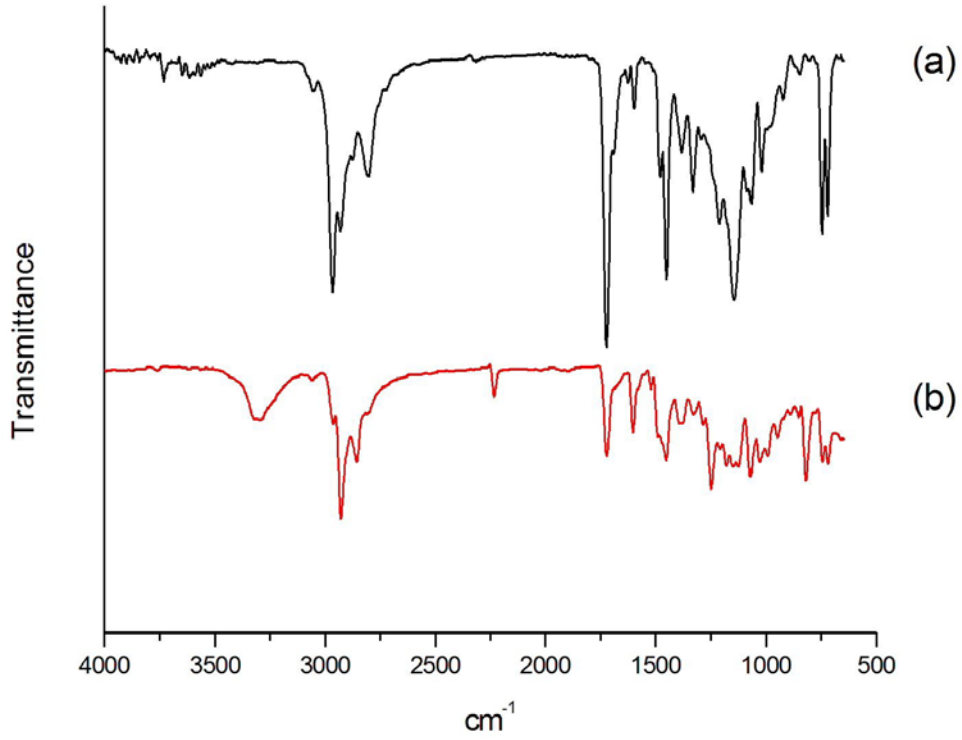


**Figure 4.45 :** FT-IR spectrum of poly(N-vinylcarbazole)-co-poly(2-(Dimethylamino)ethylmethacrylate)(C3)(a);hydrogen bonded side-chain liquid crystal copolymer(C3-LC8)(b).

### 4.3.2 Thermal and mezophase properties of 8-(4-cyanobiphenyl-4'-oxy) octan-1 ol (LC8)

The DSC heating and cooling scans for LC8 shown in Figure 4.46. The heating scan for LC8 shown in Figure 4.46 shows two sharp peaks at 76.2 °C and 90.7 °C corresponding to melting points of polymorphic crystal structure and a broad peak at 112.6°C corresponding isotropic transition respectively. The textures of the mesophase was identified during both heating and cooling cycles as being a nematic mesophase at 106 °C.

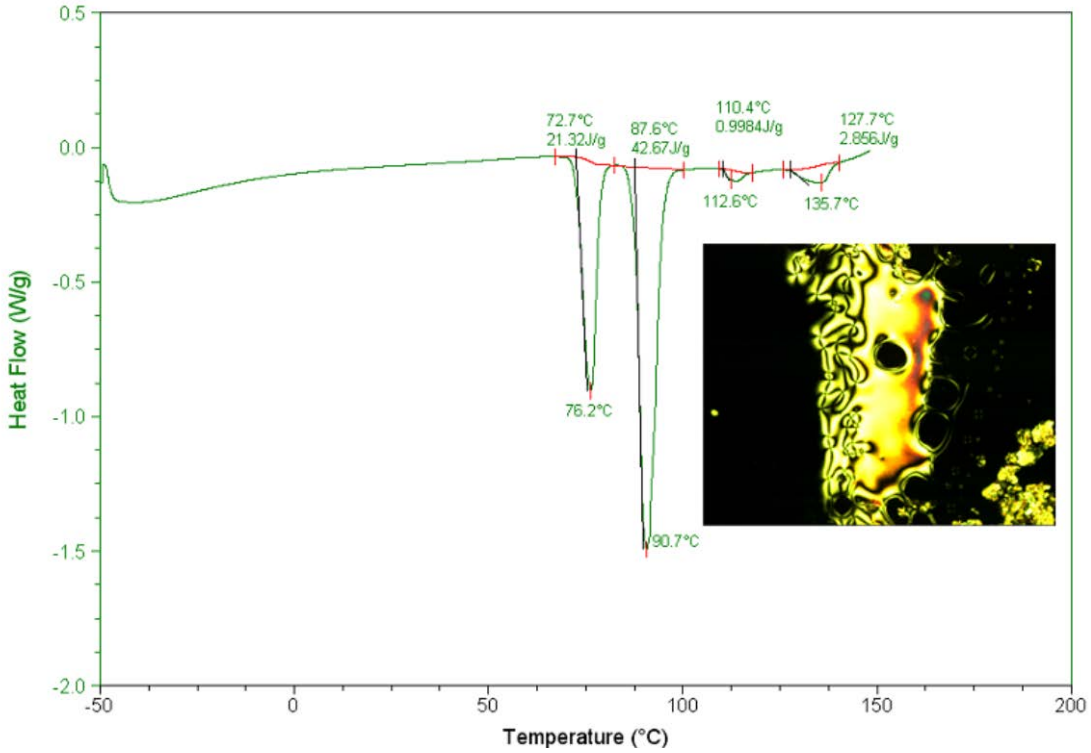


**Figure 4.46 :** The DSC heating and cooling scans for LC8.

### 4.3.3 Thermal and mezophase properties of H-bonded side chain LC copolymers

Thermal and liquid crystalline properties of H-bonded LC copolymers containing different ratios carbazole groups (C1, C2 and C3) and H-bonded liquid crystalline homopolymer HB-P were investigated by DSC and POM.

Investigations by DSC and POM showed that all compounds exhibit one liquid-crystalline mesophase. The DSC and POM observations revealed that all of the compounds exhibit enantiotropic nematic phase liquid crystals. Results are summarized in Table 4.13.

**Table 4.13 :** Thermal parameters of the compounds determined by DSC.

| Code | Phase Transition Heating (˚C) | | | Corresponding ΔH, J/g |
|---|---|---|---|---|
| HB-P | 90K | 78N | 107I | 41.32 |
| C1 | 90K | 104N | 107I | 30.29 |
| C2 | 90K | 80N | 130I | 26.55 |
| C3 | 85K | 74N | 96I | 18.18 |

The DSC heating scans for HB-P (Fig 4.47 a) and copolymers C1 (Figure 4.47 b), C2 (Figure 4.47 c) and C3 (Figure 4.47 d) show single peaks at 91,17°C, 91.11 °C, 88.65 °C and 89.80 °C, respectively corresponding to transition to izotropic phase which is compatible with the POM results. A mesophase region was not detected during heating or cooling scans by DSC. Glass transition temperature for the copolymers can not be detected.

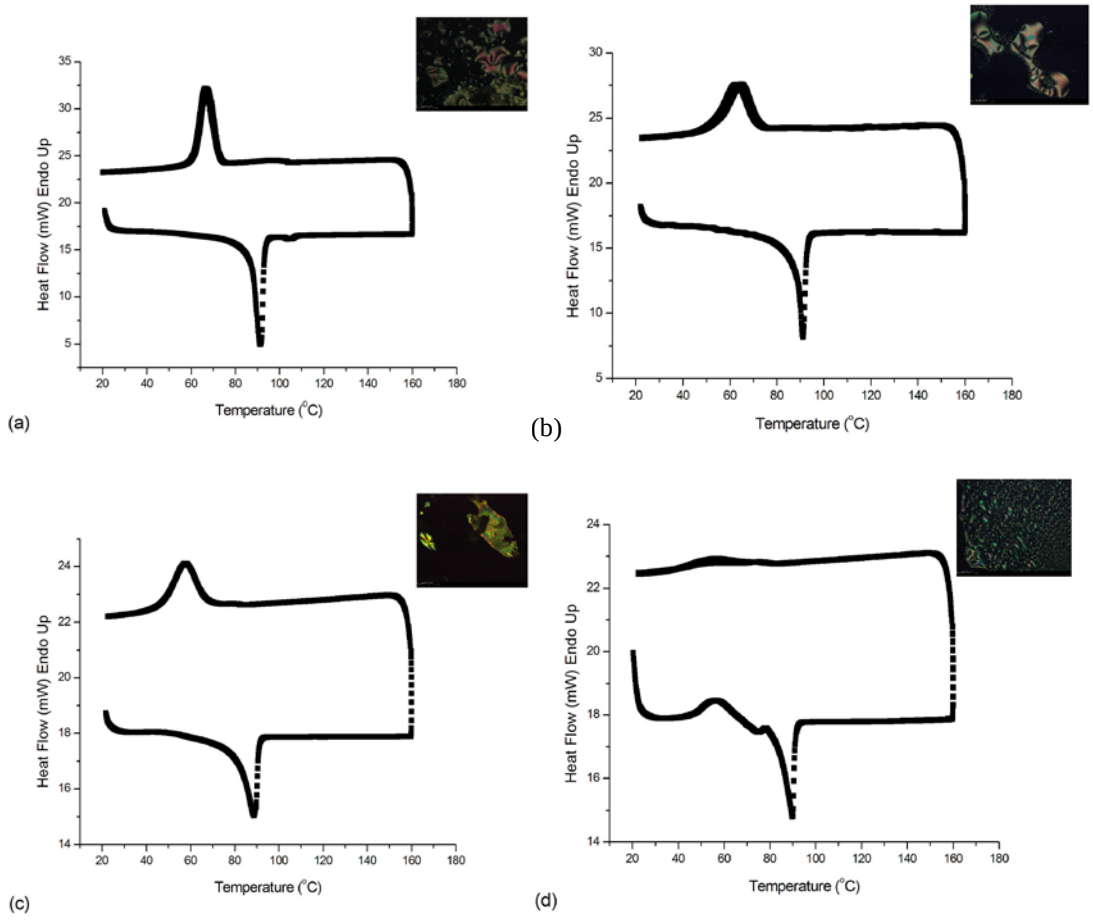


**Figure 4.47 :** DSC thermograms of HB-P (a), C1 (b), C2 (c), and C3 (d) at a rate 10 K.min-1 and mesophase textures.

### 4.3.4 Dielectric properties

For the liquid crystals studied, the complex dielectric constant is defined as,

$$\varepsilon^*(\omega) = \varepsilon'(\omega) - i\varepsilon''(\omega) \qquad \textbf{(4.21)}$$

where is the real and is the imaginary parts of the dielectric constant. Angular frequency ω referred to by the radial frequency, ω=2πf where, f is the frequency (measured in hertz). The dispersion curves of the 8-(4-cyanobiphenyl-4'-oxy) octan-1-ol (LC8) and H-bonded Side Chain LC Copolymers (HB-PLC) doped LC8 coded

LCs at room temperatures (RT) are shown in Figure 4.48. The real part of the dielectric constant decreases with increasing frequency. But, at lower frequencies, decreases significantly with increasing doped 1% HB-PLC(w/w). This suggests that the doped HB-PLC facilities molecular reorientation in liquid crystals.

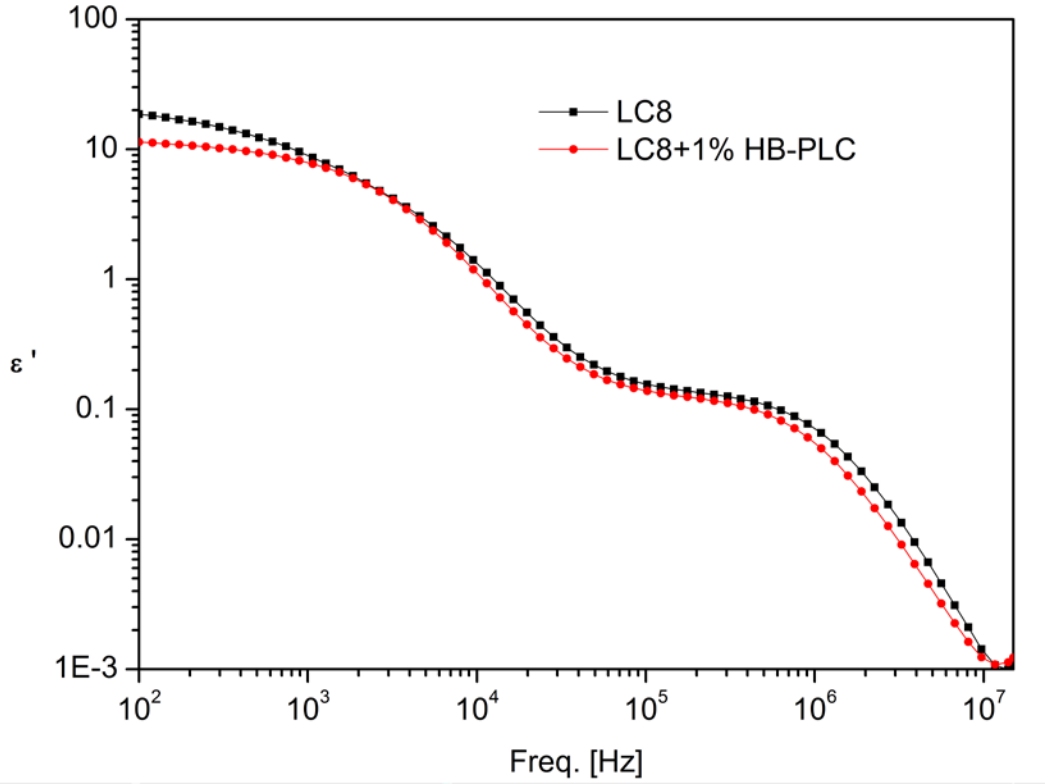


**Figure 4.48 :** Dependence of real dielectric constant on frequency ( $\varepsilon'$ -log*f*) plots of LC8 and LC8+1%HB-PLC**.**

Figure 4.49 show the absorption curves of the LCs. The absorption curves of the LCs shows a dielectric relaxation peak. The position of the peak shifts to higher frequencies with doped HB-PLC. This suggests that a doping-dependent relaxation process is taking place in LCs. Furthermore, the positions of the relaxation peak are changed with the orientation configurations of pure LC8 and LC8+HP-PLC liquid crystals. The maximum peak value is defined as dielectric relaxation frequency. The position of the peak shift to the higher frequencies by the doping 1% HB-PLC.

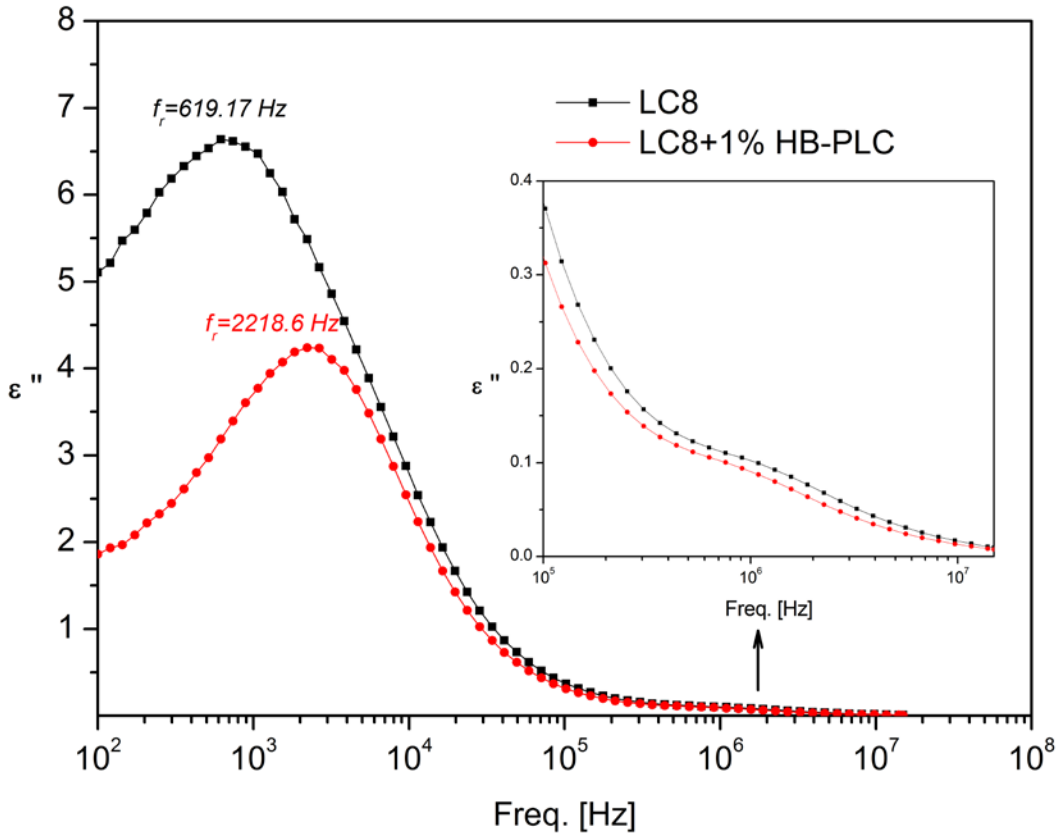


**Figure 4.49 :** Dependence of imaginary dielectric constant on frequency ($\varepsilon''$-log*f*) plots of LC8 and LC8+1%HB-PLC**.**

The dielectric dispersion curves are described by the Cole-Cole relation [103-105],

$$\varepsilon^*(\omega) = \varepsilon_\infty + \frac{\varepsilon_s - \varepsilon_\infty}{1 + (i\omega\tau_o)^{1-\alpha}} \qquad \textbf{(4.22)}$$

where $\varepsilon^*(\omega)$ is the complex dielectric constant, $\varepsilon_s$ is the limiting low-frequency dielectric constant and $\varepsilon_\infty$ the limiting high-frequency dielectric constant, $\tau_o$ is the average relaxation time, $\omega$ is the average angular frequency, α is the distribution parameter.

The dielectric strength $(\Delta\varepsilon) = \varepsilon_s - \varepsilon_\infty$, and all parameters except $\tau$ have been designated from the experimental results are shown in Table 4.14. $\tau$ is the characteristic or principal relaxation time, $\alpha$ $(0<\alpha<1)$ is an empirical parameter which is related to the width of the relaxation peak, and $\omega$ is the angular frequency. If the centers of the semicircles lie $\varepsilon'$ axis, α is zero (Debye type) [26]. The relaxation phenomenon is analyzed by Cole-Cole plots. The plots of $\varepsilon''$ vs $\varepsilon'$ for LC8 and LC8/HB-PLC LCs are shown in Figure 4.50. The plots indicate semi-circles

and are passing through the origin. The center is located on the real axis which is explained by Debye type properties. The parameter, $\alpha$, has values different from zero for LCs. For a mono-dispersive relaxation process, one expects the circle center is located exactly on the ε'-axis, whereas for a poly-dispersive process, the circle center will be located below the ε'-axis. It is evident from these plots that the relaxation process differs from the mono-dispersive Debye type process (for which α = 0) [106], and poly-dispersive situation non-Debye type process (for which $\alpha \neq 0$). The plots obey Cole-Cole type dispersion with a distribution of relaxation times. The presence of the semi-circle center will be located below and the complex dielectric constant shows the poly-dispersive situation non-Debye type of the dielectric properties of the pure LC8 and LC8/HB-PLC LCs samples.

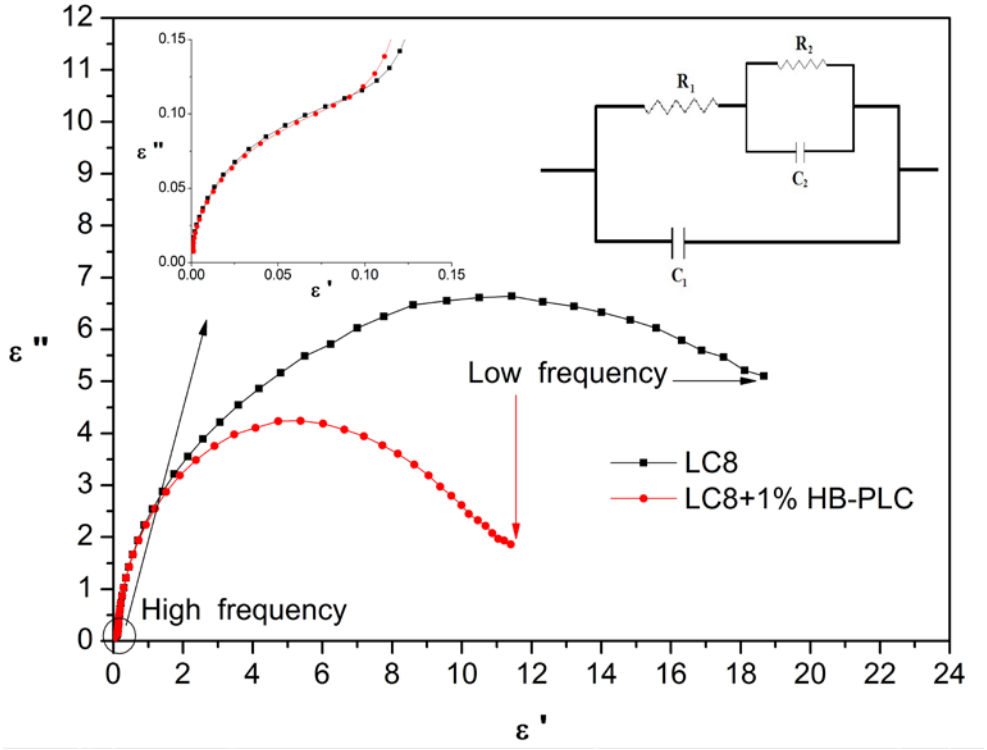


**Figure 4.50 :** Cole-Cole plots of the LCs of LC8 and LC8+1%HB-PLC.

As a result, the relaxation for LC8 and LC8/HB-PLC are a non-Debye type due to $\alpha$ $\alpha \neq 0$. This behaviour is probably due to the dipolar rotation around the long molecular axis. The $\varepsilon_s$ and $\varepsilon''_{max}$ values were calculated from the Cole-Cole curves and are given in Table 4.14. $\varepsilon_s$ values decrease with doped HB-PLC. This suggests that $\varepsilon_0$ values of the relaxation process are associated with the reorientation of molecules [106].

**Table 4.14 :** The dielectric parameters of LC8 and LC8/HB-PLC LCs.

| Sample | $\varepsilon_s$ | $\varepsilon_\infty$ | $\Delta\varepsilon$ | $\varepsilon''_{max}$ |
|---|---|---|---|---|
| LC8 | 18.664 | 0.00104 | 18.663 | 6.63 |
| LC8/HB-PLC | 11.399 | 0.00170 | 11.398 | 4.23 |

Depending on the distinctive orders of magnitude for the relaxation time, which is defined as the time-constant RC in the equivalent circuit to be an indication of the transport process, a series array of parallel RC elements may give rise to independent or overlapping semi-circular arcs in the two complex planes. Thus, the Cole–Cole plots can be accurately represented by an equivalent RC circuit model in the inset in Figure 4.50.

## 5. CONCLUSION

In this thesis, new conducting polymers, PANI and polythiophene based composites were prepared and characterized.

Propiolic acid doped polyaniline was synthesized and electrical characterizations were investigated. The impedance behavior decrease with the increases temperature in the lower frequency and it has critical resonance frequency in the higher frequency for undoped PANI. Nevertheless the change of impedance with respect to temperature was not regular at low frequency, but max peak values appeared and critical resonance frequency disappeared at high frequency. This was seen as the same for the AC conductivity behavior. The critical frequency and maximum peak frequency values for undoped PANI are smaller than doped PANI, respectively. The impedance of doped PANI material decreases with the ionic conductivity increases for undoped PANI material.

Conducting polymer materials are very important novel materials. Chalcone subtitued PANI was synthesized and characterized. The impedance values monotically decreases with frequency of the new synthesized ionic polymeric materials. There liable results correlated by Kramers–Kronig relations and impedance variation exhibits new conductive polymer materials. The phase angle for new aniline derivative shows molecular behavior between $10^2$ Hz and $10^7$ Hz. The dipolar effects for phase angle (~$20^0$) are seen in the frequency range of low-frequency ($10^2$–$10^3$ Hz) regime. The phase angle of the loaded aniline and HBr in the chalcone originated from the ionic effects between $10^3$–$10^5$ Hz from the phase angle. The electronic properties rise in the frequency range of $10^5$–$10^7$ Hz. In addition, the phase angles are nearly $90^0$ for all ions loaded Cs-PANI near $10^7$ Hz frequency. Therefore, the ionic impedance depends on the frequency for new polymeric materials synthesized in the loaded polyaniline and HBr for the chalcone. The angular frequency dependency of AC conductivity of the Cs-PANI obeyed in terms of the correlated barrier hopping (CBH) model.

In this study, side chain hydrogen bonded liquid crystalline copolymers similar H-bonding approaches are applied to the carbazole containing photoconductive copolymer consisting of N,N-dimethyl amino moieties as H-bond acceptor in the presence of 8-(4-cyanobiphenyl-4 (-oxy)octan-1-ol(LC8) as a hydrogen bond donor LC8 and HB-PLC have been confirmed ,using FTIR,DSC, POM studies. Dielectric properties of HB-PLC in LC8 nematic liquid crystal have been investigated by the dielectric spectroscopy method. Pure LC8 and HB-PLC doped LC8 liquid crystals exhibit a relaxation process coordinating from log–log plotting analyzed with the real part of dielectric constant. The obtained results suggest that dielectric relaxation process taken place in LCs is a non-Debye type relaxation behavior. It is observed that doping of the liquid crystals with HB-PLC alters dielectric behavior and relaxation frequency ($f_r$) of LCs. The dielectric strength values of the LCs decrease with HB-PLC doping. The proposed doping methods in the new synthesis HB-LCP and LC8 coded nematic meso phase system are investigated by Liquid Crystal Cells. They are characterized with the inclusion of equivalent two RC circuits of Cole–Cole plot for a powerful stimulation of cells for displays.

The second part of the thesis, conducting polymer composites were prepared and characterizations were performed by using spectroscopic and physical methods.

Polyaniline-NanoClay composites were successfully obtained by polymerizing aniline in the presence of ammonium persulfate, boric acid and NanoClay by chemical oxidative method. From these XRD patterns, FT-IR and the SEM photographs are observed intercalation of PANI in NanoClay. This justified the objective that this clay can be used for synthesizing PANI+NanoClay composite. The shifts in IR peaks of the PANI+NanoClay samples suggest interaction between the PANI+NanoClay composites. The morphological study from the SEM analysis shows the compact morphology with the increase in NanoClay. The dielectric strength $\Delta\varepsilon$ decreases with increases the amount of the contribution of nanoclay. This result is consistent with the electrical behavior of the PANI+20%NC material. According to dissipation factor plots, the materials present the first relaxation times at low frequencies and second relaxation times at high frequencies. It is shown that lowest first and lowest second relaxation time is PANI+5%NC and PANI+20%NC, respectively. Four point probe measurements are used to improve the dispersion of surface electrical conductivity of PANI and PANI+NanoClay composites. The dielectric strength decreasing value exhibits low dielectric and the surface resistivity

increasing value exhibits high resistance. Doped new polymers play an essential role in the high-quality and decreased-porosity strong materials with increases the amount of the contribution of NanoClay.

PANI/GH powder composites have been prepared by oxidative polymerization of aniline in the presence of different weight percentage of graphite powder and boric acid as a doping agent. The dispersion of graphite powder within the PANI have evidenced by SEM and FT-IR examinations. The frequency evolution of real part ($Z^{'}$), imaginary part ($Z^{''}$) of the impedance, the real part of the dielectric constant, and the AC conduction for PANI doped 2%, 5% and 10% GHs have been investigated using the impedance spectroscopy at room temperature. The critical frequency decreases with the doping.

In this work, the dipolar polarization behaviors in the high frequency regions have been obtained for PANI doped 2%, 5% and 10% GHs at RT. The absorption coefficient observed nearly-Debye type mechanism for the all samples. The ionic conduction mechanism for PANI doped 2%, 5% and 10% GHs were prevented for the s parameter the system alters its conductivity from dc to Correlated Barrier Hoping (CBH) Mechanism.

PANI-Magnetite composites were prepared different weight percentafe of magnetite as 2%,5% and 10% The EPR, ac conductivity and impedance properties of the magnetite doped polyaniline composites have been investigated. Magnetic measurements were studied between 500 G-7000 G. g factor of the composites were found as between 2.005 and 2.3248 increasing of magnetite quantity.

The ionic conductivity properties for magnetite, PANI and magnetite doped 2%, 5% and 10% PANI were prevented tree regions for the “s” parameter the system alters its conductivity types from dc in the low frequency region to Correlated Barrier Hoping (CBH) Mechanism in the high frequency regions.

## REFERENCES


**[1] Pei , J., Yu, W. L., Huang, W., Heeger, A. J.** (2000). A novel series of efficient thiophene-based light-emitting conjugated polymers and application in polymer light emitting diodes. *Macromolecules, 33,* 2462-2471.

**[2] Gurunathan, K., Vadivel Murugan, A., Marimuthu, R., Mulik, U. P., Amalanerkar , D. P., Mater, J.** (1999). Electrochemically synthesised conducting polymeric materials for applications towards technology in electronics, optoelectronics and energy storage devices. *Materials Chemistry and Physics, 61,* 173-191.

**[3] Bhadra, S., Singha , N.K., Khastgir , D.** (2006) Polyaniline by new miniemulsion polymerization and the effect of reducing agent on conductivity. *Synth. Met., 156,* 1148–1154.

**[4] Bhadra, S., Chattopadhyay, S., Singha, N.K., Khastgir, D.** (2008). Improvement of conductivity of electrochemically synthesized polyaniline. *Appl, J.. Polym Sci., 108,* 57-64.

**[5] Selvam, P., Nanjundan, S.,** (2005). Synthesis and characterization of new photoresponsive acrylamide polymers having pendant chalcone moieties. *Reactive & Functional Polymers, 62,* 179–193

**[6] Tazuke, S.** (1982). *Developments in Polymer Photochemistry,* Applied Science; Publishers, London, UK.

**[7] Reichmanis, E., Nalamasu, O., Houlihan, F.M, Novembre, A.E.** (1999). Radiation Chemistry of Polymeric Materials: Novel Chemistry and Applications for Microlithography. *Polym. International., 48,* 1053.

**[8] Sakai, Y., Ueda, M., Fukuda, T., Matsuda, M,.** (1999). Synthesis and properties of a second-order nonlinear optical side-chain polyimide. *Polym, J.. Sci. Part A: Polym. Chem.,* 37, 1321-1329.

**[9] Ohe, Y., Kume, M., Demachi, Y., Taguchi, T., Ichimura, K..** (1999). Application of a novel photopolymer to a holographic head-up display, *Polym. Adv. Technol., 10,* 544-553.

**[10] Perny, S., Le Barny, P., Delaire, J., Buffeteau, T., Sourisseau, C.,** (2000). Molecular orientation and liquid crystal alingment properties of new cinnemate-based ohotocrosslinkable polymers. *Liq. Cryst., 27,* 341.

**[11] Kawatsuki, N., Sai, I., Yamamota, T.,** (1999). Linearly polarized ultraviolet photoreaction of photocrosslinkable polymers comprising the p-phenylenediacrylate group and photoalignment control of liquid crystals on the resultant film. *Polym, J.. Sci. Part A: Polym. Chem., 37* 4000.

**[12] Erddalane, A., Fouassier, J.P., Morlet-Savary, F., Takimoto, Y.,** (1996). Efficiency and excited state processes in a three-component system, based on thioxanthene derived dye/amine/additive, usable in photopolymer plates. *Polym, J.. Sci. Part A: Polym. Chem. 34,* 633.

**[13] Boichuk, V; Kucheev, S; Parka, J; Reshetnyak, V; Reznikov, Y; Shiyanovskaya, I; Singer, KD; Slussarenko, S**. (2001). Surface-mediated light-controlled Friedericksz transition in a nematic liquid crystal cell. *J. Appl.Phys. 90,* 5963-5967.

**[14] Han, X., Zhang, S., Shanks, R. A., Pavel, D.,** (2008). Poly(4-vinylpyridine)-based hydrogen bonded side-chain liquid crystal polymers. *React. Funct. Polym., 68,* 1097-1102.

**[15] Stewart, D., Imrie, C. T.,** (1996). Poly(4-vinylpyridine)-based hydrogen bonded side-chain liquid crystal polymers. *Liquid Crystals, 68,* 1097-1102.

**[16] Alder, K. I., Stewart, D., Imrie, C. T.,** Mater, J.. Chem (1982)

**[17] Gustafsson, G., Cao, Y., Treacy, G.M., Klavetter, F., Colaneri, N., Heeger, A.J.,** (1992). Flexible light-emitting diodes made from soluble conducting polymers, *Nature* 357, 477–479.

**[18] Riede, A., Helmstedt, J., Riede, V., Zemek, J., Stejskal, J.,** (2000). In situ polymerized polyaniline films. 2. Dispersion polymerization of aniline in the presence of colloidal silica. *Langmuir, 16,* 6240–6244.

**[19] Kar, P.,** *Doping in conjugated polymers* (2013), Wiley.

**[20] Drobny, J. G.** (2012). *Polymers for electricty and electronics Materials, Properties, and Applications,* Drobny Polymer Associates Merrimack, New Hampshire, Wiley.

**[21] Chandrasekhar, P.** (1999). *Conducting Polymers: Fundamentals and Applications,* Springer.

**[22] Zhou, H., Lin, Y., Yu, P., Su L., Mao, L.,** (2009). Doping polyaniline with pristine carbon nanotubes into electroactive nanocomposite in neutral and alkaline media. *Electrochemistry Communications, 11,* 965–968

**[23] Parajuli, R. R.** (2011) Developing conducting polymer nanocomposites with carbon nanomaterials for molecular detection and fuel cell applications, newark, PhD Thesis, The State University of New Jersey, New Jersey

**[24] Yang X.** (2012). *Semiconducting Polymer Composites Principles, Morphologies, Properties and Applications*, Wiley.

**[25] Huang, J1., Kaner, RB.** (2006). The intrinsic nanofibrillar morphology of polyaniline. *Chem Commun (Camb). 28,* 367-76.

**[26] Henry, D. T., M. D'Arcy, J., Yue Wang, Beltramo, P. J., Strong, V. A., Kaner, R. B.** (2010). The oxidation of aniline to produce ''polyaniline'': a process yielding many different nanoscale structures. *Journal of Materials Chemistry, 21,* 3534-3550.

**[27] Parajuli, R. R.** (2011) Developing conducting polymer nanocomposites with carbon nanomaterials for molecular detection and fuel cell applications, newark, *PhD Thesis*, The State University of New Jersey, New Jersey

**[28] Yılmaz, F.** (2007). Polyanılıne: synthesıs, characterızatıon, solutıon propertıes and composites, *Ph.D. Thesis*, Middle East Technical University, Ankara

**[29] Url-1** <*http://lbytpmd.seu.edu.cn/nano/?type=detail&id=341*>, date retrieved 01.06.2015.

**[30] Roncali, J.** (1992). Conjugated Polythiophenes: Synthesis, Functionalization and Applications. *Chem. Rev*., *92*, 711-738.

**[31] Druy, M. A., Rubner, M. F., Walsh, S. P.** (1986). An experimental approach towards the synthesis and characterization of environmentally stable conducting polymers. *Synthetic Metals, 13*, 207.

**[32] Toshima N., Hara S.** (1995). Direct Synthesis of Conducting Polymers from Simple Monomers, *Prog. Polym. Sci., 20*, 155-183.

**[33] Url-2** <*http://upload.wikimedia.org/wikipedia/commons/thumb/0/0e/Poly.png*>, date retrieved 01.06.2015.

**[34] Huang, C. F., Hsieh, Y.A., Hsu, S. C., Matyjaszewski, K.** (2014). Synthesis of poly (N-vinyl carbazole)-based block copolymers by sequential polymerizations of RAFT-ATRP. *Polymer, 55*, 6051-6057.

**[35] Grazulevicius J.V., Strohriegl P., Pielichowski J., Pielichowski K.** (2003). carbazole containing polymers: synthesis properties and application. *Prog Polym Sci., 28*, 1297-353.

**[36] Petukhova, A., Greener, J., Liu, K., Nykypanchuk, D., Nicolay, R., Matyjaszewski K., et al.** (2012). Standing Arrays of Gold Nanorods End-Tethered with Polymer Ligands. *Small*, 8, 731-737**.**

**[37] Sawamoto, M, Fujimori, J, Higashimura, T.** (1987). Living cationic polymerization of N-vinylcarbazole initiated by hydrogen iodide. *Macromolecules*, *20*, 916-920.

**[38] Url-3** <*http://www.mpbio.com/images/product-images/molecular-structu.png*>, date retrieved 01.06.2015.

**[39] Url-4** <*http://www.jncasr.ac.in/shruti/chapter2.pdf*>, date retrieved 01.06.2015.

**[40] Url-5** <*http://upload.wikimedia.org/wikipedia/commons/0/05/PEDOT.png*>

**[41] Balcerzak E. S.** (2011) Polypyrrole Composites: Electrochemical Synthesis, Characterizations and Applications in *Electropolymerization*, InTech, Croatia

**[42] Url-6 <***https://commons. Polypyrrole.png*>, date retrieved 06.06.2015.

**[43] Url-7** <*http://upload.wikimedia.org/wikipedia/commons/5/58/Trans-%28.png*>, date retrieved 06.06.2015.

**[44] Börüban, Ç.** (2007). Synthesis and characterization of polypyrrole/ montmorillonite and polypyrrole/polypropylene composıtes, *Ph.D. Thesis*, Middle East Technical University, Ankara

**[45] Ahlatcioğlu, E., Şenkal, B. F., Okutan, M.** (2014). Preparation and Electrical Characterization of Poly(Aniline) NanoClay Composites *High temperature materials and processes, 34,* 341–346.

**[46] Suh, D. J., Park O. O.** (2002). Nanocomposite structure depending on the degree of surface treatment of layered silicate. *Journal of Applied Polymer Science, 83*, 2143–2147.

**[47] Phang, S.W., Kuramoto N.** (2010). Microwave absorption property of polyaniline nanocomposites containing TiO2 and Fe3O4 nanoparticles after FeCl36H2O treatment. *Polym.Compos., 31,* 516-523.

**[48] H.B.Gu, Y.D.Huang, X.Zhang, Q.Wang, et al.** (2012). Magnetoresistive polyaniline-magnetite nanocomposites with negative dielectrical properties. *Polymer, 53,* 801.

**[49] Kurlyandskaya, G.V., Cunanan, J., Bhagat, S.M., Aphesteguy, J.C., Jacobo, S.E.** (2007). Field-induced microwave absorption in $Fe_3O_4$ nanoparticles and $Fe_3O_4$/polyaniline composites synthesized by different methods. *J. Phys. Chem. Solids, 68,* 1527.

**[50] Jolivet, J.P., Tronc, E.** (1998). *J. Colloid Interface Sci*., 125, 688.

**[51] Url-8** <*http://prliuerve.lehpgh.edu/cgi/vi02&context=cas-lehighreview-vol-15*> date retrieved 06.06.2015.

**[52]Url-9** <*http://shtyduldirect.co.tz/notes/vienotes/cdDw9yJ0Pt7jhynq_SMvg*>,date retrieved 06.06.2015.

**[53] Shioyama, H., Tatsumi, K., Iwashita, N.** (1998). On The Interaction between The Potassium-GIC and Unsaturated Hydrocarbons. *Synth Met, 96*,229.

**[54] Url-10** <*http://www.spring8.or.jp/en/news_publications/press_LP12/120806/*>, date retrieved 15.06.2015.

**[55] Koyun A., Ahlatcıoğlu E. and Koca İpek Y.** (2012). Biosensors and Their Principles in *A Roadmap of Biomedical Engineers and Milestones,* Intech, Croatia.

**[56] Paine, R. T., Narula, C. K.** (1990). Synthetic routes to boron nitride. *Chem Rev 90,* 73-91.

**[57] Narula, C. K., Schaeffer, R., Paine, R. T. J Am** (1987) Synthesis of boron nitride ceramics from poly(borazinylamine) precursors. *Chem Soc, 109*, 5556-5557.

**[58] Pouch, J.J., Alterovitz, S.A.** (1990). Synthesis and Properties of Boron Nitride in *Materials Science Forum Trans Techn.,* p. 426., Switzerland.

**[59] Meller A. (**1983). Boron Compounds in *Gmelin Handbuch der Anorganische* Chemie, (Second ed.), Springer-Verlag, Berlin.

**[60] Xiao, Y., Yan, X. H., Cao, J. X., Ding, J. W., Mao, Y. L., Xiang, J.** (2004). Specific heat and quantized thermal conductance of single-walled boron nitride nanotubes. *Phys. Rev. B., 69*, 205415.

**[61] Chang, C. W.; Han, W. Q.; Zettl, A.** (2005) Thermal conductivity of B–C–N and BN nanotubes. *Appl. Phys. Lett., 86*, 173102.

**[62] Singh, S.** (2002). Liquid Crystal Fundemantals, Singapore.

**[63] Url-11** <*http://chemwiki.ucdavis.edu/Physical_Chemisty/Physical_Properties*>, date retrieved 06.06.2015.

**[64] Kaniappan1, K., Murugavel, S. C., Thangadurai, T. D.** (2014). A Review on Photopolymers for Polymer Nanocomposite Applications. *J. Environ. Nanotechnology, 3,* 01-15

**[65] Thaker, B. T., Patel, D. M., Kanojiya, J. B.,** (2009). New Liquid Crystalline Compounds Involving Ester-Chalcone Linkages Having 1,3,5-Trisubstituted Pyrazole as a Terminal Group. *Molecular Crystals and Liquid Crystals, 509,* 145-164

**[66] Chao, C. Y., Xuefa Li, Christopher K. Ober,** (2004). Directing self-assembly in macromolecular systems: Hydrogen bonding in ordered polymers. *Pure and Applied Chemistry Vol. 76,* 1337

**[67] Selvam, P., Nanjundan, S.**, (2005). Synthesis and characterization of new photoresponsive acrylamide polymers having pendant chalcone moieties. *Reactive and Functional Polymers, 62*, 179–193

**[68] Balaji, R., Nanjundan, S.** (2001)**.** Synthesis and characterization of photocrosslinkable functional polymer having pendant chalcone moiety," *Reactive and Functional Polymers 49*, 77–86

**[69] Okutan M. (**2010). Fulleren ve Azo Boya Katkılı Nematik Sıvı Kristal Sistemlerde Dielektrik ve Optik Spektroskopi Yöntemleri İle Moleküler Durulma Zamanlarının ve Kırılma İndisi Değişimlerinin İncelenmesi, Ph.D. Thesis, Gebze Technical University, Gebze, Kocaeli.

**[70] Ahlatcioğlu, Şenkal, E., B. F., and Okutan, M.** (2014). Preparation and Electrical Characterization of Poly(Aniline) NanoClay Composites, *High Temp. Mater. Proc. 34*, 341–346.

**[71] Knight, R. J., Nur, A.,** (1986). *Society of Professional Well Log Analysts Twenty Seventh Annual Logging Symposium*, Houston, Texas, June 9–13.

**[72] Url-12** <*http://chemwiki.ucdavis.edu/uMaterials/Optics/Dielectric_Polarizatn*> date retrieved 07.06.2015.

**[73] Ahlatcıoğlu E., Senkal B. F., Okutan M., Gursel Y.** (2014). Preparation and polymerization of chalcone substituted aniline and investigation of impedance properties. *Materials Science in Semiconductor Processing 28*, 103–107.

**[74] H.E., Atyia, A.M., Farid, N.A. Hegab,** (2008). AC conductivity and dielectric properties of amorphous GexSb 40− xSe 60 thin films, *Physica B, 403* 3980.

**[75] Ahlatcıoğlu, E., Gursel, Y., Okutan, M., Senkal, B.F.,** (2014). Preparation of poly (N-vinylcarbazole)-co-poly (2-(dimethylamino)ethyl methacrylate) based hydrogen bonded side-chain liquid crystal copolymer, *Materials Science in Semiconductor Processing, 28,* 144–150.

**[76] Ahlatcıoğlu Özerol, E., Şenkal, B.F., Okutan, M.** (2015). Preparation and characterization of graphite composites of polyaniline, *Microelectronic Engineering, 146,* 76–80.

**[77] Zeng, X., Ko, T.,** (1997). Structure–Conductivity Relationships of Iodine-Doped Polyaniline. *J. Polym. Sci. Part B: Polymer Physics, 35*, 1993–2001.

**[78] Atyia, H.E., Farid, A.M., Hegab, N.A.** (2008). AC conductivity and dielectric properties of amorphous GexSb 40− xSe 60 thin films, *Physica B, 403* 3980-3984.

**[79] Afifi, M.A., Bekheet, A.E., Elwahhab, E. A., Atyia, H.E.** (2001). AC conductivity and dielectric properties of amorphous, $In_2Se_3$ films, *Vacuum, 61,* 9-17.

**[80] Ghosh, A.** (1990). Frequency-dependent conductivity in bismuth-vanadate glassy semiconductors. *Phys. Rev. B,* 41, 1479.

**[81] Fouad, S.S., Sakr, G.B., Yahia, I.S., Abdel-Basset, D.M., Yakuphanoglu, F.** (2013). Impedance spectroscopy of p-ZnGa2Te4/n-Si nano-HJD. *Physica B, 415,* 82–91.

**[82] Meirhaeghe, R.L. V., Dutoit, E.C., Cardon, F., Comes, W.P.** (1976). On the application of the Kramers-Kronig relations to problems concerning the frequency dependence of electrode impedance, *Elecrochim. Acta, 21* 39–43.

**[83] E.C. Dutoit, et al.,** (1975). Investigation on frequency-dependence of impedance of nearly ideally polarizable semiconductor electrodes CDSE, CDS and $TIO_2$. *Physical Chemistry Chemical Physics, 79*, 1206-1213.

**[84] N. N. Binitha and S. Sugunan,** (2008). Polyaniline/pillared montmorillonite clay composite nanofibers. *Journal of Applied Polymer Science*, *107* 3367–3372.

**[85] Knight, R. J. and Nur, A.,** (1986) *Society of Professional Well Log Analysts Twenty Seventh Annual Logging Symposium,* Houston, Texas, June 9–13

**[86] Raju G.G.,** (2003). *Dielectrics in Electric Fields*, Marcel Dekker, New York.

**[87] Pouch, J.J., Alterovitz, S.A.** (1990). Synthesis and Properties of Boron Nitride in *Materials Science Forum Trans Techn.,* p. 426., Switzerland.

**[88] Raju G.G.,** (2003). *Dielectrics in Electric Fields*, Marcel Dekker, New York.

**[89] Meller A. (**1983). Boron Compounds in *Gmelin Handbuch der Anorganische* Chemie, (Second ed.), Springer-Verlag, Berlin.

**[90] Barsoukov, E., Macdonald, J.R.** (2005). *Impedance Spectroscopy Theory, Experiment and Applications,* (Second ed.), John Wiley & Sons Inc., New Jersey.

**[91] A.M., Farid, Atyia H.E., Hegab, N.A.** (2008). AC conductivity and dielectric properties of amorphous GexSb 40− xSe 60 thin films, *Physica B, 403* 3980–3984.

**[92] Tiwari, T., Srivastava, N., Srivastava, P.C.,** (2013). Ion Dynamics Study of Potato Starch. *Int. J. Electrochem., 2013,* 1–8.

**[93] Elliott, S.R.,** (1987). A.c. conduction in amorphous chalcogenide and pnictide semiconductors, *Adv. Phys.*, 36, 135-218.

**[94] Mathavan, T., Umapathy, S., Jothirajan, M. A., Benial, A. M. F.**,(2012). Spectroscopic Studies on Threonine Doped Polyaniline. *Composite, 45,* 588-593.

**[95] Jonscher, A.K.,** (1977). The 'Universal' Dielectric Response. *Nature, 267*,673-679.

**[96] Elliott, S.R.,** (1987). A.c. conduction in amorphous chalcogenide and pnictide semiconductors, *Adv. Phys.*, 36, 135-218.

**[97] Paine, R. T., Narula, C. K. (**1990). Synthesis and thermal decomposition of B-N compounds. *Chem Rev, 90*, 73.

**[98] Narula, C. K., Schaeffer, R., Paine, R. T. (**1987). Synthesis of boron nitride ceramics from poly(borazinylamine) precursors. *J Am Chem Soc, 109,* 5556-5557.

**[99] Pouch, J.J., Alterovitz, S.A.** (1990). Synthesis and Properties of Boron Nitride in *Materials Science Forum Trans Techn.,* p. 426, Switzerland.

**[100] Meller A. (**1983). Boron Compounds in *Gmelin Handbuch der Anorganische* Chemie, (Second ed.), Springer-Verlag, Berlin.

**[101] Xiao, Y., Yan, X. H., Cao, J. X., Ding, J. W., Mao, Y. L., Xiang,** (2004). Specific heat and quantized thermal conductance of single-walled boron nitride nanotubes. *Phys. Rev. B., 69*, 205415.

**[102] Johscher, A.K.** (1983). *Dielectric Relaxation in Solids,* Chelsea Dielectrics Press, London,

**[103] Cole, K.S., Cole, R.H.** (1941). Dispersion and Absorption in Dielectrics I: Alternating Current Characteristics. *J.Chem. Phys., 9,* 341-351.

**[104] Bunget, I., Popescu, M.,** (1984). *Physics of Solid Dielectrics*, Elsevier Publishing Company, NewYork.

**[105] Chelkowski, A.** (1980). *Dielectric Physics*, Elsevier Publishing Scientific Publishing Company, NewYork.

**[106] Saha, S., Sinha, T.P.,** (2002). Structural and Dielectric Studies of Ba (Fe0.5Nb0.5)O3, *J.Phys.Condens.Matter, 14,* 249–258.

**[107] Url-13** <*http://www3.imperial.ac.uk/pls/portallive/doc/1/11949698.PDF*>, date retrieved 10.06.2015.

**[108] Url-14** <*http://chemwiki.ucdavis.edu/Physical_Chemistry/Spectroscopy/*>, date retrieved 15.06.2015.

**[109] Url-15** <*http://www.st-andrews.ac.uk/~mmave/epr/what-is-epr/*>,date retrieved 15.06.2015.

## CURRICULUM VITAE

**Name Surname:** Esma ÖZEROL

**Place and Date of Birth:** Fatih, 08/06/1984

**E-Mail:** esma_ahlatcioglu@yildiz.edu.tr

**EDUCATION:**

**B.Sc.:** ISTANBUL UNIVERSITY, PHYSIC

**M.Sc.:** ISTANBUL TECHNICAL UNIVERSITY POLYMER SCIENCE AND TECHNOLOGY

**PROFESSIONAL EXPERIENCE AND REWARDS:**

**PUBLICATIONS, PRESENTATIONS AND PATENTS ON THE THESIS:**

- **Ahlatcıoğlu, E.**, Okutan, M., Şenkal, F. B. (2014). Preparation of Propiolic Acid Doped Polyaniline and Investigation of Opto-electronic Properties. *Key Engineering Materials, 605*, 531-535.
- **Ahlatcıoğlu, E.**, Şenkal, B. F., Okutan, M. (2014). Preparation and Electrical Characterization of Poly(Aniline) NanoClay Composites. *High Temperature Materials and Processes, 34*, 341–346.
- **Ahlatcıoğlu, E.**, Şenkal, B. F., Okutan, M., Gürsel, Y. (2014). Preparation and polymerization of chalcone substituted aniline and investigation of impedance properties. *Materials Science in Semiconductor Processing, 28*, 103-107.
- **Ahlatcıoğlu, E.**, Gürsel Y., Okutan, M., Şenkal, B. F. (2014). Preparation of poly (N-vinylcarbazole)-co-poly(2-(dimethylamino)ethyl methacrylate) based hydrogen bonded side-chain liquid crystal copolymer. *Materials Science in Semiconductor Processing, 28*, 144-150.
- **Ahlatcıoğlu Özerol, E.**, Şenkal, F. B., Okutan M. (2015). Preparation and characterization of graphite composites of polyaniline. *Microelectronic Engineering, 146*, 76-80.

- **Ahlatcıoğlu, E.**, Okutan, M., Şenkal, B. F. (2013). Preparation of Propiolic Acid Doped Polyaniline and Investigation of Opto-Electronic Properties. 3rd International Conference on Materials and Applications for Sensors and Transducers. (Poster Presentation).
- **Ahlatcıoğlu, E.**, Şenkal, B. F., Okutan, M., Çelik Bozdoğan, A. (2015). Preparatıon And Characterızatıon Of Poly (Thiophene) Modified Nanoclay Composıtes. Oemt 2015 (Poster Presentation).
- **Ahlatcıoğlu, E**, Çelik Bozdoğan, A., Bozdoğan, A., Şenkal, B. F., Okutan, M. (2015). Structural, Magnetıcal and Electrıcal Propertıes Of Magnetıte Doped Polyanılıne. Oemt 2015 (Poster Presentation).
- **Ahlatcıoğlu, E.**, Şenkal, B. F., Okutan, M. (2014). Preparation and Characterization of graphite composites of Poly ( Thiophene) and Poly (aniline). International Nanoscience and Nanotechnolgy for Next Generation (NaNoNG) 2014 (Poster Presentation).
- **Ahlatcıoğlu, E.**, Şenkal, B. F., Yakuphanoğlu, F., Okutan, M. (2014). Preparatıon and Characterızatıon Of Poly (Thıophene)-Boron Nıtrıde Composıtes. International Nanoscience and Nanotechnolgy for Next Generation (NaNoNG) 2014 (Poster Presentation).
- **Ahlatcıoğlu, E.**, Şenkal, B. F., Okutan, M., Gürsel, Y. (2014). Preparation and Polymerization of Chalcone Substituted Aniline and Investigation of Electro-optical Properties. 1 st International Semiconductor Science and Technology Conference (Poster Presentation).
- **Ahlatcıoğlu, E.**, Barım, G., Gürsel, Y., Okutan, M., Şenkal, B. F. (2014). Preparation of poly (N-vinyl carbazole)-co-poly(2-(Dimethylamino)ethyl methacrylate) based hydrogen bonded side-chain liquid crystal copolymer. 1st International Semiconductor Science and Technology Conference (Poster Presentation).

## OTHER PUBLICATIONS, PRESENTATIONS AND PATENTS :

- **Ahlatcıoğlu E.,** Şenkal B.F., Yakuphanoğlu F., Mansour Sh.A. (2013). Synthesis of new organic semiconductors based on poly(2-anilinoethanol) doped with different acids and investigation of their electro-optical properties. *Polymer Engineering & Science*, *53*, 251-256.

- Gürsel, Y., Şenkal B.F., Yilmaz Canli, N., Güven Özdemir, Z., **Ahlatcıoğlu E.,** Yilmaz, Ö. F., Okutan, M. (2015). Addition of single-wall carbon nanotubes to a liquid crystal material: Impact on dielectric properties. *Materials Science in Semiconductor Processing*, *34*, 182-188.
- *A Roadmap of Biomedical Engineers and Milestones*, Chapter: Biosensors and Their Principles (2012)., Koyun, A., **Ahlatcıoğlu E.,** İpek, Y., intech, Editor: Sadik Kara, (Book Chapter).
- **Ahlatcıoğlu E.,** Yakuphanoğlu, F., Şenkal B.F., (2012). Poli (Akrilik Asit) İle Modifiye Kilin Hazırlanması Ve Modifiye Kil Ortamında Polianilin Sentezi ve Karakterizasyonu. 4. Ulusal Polimer Bilim ve Teknolojisi Kongresi, (Poster Presentation).
- **Ahlatcıoğlu E.,** Şenkal B.F., Yakuphanoğlu, F., (2010). Poli(2-Anilinoetanol) Organik Yarıiletken Polimerin Sentezi Ve Elektro-Optik Özelliklerinin İncelenmesi. 3.Ulusal Polimer Bilim ve Teknolojisi Kongre ve Sergisi, (Poster Presentation).